Kinetic Modelling of Biomass Gasification in an Indirectly Heated Bubbling Fluidized Bed Steam Reformer

Maarten Kwakkenbos

TU Delft

Kinetic Modelling of Biomass Gasification in an Indirectly Heated Bubbling Fluidized Bed Steam Reformer

A Performance Assessment

by

M. Kwakkenbos

to obtain the degree of Master of Science
at the Delft University of Technology,
to be defended publicly on Monday February 3, 2020 at 02:00 PM.

This thesis is confidential and cannot be made public until February 03, 2022.

An electronic version of this thesis is available at `http://repository.tudelft.nl/`.

ŤUDelft

Preface

In September 2012, I started my masters in Mechanical Engineering at the Faculty on Mechanical, Maritime and Materials Engineering at the Delft University of Technology. For my minor in 2015, I followed a six months program in spaceflight engineering at the Faculty of Aerospace Engineering. I have had the luxury of experiencing multiple fields of work as interesting to me. In order to make a well informed decision for my master program, I started a six month internship at Arcadis and I have travelled through South East Asia for three months. During my internship, I had been most interested in projects on the topic of sustainable energy. During my travels, I learned that in order to preserve nature, wildlife and a wealthy living standard, the world needs engineers to innovate towards sustainable production and the managements of the Earth's limited resources.

In 2017, I started the masters program Sustainable Energy Technology at the Faculty of Electrical Engineering, Computer Science and Mathematics at the Delft University of Technology. Looking back at how different resources for energy transportation and consumption have developed in the past centuries, I concluded that energy can be stored, transported and consumed best when stored in a chemical bond. For this reason, it is still a challenge to shift our consumption away from highly energy dense fossil fuels. As a result, I have chosen to focus on courses that consider sustainable energy as an (electro-) chemical carrier.

In order to provide myself with a deeper understanding of the currently ongoing energy transition, I decided to learn more about three large stakeholders in the energy transition: The government, small innovative tech start-ups and large fossil fuel consuming/producing companies. To deepen my knowledge from the government's perspective, I entered a project at the department of Economic Affairs and Climate of the Dutch national government, designing policy instruments enabling sustainable energy growth. For the perspective of tech start-ups on the energy transition, I followed a six months extra course in technical entrepreneurship. In order to really understand the energy transition, I did an internship at commonly named culprit, Shell, and find out what position companies such as Shell take in the energy transition . These projects, along with my studies, have shown that sustainable innovation is not only an important topic in energy production but in the chemical industry as well. I became increasingly interested in finding sustainable solutions for two topics. First, the production of sustainable chemical feed and secondly, the production of sustainable chemicals for large scale energy storage. My interests have brought me to the department of Large Scale Energy Storage at the faculty of Mechanical, Maritime and Materials Engineering at the Delft University of Technology. I found the Indirectly Heated Bubbling Fluidized Bed Steam Reformer [IHBFBSR] project as an extension of my interests.

The IHBBFBSR project is involved in biomass conversion for energy production. From a sustainable perspective there are both advantages and disadvantages towards the utilization of biomass for sustainable production. I have been determined to learn about these advantages and disadvantages though this project and I aim to form a clear opinion about the role of biomass in the energy transition.

M. Kwakkenbos
Delft, January 2020

List of Acronyms and Symbols

Acronyms

Acronyms	Full Expression
A	Austria
a.r.	as received
atm	atmosphere
BAU	Business as Usual
BBM	Black Box Model
BFB	Bubbling Fluidized Bed
CC	Carbon Conversion
CCBM	Counter Current Back Mixing model
CFB	Circulating Fluidized Bed
CFD	Computational Fluid Dynamics
CGE	Cold Gas Efficiency
CHP plants	Combined Heat and Power plants
CSTR	Continuously Stirred Tank Reactor
DAE	Distributed Activation Energy
d.a.f.	dry ash free
d.b.	dry basis
DHM	Davidson-Harrison Model
dLUC	direct Land Use Change
DNS	Direct Numerical Simulation
DPM	Discrete Particle Model
ECN	Energie Centrum Nederland
EEM	Eulerian-Eulerian Model
EF	Entrained Flow
ELM	Eulerian-Lagrangian Model
EM	Equilibrium Model
ER	Equivalent Ratio
FB	Fluidized Bed
FC	Fixed Carbon
FERCO	Future Energy Resources Corporation
FM	Fluidization Model
GB	Green Biomass
GER	Germany
HHV	Higher Heating Value
HPLC	High-Performance Liquid Chromatography
HPR	Heat Pipe Reformer
IHBFBSR	Indirectly Heated Bubbling Fluidized Bed Steam Reformer
iLUC	indirect Land Use Change
IPCC	International Panel of Climate Change
KLM	Kunii-Levenspiel Model
ktoe	kilo tonnes of oil equivalent
LCA	Life Cycle Analysis
LHV	Lower Heating Value

Acronyms	Full Expression
LMHW	Langmuir-Hinshelwood
NDIR	Non-Dispersive Infrared Spectroscopy
NL	the Netherlands
PFR	Plug Flow Reactor
PMSC	Progressive Model with Shrinking (Reacting) Core
RB	Red Biomass
S	Sweden
SB	Steam to Biomass Ratio
SNG	Synthetic Natural Gas
SUCM	Shrinking Unreacted Core Model
SUPM	Shrinking Unreacted Particle Model
TB	Twin Bed
TFC	Total Final Consumption
TFM	Two-Fluid Model
TGA	Thermo-Gravimetric Analysis
TNO	Nederlandse Organisatie voor toegepast-natuurwetenschappelijk onderzoek
TPES	Total Primary Energy Supply
UCM	Uniform Conversion Model
UNEP	United Nations Environmental Program
US	United States of America
VM	Volatile matter
WMO	World Meteorological Organization

Symbols

Symbol	Parameter	Unit
$a_{s,m}$	Specific area on a mass basis	$m^2 \cdot kg^{-1}$
$a_{i,p}$	The number of atoms of the p-th element in species i	[-]
A_p	The total number of atoms of element p present in the reactor	[-]
A_j	Arrhenius constant for reaction j	s^{-1}
A_{cross}	Cross-sectional area	m^2
$[A]^a$	Concentration of species A to the power of stoichiometric coefficient a	$[kmol \cdot m^{-3}]^a$
Bi_t	Dimensionless thermal Biot number	[-]
Bi_m	Dimensionless mass Biot number	[-]
C_i^{n-1}	Concentration of species i for an n-th order reaction	$kmol \cdot m^{-3}$
$C_{p,i}$	Specific heat of species i	$J \cdot kg^{-1} \cdot K^{-1}$
CC	Carbon Conversion	[-]
CGE	Cold Gas Efficiency	[-]
d_j	Diameter of structure j	m
$D_{i,eff}$	Effective diffusion coefficient	$m^2 \cdot s^{-1}$
$D_{i,j}$	Binary diffusion coefficient of species i in j	$m^2 \cdot s^{-1}$
$E_{a,j}$	Activation energy for reaction j	$kJ \cdot kmol^{-1}$
$\dot{F}_i$	Molar flow of species i	$kmol \cdot s^{-1}$
$G_{f,i}^0$	Gibbs free energy of formation of species i	$kJ \cdot kmol^{-1}$
h_{eff}	Effective heat transfer coefficient	$W \cdot m^{-2} \cdot K^{-1}$
h_{conv}	Convective heat transfer coefficient	$W \cdot m^{-2} \cdot K^{-1}$
h_{rad}	Radiative heat transfer coefficient	$W \cdot m^{-2} \cdot K^{-1}$
h_m	Effective mass transfer coefficient	$[m \cdot s^{-1}]$

Symbol	Parameter	Unit
$H_{f,i}^0$	Enthalpy of formation	$kJ \cdot kmol^{-1}$
HHV_i^b	Higher heating value of component i on a 'b' basis.	$MJ \cdot kg^{-1}$
$k_{i,\text{eff}}$	Effective thermal conductivity of species i	$W \cdot m^{-1} \cdot K^{-1}$
$k_{i,\text{per}}$	Perpendicular thermal conductivity of species i	$W \cdot m^{-1} \cdot K^{-1}$
$k_{i,\text{par}}$	Parallel thermal conductivity of species i	$W \cdot m^{-1} \cdot K^{-1}$
k_j	Reaction rate coefficient for reaction j	Depends on order
LHV_i^b	Lower heating value of component i on a 'b' basis.	$MJ \cdot kg^{-1}$
L_{Fixed}	Bed height for fixed bed configuration	m
L_{mf}	Bed height at minimum fluidization	m
L_{Fluid}	Bed height for fluidized bed configuration	m
$\dot{m}'''$		
m_i^b	Mass of component i on a 'b' basis.	kg
M_{bed}	Mass of the bed material	kg
MW_i	Molecular weight of species i	$kg \cdot kmol^{-1}$
n	Reaction order	[-]
Nu	Dimensionless Nusselt number	[-]
p_j	Pressure of reactor/stream j	bar or atm
P_{burn}	Power delivered by the burners	W
Py	Dimensionless Pyrolysis number	[-]
Py'	Dimensionless Pyrolysis' number	[-]
r	Particle radius	m
r_l	Particle radius at radial location l	m
r_j	Reaction rate of reaction j	$kmol \cdot m^{-3} \cdot s^{-1}$
R_g	Universal gas constant of 8.314	$kJ \cdot K^1 \cdot kmol^1$
R_{heating}	Heating rate	$K \cdot s^{-1}$
Re	Dimensionless Reinolds number	[-]
SB	Steam to biomass ratio [SB]	[-]
Sc	Dimensionless Schmidt number	[-]
Sh	Dimensionless Sherwood number	[-]
t_{heating}	Heating time	s
T_j	Temperature of reactor/stream j	°C or K
Th_n	Thiele modulus for an n-th order reaction	[-]
U_i	Velocity of species i	$m \cdot s^{-1}$
V_{CSTR}	Volume of the bedzone	m^3
Y_i^b	Mass fraction of component i on a 'b' basis.	wt %

Greek Symbol	Parameter	Unit
ϵ	Voidage	%
ϵ_{Fixed}	Bed voidage for fixed bed configuration	[-]
γ_i	Relative volume fraction of gas species i compared with the total amount of gas	vol%
λ	Equivalent ratio [ER]	[-]
v_i	Kinematic viscosity of species i	$m^2 \cdot s^{-1}$
ρ_i	Density of species i	$kg \cdot m^{-3}$

Subscripts

Subscript	Meaning
b	Biomass
bulk	Bulk of emulsion or solids bulk including voidage
c	Char
conv	convective
eff	effective
f	formation
g	gas
m	mass
n	reaction order
p	Particle
pyr	pyrolysis
$pyr - H_2O$	Pyrolytic water
r_0	location at the shell of the particle at distance r of the center of the particle
rad	radiative
s	solid
∞	homogeneous emusion bulk

Species

Species	Molecule	Steam Class
CO	Carbon monoxide	Conventional vapour
CO_2	Carbon dioxide	Conventional vapour
H_2	Hydrogen	Conventional vapour
CH_4	Methane	Conventional vapour
H_2O	Water/steam	Conventional vapour
C_6H_6	Benzene	Conventional vapour
C_7H_8	Toluene	Conventional vapour
$C_{10}H_8$	Naphthalene	Conventional vapour
C_5H_6OH	Phenol	Conventional vapour
O_2	Oxygen	Conventional vapour
N_2	Nitrogen	Conventional vapour
C	Carbon/Char	Conventional solid
S	Sulfur	Conventional vapour
NH_3	Ammonia	Conventional vapour
H_2S	Hydrogen Sulfide	Conventional vapour
HCl	Hydrogen chloride	Conventional vapour
Cl_2	Chlorine gas	Conventional vapour

Summary

The effort to reduce global anthropogenic carbon dioxide emissions has caused a growing interest in the use of sustainable energy sources. In addition, the chemical and energy sectors aim to be less dependent on fossil resources to ensure their continuity. One of the potentially sustainable energy sources considered as an alternative for the currently used fossil sources is biomass. Biomass is organic matter that originates from plants or animals which can be used as chemical energy carrier for fuels or for the production of chemical feed stock[6]. Biomass is considered a sustainable energy source for the reason that as much carbon dioxide is taken out of the atmosphere, for biomass growth, as carbon dioxide is being released into the atmosphere upon combustion for energy consumption. Biomass is also seen as potential non-fossil resource for the production of chemical feed for the reason biomass can be cultivated.

Gasification is a thermochemical process that converts carbonaceous materials like biomass into useful convenient gaseous fuels or chemical feedstock[6]. Gasification takes place at high temperature in the presence of a gaseous agent. Gasification is aimed at increasing the overall energy density of biomass by producing gaseous energy carriers with a higher energy density than the original biomass feed. Typical gaseous products from gasification are hydrogen, carbon monoxide, carbon dioxide and methane[12][6]. Conventional gasifiers combust a fraction of the biomass or char in order to provide heat to the reduction reactions. This has two disadvantages. First, the flue gasses are mixed with the product gas and need to be separated in order for the product gas to be used efficiently. Secondly, the air that is used for partial biomass combustion mainly consists out of nitrogen. The nitrogen does not react in the gasification process and dilutes the gasification product significantly.

The Indirectly Heated Bubbling Fluidized Bed Steam Reformer [IHBFBSR] set-up at the TU Delft is a novel indirectly heated gasifier or allothermal gasifier. The combustion of natural gas takes place in a separate combustion chamber inside the reactor chamber. Steam gasification can therefore be performed in the absolute absence of oxygen. A radiant tube facilitates heat transfer from the combustion to the reaction chamber. The radiant tubes are installed at the top and bottom of the IHBFBSR and work according to the heat from inside to outside principle.

The aim of this study is to assess the performance of the IHBFBSR set-up at the TU Delft and compare its performance with other existing allothermal gasifiers. The main research question of this study is stated as: "How does the Indirectly Heated Fluidized Bed Reactor perform in terms of product yield, product quality and energy efficiency and how does its performance compare to other indirectly heated gasifiers?"

In order to answer this question, both an equilibrium model and a kinetic model have been designed. The molar fractions of the permanent gasses CO, CO_2, H_2 and CH_4, produced by the kinetic model, have been validated by experiments with the IHBFBSR for four different values of the equivalent ratio. In addition, the experimentally determined carbon conversion [CC] resembles the carbon conversion as calculated by the model. The cold gas efficiency [CGE] cannot be validated for the reason that the yield of tar species has not been determined experimentally. Nevertheless, the results from the model are in the range of 65-70% around the sub-optimal process conditions. These values of the CGE resemble the CGE reported in literature of similar allothermal biomass gasification set-ups. The kinetic model is used in order to find (sub)-optimal process conditions for the IHBFBSR. The conditions are sub-optimal for the reason that not all influencing process parameters have been reviewed within the scope of this study.

This study shows that the pyrolysis step in the IHBFBSR is rate limited by internal heat transfer. In addition, the char oxidation reaction is limited by mass transfer of oxygen to the char particle.

Sub-optimal conditions for the IHBFBSR take place at a reactor temperature of 850 [°C], which is the maximal controlable temperature of the reactor. At this temperature, the carbon limit is reached for an equivalent ratio of 0.23. By definition, the CC equals 100% at the carbon limit. In reality, the CC will not be 100% due

to a fraction of unreacted biomass, the condensation of tars in the reactor or the formation of other contaminants. The only measured CC of the IHBFBSR from experimental data equals 76%. The CGE at the carbon limit equals 69.7%. Optimal process conditions are where the particle size of the bed material is maximized without loosing the fluidization behaviour of the bed. The maximum particle size equals 600 micron. The gas composition and char fraction as function of the equivalent ratio is visualized in figure 1. The gas composition and char fraction as function of the reactor temperature is visualized in figure 2. The figure show the gas composition at the carbon limit when the char fraction reaches zero.
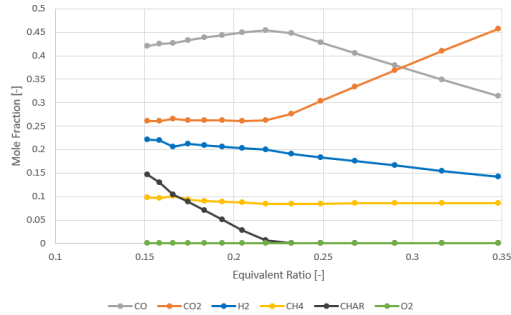
Figure 1: The Sensitivity Analysis on the Product Gas Composition as Function of the Equivalent Ratio λ.
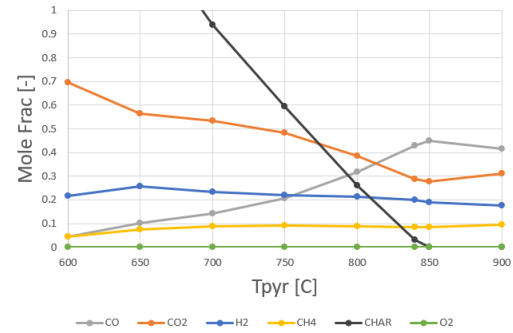
Figure 2: The Sensitivity Analysis on the Product Gas Composition as Function of the Reactor Temperature T_r.

With these results for the CC and CGE, the IHBFBSR performs similar with respect other allothermal gasification technologies. The technologies considered in this study for comparison include: MILENA [NL], Heat Pipe Reformer [GER], FIFCB [A] and Ferco's SilvaGas [US]. Main advantages of the IHBFBSR over the other technologies are the complete separation of the combustion and gasification reaction chambers, and effective heat control by the external heat source. A challenge that needs to be overcome before scaling up the IHBFBSR technology is the bed removal strategy. Circulating fluidized bed would for instance solve this problem and make the technology scalable.

The overall efficiency of the system can be increased by heat transfer between the inlet and outlet gasses of the burners and by the separation and combustion of tars and char to add heat to the process.

The main purpose of the research on allothermal gasifiers is to remove the combustion process from the gasification process. It is therefore crucial to do experiments with steam in the future. It is proposed to validate the current kinetic model for steam gasification and compare its performance with other allothermal gasifiers. What makes this allothermal gasifier unique compared to other allothermal gasifiers is the use of radiant tube burners. It is therefore advised to study the heat transfer between these radiant tubes and the gasification reaction chamber thoroughly.

For this study, it is chosen to use a limited fluidization model as part of the kinetic model. The bedzone has been modelled as a homogeneous steady state emulsion phase. This has been the result of limited project duration. It is advised to upgrade the kinetic model with a more detailed fluidization model. In addition, it is advised to look into possibilities to model the internal heat transfer limitation in the pyrolysis process and the mass transfer limitation in char oxidation to further extend.

Contents

1

Introduction

1.1. Biomass as a Sustainable Energy Source

In 2017, roughly 7.55 billion people lived on Earth[61]. In that year, the entire population needed clean water, food, housing, education, health care, energy and a space to live, but unfortunately, not everyone on Earth has access to the resources to fulfill their needs. To make this challenge even more difficult to solve, the global population is growing at a rate of 1.109% (rate in 2018) [65] yielding an increased demand for natural resources. A distinction can be made between fossil resources and resources that can be regrown. At the current consumption rate, the Earth is being depleted from its fossil resources.

The past few decades the public interest in fossil resource depletion, for the production of energy, has grown. The greenhouse gasses emitted upon the combustion of fossil fuels such as coal, oil and natural gas are named as one of the main causes for global warming. Human activities are estimated to have already caused a global temperature increase of 1.0 °C by the emission of greenhouse gasses with respect to the pre-industrial average[3].

In order to provide a clear scientific view on the root causes and consequences of global warming, the United Nations Environmental Program UNEP and World Meteorological Organization WMO founded the International Panel of Climate Change, IPCC[3]. In one of their latest reports (2018), the IPCC concludes that the consequences of global warming will have a devastating impact on health, livelihoods, food security, water supply, human security, biodiversity and economic growth on a global scale[3]. Direct consequences of global warming as described by the IPCC are:

- Sea level rise as the result of polar ice melting

- Increase in the magnitude of hurricanes and increase of frequency and magnitude of extreme storms in several regions

- Change in biodiversity and extinction of species.

- Change in regional climates such as heavy precipitation and droughts.

The IPCC report states that human activity is not the only cause of global warming. Several natural processes contribute as well to the emission of greenhouse gasses[3]. Nevertheless, it is evident that the global population will have to react to the consequences of global warming hence the need to reduce the anthropogenic contribution to greenhouse gas emissions.

The global energy consumption increases severely. Not only due to a growing population but also because the energy needs of each individual increase. In 2018, global energy consumption increased at nearly twice the rate compared to the average growth rate in 2010[22]. Main reasons are an increase in energy demand for heating and cooling and an increase in demand for electricity. As a result of higher energy consumption, CO_2 emissions rose 1.7% in 2018 and hit a new record[22].

1

In 2016, 81% of the global Total Primary Energy Supply [TPES] originates from fossil fuels which release carbon dioxide upon combustion. The shares of coal (27%), oil(32%) and natural gas (22%) are illustrated in figure 1.1[21].
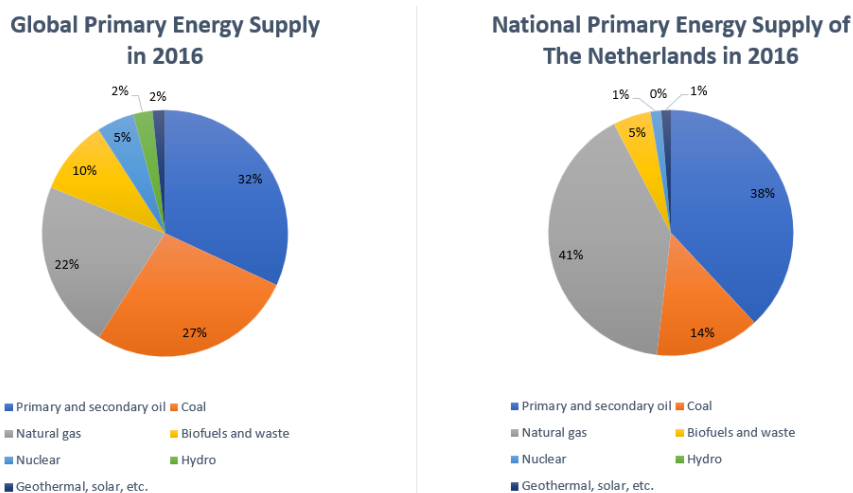

Figure 1.1: Energy sources Shares for Global and Dutch National Total Primary Energy Supply (TPES) in 2016[21].

Only 14% of the global TPES originates from non-fossil fuels such as biomass energy (10%), hyrdo power (2%) and other renewables (2%) including solar and wind energy. Note that electricity is not a primary energy resource and is produced by an energy conversion step as product from primary energy sources. The missing 5% from the TPES balance originates from nuclear energy. Nuclear fuel is a depletable non-fossil resource, but does not produce large scale greenhouse gas emission as is the case for the other fuels[21]. Instead, it produces small amounts of toxic nuclear waste.

When the global statistics from figure 1.1 are compared to the TPES of The Netherlands, it can be observed that The Netherlands is also highly dependent on fossil energy sources and that the energy supply is dominated by natural gas (41%) and oil (38%)[21]. For the reason that The Netherlands has nationally owned natural gas fields, natural gas has been the favorite energy carrier for domestic heating, cooking and in agricultural and industrial processes. The high supply of primary oil products can be attributed to the (petro-)chemical refineries based in the Netherlands. Although a large share of the nationally produced secondary oil leaves the country as export product (55.2%)[21], a significant share is being consumed nationally. The nationally consumed secondary oil products are mainly consumed by the transport sector (44.0%) and (petro-)chemical industry (36.8%)[21].

Not only the energy sector depends mainly on fossil resources. As illustrated in figure 1.2, the main feedstock for the chemical sector consists of fossil resources as well. Since the chemical industry remains by far the largest industrial user of energy sources [7], which also mainly originate from fossil resources, their dependency on fossil resources is two-fold.

In 2015, 175 parties agreed to put an effort to reduce anthropogenic carbon dioxide emissions as a result of the Paris Agreement. The common goal is to prevent global temperature from exceeding an increase of 2.0 $^\circ C$ above pre-industrial levels with a serious effort to stay below 1.5 $^\circ$C[60]. In order to meet this goal it is possible to define a global carbon dioxide emissions limit or a remaining carbon dioxide budget. In 2018, IPCC estimated the remaining carbon dioxide budget that has a 50% chance of reaching the 1.5 $^\circ$C goal at 580 Gt CO_2[3]. The remaining budget is being depleted by current global emissions of around 39-45 Gt CO_2 per year[3]. This means that, within 13 years at the current rate, the 1.5 $^\circ C$ goal will probably not be met. All participating countries of the Paris Agreement have committed to adopt a national policy strategy to ensure the remaining carbon dioxide budget will not be exceeded.
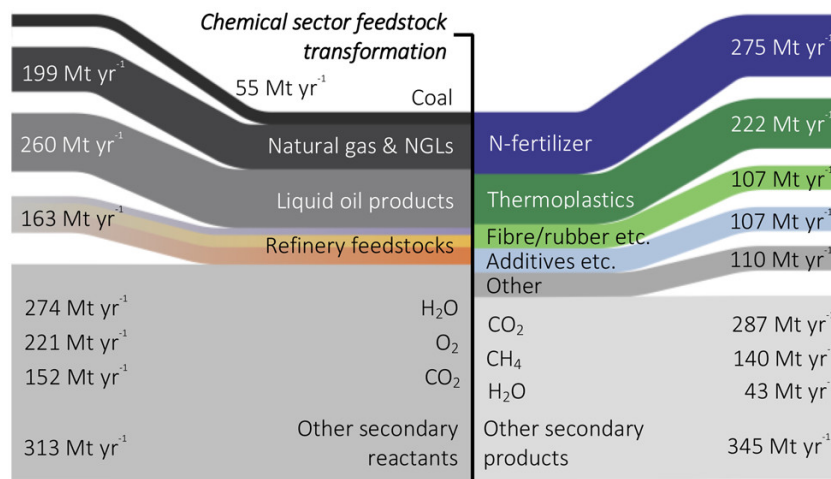
Figure 1.2: Feedstock Origin for the Global Chemical Industry[7].

The effort to reduce global anthropogenic carbon dioxide emissions has caused a growing interest in the use of sustainable energy sources. In addition, the chemical and energy sectors aim to be less dependent on fossil resources to ensure their continuity.

Examples of sustainable energy sources are hydro-, wind and solar energy which can be used for electricity production. Sustainable fuels, such as hydrogen and biofuels, can be produced using sustainable electricity and can be deployed in the industry and transport sector where electrification is not an option. Geothermal energy, heat pumps and the utilization of residual heat can provide energy for domestic heating purposes.

One of the potentially sustainable energy sources considered as an alternative for the currently used fossil sources is biomass. Biomass is organic matter that originates from plants or animals which can be used as chemical energy carrier for fuels or for the production of chemical feed stock[6]. Biomass is considered a sustainable energy source for the reason that as much carbon dioxide is taken out of the atmosphere, for biomass growth, as carbon dioxide is being released into the atmosphere upon combustion for energy consumption. Biomass is also seen as potential non-fossil resource for the production of chemical feed for the reason biomass can be cultivated. This study will mainly focus on the research of biomass as a sustainable energy source, but bear in mind that biomass can also contribute to a less fossil dependent feedstock for the chemical industry.

Historically, biomass has been the main energy source for residential heating and cooking. After the introduction of other energy carriers such as coal, oil, natural gas and nuclear energy, the share of biomass in the global energy mix has decreased substantially. In 2016, 9.8% of the global TPES originated from biomass[20]. This equals a consumption of $56.5 \, \text{EJ} \cdot \text{yr}^{-1}$. In certain areas, biomass is still widely used in the residential sector as energy source for cooking and heating. The global biomass consumption in the residential sector equals 69% of the total final consumption of biomass in 2016[20]. 8.9% of the global TPES of biomass has been used for electricity production in 2016[20].

Berndes et all.[8] compares seventeen different studies which assess the global availability of biomass for consumption. Their work concludes a large variety in the approximated future contribution of biomass in the global energy supply. The availability varies between $100 \, \text{EJ} \cdot \text{yr}^{-1}$ to over $400 \, \text{EJ} \cdot \text{yr}^{-1}$ in 2050[8].

The Dutch government estimates the national biomass availability at 115-753 PJ in 2030[63]. Woody biomass is particularly interesting for biomass gasification. Boosten and Oldenburger[9] have analyzed the availability of woody biomass for energy production in The Netherlands. In their study, two scenarios are used. The business as usual (BAU) indicating a biomass availability as observed in 2014. For the PLUS scenario the Dutch government will make an effort to realize a higher biomass availability to reach a consumption of 40 PJ in 2050. Table 1.1 illustrates from which sources biomass can be made available for energy production.

Table 1.1 illustrates that woody biomass is only expected to contribute 18.3 PJ to the biomass availability in 2020[63]. This is only a small fraction of the estimated biomass availability estimate of 115-753 PJ (2030). Other biomass types that can be used for energy production are wet biomasses from the industrial and agricultural sector, but due to their high moisture content and high level of contaminants, this biomass type is not favourable for gasification. In the Netherlands, 67% of all woody biomass is used in CHP plants, often in combination with coal[10]. This means that the biomass is directly combusted after a drying and pelletizing pre-treatment step. The use of biomass for the production of gasification products is less common on an industrial scale.

Table 1.1: Woody Biomass Availability Estimation in The Netherlands according to Three Different Scenarios[9].

Scenario	Currently	Currently	BAU	BAU	PLUS	PLUS	PLUS	PLUS
Year	2014	2014	2020	2020	2020	2020	2050	2050
Unit	kton	PJ	kton	PJ	kton	PJ	kton	PJ
Woody biomass from forests, landscape, crop growth en build environment	**394**	**7.0**	**417**	**7.5**	**536**	**9.6**	**712**	**12.8**
Forest	112	2,0	121	2,2	150	2,7	210	3,8
Landscape	103	1.8	108	1.9	135	2.4	172	3.1
Crop Growth	1	0.02	10	0.2	22	0.4	45	0.8
Build Environment	178	3.2	178	3.2	229	4.1	285	5.1
Woody biomass from woods processing industry and waste sector	**499**	**9.0**	**601**	**10.8**	**769**	**13.8**	**832**	**15.0**
Wet Residual wood	13	0.2	19	0.3	45	0.8	65	1.2
Dry Residual Wood	32	0.6	43	0.8	100	1.8	143	2.6
Used Wood	454	8.2	539	9.7	624	11.2	624	11.2
non-woody biomass	**24**	**0.4**	**65**	**1.1**	**145**	**2.5**	**684**	**12.2**
Cane	0	0.0	2	0.04	8	0.1	33	0.6
Grasses	24	0.4	63	1.1	126	2.2	615	11.0
Hay	0	0.0	0	0.0	11	0.2	36	0.6
Total	**917**	**16.4**	**1083**	**19.4**	**1450**	**25.9**	**2228**	**40.0**

1.2. Allothermal Biomass Gasification as the Sustainable Link

Gasification is a thermochemical process that converts carbonaceous materials like biomass into useful convenient gaseous fuels or chemical feedstock[6]. Gasification takes place at high temperature in the presence of a gaseous agent. Examples of gasifying agents are air, steam, pure oxygen carbon dioxide or a mixture of air and steam[6]. Typical biomass feeds are woody forestry biomasses and residues, agricultural residues and energy crops. Gasification is aimed at increasing the overall energy density of biomass by producing gaseous energy carriers with a higher energy density than the original biomass feed. Typical gaseous products from gasification are hydrogen, carbon monoxide, carbon dioxide and methane[12][6]. Through bio refineries, synthesis products can be produced for the chemical industry or for energy consumption using hydrogen and carbon monoxide as primary chemical precursor[12].

Conventional gasifiers combust a fraction of the biomass or char in order to provide heat to the reduction reactions. This has two disadvantages. First, the flue gasses are mixed with the product gas and need to be separated in order for the product gas to be used efficiently. Secondly, the air that is used for partial biomass combustion mainly consists out of nitrogen. The nitrogen does not react in the gasification process and dilutes the gasification product significantly.

The IHBFBSR set-up at the TU Delft is a novel indirectly heated gasifier or allothermal gasifier. The combustion of natural gas takes place in a separate combustion chamber inside the reactor chamber. Steam gasification can therefore take place in the absolute absence of oxygen. A radiant tube facilitates heat transfer from the combustion to the reaction chamber. The radiant tubes are installed at the top and bottom of the IHBFBSR and work according to the heat from inside to outside principle. Figure 1.3 visualizes the radiant tube burners and gasification reaction chamber consisting of a bedzone and freeboard.
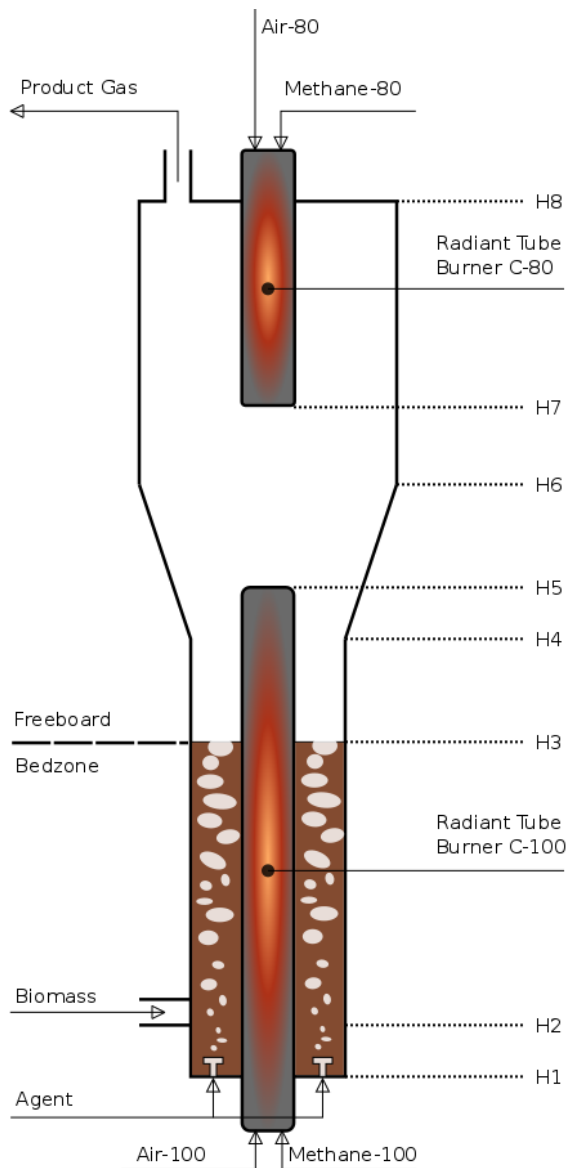
Figure 1.3: Visualization of the IHBFBSR with its Bedzone, Freeboard and Two Internal Radiant Tube Burners.

The bedzone of the bubbling fluidized bed [BFB] reactor contains bed material which facilitates efficient mass and heat transfer. The novel technology eliminates the two disadvantages of conventional biomass gasification as described in the previous paragraph. When heat is supplied from inside to outside, low energy losses and a high energy efficiency are to be expected. Disadvantages could be the reduced volume of the reaction chamber by the radiant tubes and difficulties with handling the bed material in this configuration.

For the evaluation of the performance of the gasification process two parameters are introduced. The carbon conversion and cold gas efficiency respectively are described by equations 1.1 and 1.2. The carbon conversion quantifies the amount of char that is converted into gaseous products.

For gasification at optimal conditions, it is desired to maximize the carbon conversion. In practice, it is nearly impossible to reach full char conversion. For gasification at temperatures below 1000 °C without the presence of of species in the reactor that act as catalysts, usually chemical equilibrium is not attained. Practical residence times, in particular of the gas phase, are too short[12].

$$CC = 1 - \frac{\dot{m}_{C,residue}}{\dot{m}_{C,feed}} \tag{1.1}$$

$$CGE = \frac{\sum_{i=1}^{n} \dot{m}_i \cdot LHV_i - \frac{P_{burner}}{\eta_{burner}}}{\dot{m}_{fuel} \cdot LHV_{fuel}} \tag{1.2}$$

In these equations $\dot{m}_i$ is the mass flow of molecular component i in [kg·h^{-1}]. LHV_i is the lower heating value of component i in [MJ·kg^{-1}]. It is important to mention that the cold gas efficiency is maximal at the carbon limit. In that case, carbon conversion is theoretically maximal and the yield of gasification products is steered maximally towards the production of H_2 and CO. The CCE is maximal because these products have a higher LHV than H_2O and CO_2.

In order to calculate the mass flow of a certain component, equation 1.3 is used.

$$\dot{m}_i = \dot{m}_{bulk} \cdot Y_i = \dot{m}_{bulk} \cdot y_i \cdot \frac{MW_i}{\bar{MW}_{bulk}} \tag{1.3}$$

In equation 1.3, Y_i is the mass fraction of component i in the bulk in [mass%]. y_i is the molar fraction of component i in the bulk in [mol%]. MW_i refers to the molecular weight of component i in [g·mol^{-1}]

1.3. Research Questions

The aim of gasification is to increase heating value or the energy density of a solid biomass. This is achieved by the production of gaseous fuels with higher energy densities compared to the biomass feed. The aim of allothermal or indirectly heated gasifiers is to produce a high quality product gas. The aim of this study is to assess the performance of the IHBFBSR set-up at the TU Delft and compare its performance with other existing allothermal gasifiers.

Key performance indicators [KPIs] that are used in order to quantify reactor performance are:

- Carbon conversion [CC]

- Cold Gas Efficiency [CGE]

- Gas yield of hydrogen, carbon monoxide, carbon dioxide, methane, tars and steam

- Fraction of nitrogen in the product gas

In order to optimize the performance of the IHBFBSR it is desired to have maximal carbon conversion and cold gas efficiency. In some cases, the producer gas will be used as syn-gas for the synthesis of carbohydrates. In this case it can be that a prescribed gas quality is required as well as a preferred H_2 to CO ratio. This study will reflect on the influence of several process parameters on the product quality. Parameters that are interesting for the sensitivity analysis are:

- Reactor temperature

- Equivalent Ratio [ER]

- Bed material size

The IHBFBSR set-up is not fully finalized and commissioned yet. For that reason, it has not been able to perform experiments with steam as gasifying agent. This study will focus on air-gasification in the IHBFBSR.

The main research question of this study is stated as: "How does the Indirectly Heated Fluidized Bed Reactor perform in terms of product yield, product quality and energy efficiency and how does its performance compare to other indirectly heated gasifiers?"

In order to answer this research question, several sub-questions have been formulated:

- What is the effect of the Equivalent Ratio ratio on the product selectivity, CC and CGE? For which equivalent ratios can the IHBFBSR be operated optimally? (At maximal CC and CGE)

- What is the effect of the reactor temperature on the product selectivity, CC and CGE? For which temperature(s) can the IHBFBSR be operated optimally?

- What is the effect of bed material size on the product selectivity, CC and CGE? For which bed material size can the IHBFBSR be operated optimally?

- What are (sub)optimal operation conditions in terms of ER, temperature and bed material size?

- How does the performance of the IHBFBSR compare to other allothermal gasifiers?

- How energy efficient is the IHBFBSR?

- What mechanisms, considering chemical rate, heat transfer and mass transfer, are rate limiting in biomass pyrolysis and gasification reactions in the IHBFBSR?

1.4. Methodology

In order to observe the performance of the IHBFBSR, several experiments are conducted at for several process parameter settings. Experiments are however costly. They consume significant amounts of time and resources considering that the reactor must be heated to temperatures around $850\,°C$ for each experiment. The experiments show the performance of the gasifier for specific sets of process conditions. They do not however, give optimal operation settings given a preferred product output. In order to study the performance of the IHBFBSR on a wide range of process conditions, it is chosen to design a mathematical model of the process.

A simulation or mathematical reactor model is an approximation of what is happening in the reactor by describing the most important physical processes in the form of an equation. A model can be used to predict the behaviour of the physical system without having to put the physical system in these process conditions. A good mathematical model is able to: [6]

- Predict the behaviour of the physical system in extreme and possibly dangerous process conditions.

- Find optimal process conditions for the physical system.

- Assess the performance of the process and use these results in further process design choices.

- Help to understand experimental data.

- Provide information about process scale up.

In the process of gasification, the product gas composition is highly dependent on the process conditions and reactor geometry. These parameters affect a.o. hydrodynamics, thermodynamics, heat and mass transfer and the influence of chemical pollutants. These processes are challenging to model. Most gasifiers have their own custom model for that particular reason.

Due to the high dependency between gasifier behaviour and process conditions it is important to do experiments on lab scale or with pilot plants. Experiments will give a more accurate result of the reactor performance, but a model can still be of assistance. The model can identify a useful range in which optimal process conditions are expected[6]. The amount of experiments that are needed to find these optimal conditions can therefore be limited. A model can also identify areas of concern and danger in operation. It will therefore enforce safety for the experimental work. Finally, a model can illustrate the value of a chemical process by estimating costs and revenues as well as energy efficiency. This can be necessary for the financial acquisition that is needed for a pilot plant.

1.5. Thesis Outline

This section discusses the outline of the thesis work. This first chapter has shown the need for sustainable energy sources. This introduction has shown the potential of allothermal gasification for biomass conversion with a better product gas quality compared to conventional gasification technologies. This study is aimed at assessing the performance of the IHBFBSR. It is chosen to do both experiments and design a mathematical model to reach this goal. The next chapters will describe the (acquisition of) the results that lead to the performance assessment.

Chapter 2 introduces background information that is necessary to understand the physics and chemistry involved in biomass gasification. In addition, this chapter provides an overview of conventional gasification technologies. Also, an overview of currently existing allothermal gasification technologies is given.

Chapter 3 discusses the experimental set-up of the IHBFBSR. This chapter contains detailed information on the input streams of the gasifier, gasifier dimensions and describes the measurement equipment used to produce experimental data. The experimental procedure is discussed and the results are shown.

Chapter 4 describes the design of the mathematical model for the IHBFBSR. First, various options for gasifier modelling are introduced. Mass and heat transfer in the gasifier will be discussed as well in order to account for mass and/or heat transfer limitations in the model. The third section introduces the design choices for the model of the IHBFBSR. Important design aspects are the pyrolysis process model, modelling of tar production and destruction, and the choice for both an equilibrium and kinetic model.

Chapter 5 validates the kinetic model with experimental data from the IHBFBSR. Now that the model is validated, it is possible to use the model to reflect on the performance of the IHBFBSR and optimize its performance. The second section reflects on the possible causes of the error between experimental data and the model. The third section gives a sensitivity analysis with as variables: equivalent ratio [ER], reactor temperature and bed material size. The model is used in order to reflect on the key performance indicators [KPIs] as introduced in section 1.3. In addition, the model is used to discuss the performance of the reactor from an energy perspective. An energy balance is made over the model components and burner efficiencies are stated. The results are analyzed and they enable to reflect on the limits of both the IHBFBSR and the limits of its model.

The conclusions of this study can be found in chapter 6. This chapter reflects on the methodology of this study and proposes subjects for further development.

2

Literature study

2.1. Biomass Classification and Properties

Biomass is organic matter that originates from plants or animals which can be used as chemical energy carrier for fuels or for the production of chemical feed stock. Also, biomass includes gasses and liquids recovered from the decomposition of non-fossilized and biodegradable organic materials[6]. Several methods exist in order to classify biomass and distinguish between different types of biomass[12]. The first classification method is based on the origin of biomass. The second method describes the main structural organic constituents. Thirdly, the proximate analysis classifies the biomass based on moisture, volatile matter, fixed carbon and ash content. Finally, the ultimate analysis describes the elemental biomass composition. Another identification method, which has not been used in this study, is taxonomy, describing the biological origin of the biomass. This chapter reflects on the four aforementioned classification methods and introduces the higher- and lower heating value as a benchmark to assesses the thermochemical performance of biomass as a fuel.

2.1.1. Origin of Biomass

For the origin of biomass, a distinction is made between five categories.

- **Forestry products, residues and wastes**
  Wood logs, and wood chips are considered primary forestry biomass. Wood residues and wastes from the wood industry are considered secondary forestry biomass. Tertiary forestry biomass is described as demolition wood from wood industry products.

- **Agricultural products, residues and wastes**
  Agricultural products, residues and wastes are also referred to as herbaceous species. The sugar-rich or edible parts of food crops are considered primary agricultural biomass. Plant residues such as nut shells and molasses are considered secondary agricultural biomass. Tertiary agricultural biomass includes manure from animals. Generally, agricultural biomass has a higher moisture content than forestry biomass and contains more nutrient components which will result in a higher ash content[62].

- **Industrial and Municipal Wastes**
  Manure and industrial organic waste can be found in this category. This type of biomass often has a high moisture content.

- **Aqueous Biomass**
  Biomass from algae and micro-algae such as see weeds. This category of biomass is particular interesting because it does not compete with the food industry for land use. Nevertheless, aqueous biomass has a high moisture content which is often a disadvantage in energy carrier cultivation.

- **Energy Crops**
  Fast growing, sugar or starch rich crops, such as sugar cane, straw and miscanthus, are cultivated for the energy industry. These plant species often have a high energy yield and a short cultivation period to maximize energy production.

2.1.2. Main Organic Constituents
Biomass from plants mainly consists of cellulose, hemi-cellulose and lignin[12].

Cellulose $(C_6H_{10}O_5)_n$ is a homopolysaccharide consisting of multiple glucose monosaccharides. Glucose is a C6-sugar which means that it contains six carbon atoms. It is the most common bio polymer. Most biomass contains 40-50% cellulose on a dry fuel basis[12]. Cellulose is completely insoluble in aqueous solutions[12]. The molecular structure of cellulose is visualized in figure 2.1.
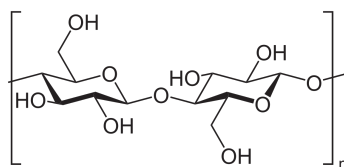
Figure 2.1: Molecular Structure of Cellulose [55].

Hemi-Cellulose is a heteropolysaccharide consisting of multiple C5 and C6 monosaccharides (pentosans and hexosans). Most biomass contains 25-35% hemi-cellulose on a dry fuel basis[12]. Hemi-cellulose can be found in the wall region of plant cells and function as the material that holds cellulose fibres together. Several different monosaccharide combinations of hemi-cellulose exist and can be classified by the name of the main monosaccharide in their structure[12]. The molecular structure of hemi-cellulose is visualized in figure 2.2.
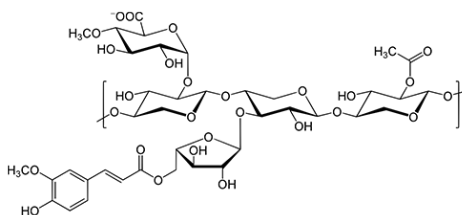
Figure 2.2: Molecular Structure of Hemi-cellulose [23].

Lignin is an amorphous polymer consisting of a heterogeneous three dimensional network of aromatic structures which can be found in the space between plant cells. Lignin provides coherence and toughness to a plant. Most biomass contains 20-30% lignin on a dry fuel basis. Lignin is relatively stable in thermal conversion and has a higher heating value than cellulose and hemi-cellulose[12]. The molecular structure of lignin is visualized in figure 2.3.
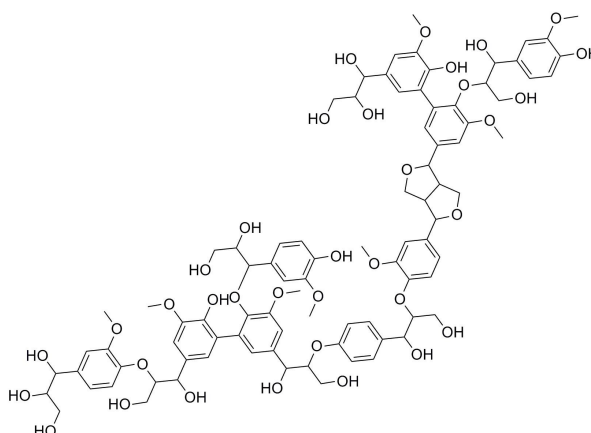
Figure 2.3: A Typical Molecular Structure of Lignin [24].

Starch is a stereo-isomer of C6 glucose and does not serve as a structural component of the plant. Starch serves as an easily accessible sugar source. The bonds between starch are weak and therefore starch is easily digestible by humans and animals. For this reason starch components are also called "free sugars"[12].

Other organic components, besides cellulose, hemi-cellulose and lignin, can be found in biomass from plants. Amongst others, these components are chitosan, chitin, oils, fats, proteins, alkaloids, antioxidants, aromatic amines, chlorophyll, hormones, vitamins, natural dyes, and terpenes[12].

Inorganic components can be found in small quantities in plant biomass. These components are essential for the plant growth and are also referred to as plant nutrients. The most abundant inorganic components in plants are nitrogen, potassium, calcium, magnesium, phosphorus and sulphur. These inorganic components remain as the ash when biomass is combusted[12].

2.1.3. Proximate Analysis

The proximate analysis is used to determine the quantities of the component classes as listed below[12]:

- Moisture content

- Volatile matter (VM) content

- Fixed carbon (FC) content

- Ash content

The biomass composition as received, (ar), is dried for 24 hours at 105 °C in the first step of the proximate analysis. The weight difference between the biomass (ar) and the biomass on a dry basis (db) quantifies the moisture content as described by equation 2.1.

$$Y_{\text{moist}}^{\text{ar}} = \frac{m_{\text{bio}}^{\text{ar}} - m_{\text{bio}}^{\text{db}}}{m_{\text{bio}}^{\text{ar}}} \qquad (2.1)$$

The volatile matter content is determined by heating a sample of biomass (db) to 550 °C in an inert environment. The mass difference quantifies the moisture content as described by equation 2.2[12].

$$Y_{\text{VM}}^{\text{db}} = \frac{\delta m_{\text{devolatilization}}}{m_{\text{bio}}^{\text{db}}} \qquad (2.2)$$

The remainder of the biomass, consisting of fixed carbon and ash will be combusted. The weight of the remaining ash is used in equation 2.3 and 2.4 to determine the ash content and fixed carbon content[12]. A detailed explanation of the basis of expression (a.r., d.b. and d.a.f.) can be found in appendix A.

$$Y_{\text{Ash}}^{\text{db}} = \frac{m_{\text{ash}}}{m_{\text{bio}}^{\text{db}}} \qquad (2.3)$$

$$Y_{\text{FC}}^{\text{db}} = 1 - Y_{\text{Ash}}^{\text{db}} - Y_{\text{VM}}^{\text{db}} \qquad (2.4)$$

From the perspective of considering biomass as a fuel, the combustible volatile matter and fixed carbon contribute positively to the heating value. The moisture content and non-combustible volatile matter contribute negatively to the heating value as it takes energy to vaporize or heat these components. The ash consists of nutrient carrying molecules that can negatively influence the heating value by the presence of oxygen in these molecules. Furthermore, some of the nutrients in the ash can cause damage to the reactor by melting and agglomerating in the rector system.

Typical values for the proximate analysis of different biomasses are shown in table 2.1. In order to compare biomass with charcoal, a typical proximate analysis of charcoal has been added as well. It can be observed that the fixed carbon content of coal is much higher than that of biomass. The volatile matter content however is much higher for biomasses.

Table 2.1: Typical Proximate Composition of Several Different Biomass Types and Coal[6],[43],[33].

Fuel	FC (%)	VM (%)	ASH (%)	Source
Redwood	18.5	80.1	1.4	[6]
Rice Straw	16.7	65.5	17.9	[6]
Sewage sludge	16.6	83.4	42.1	[43]
PRB Coal	74.0	4.2	21.8	[33]

2.1.4. Ultimate Analysis

The ultimate analysis gives the elemental composition of the biomass fuel. A sample of biomass is combusted and from the components present in the flue gas the elemental composition can be determined. Elements considered are C,H,O,N,S,Cl and ash for biomass on a dry basis. Typical values for the ultimate analysis of different biomasses are shown in table 2.2. In order to compare biomass with charcoal, a typical ultimate analysis of charcoal has been added as well.

Most woody biomasses have a relatively high carbon and oxygen content of approximately 50% and 40-45% respectively. The lower hydrogen content is often equal to approximately 6%. For wood pellets that consist out of clean wood, the ash, nitrogen and sulfur content are very low. It can be observed from the table that the ash content is significantly higher for straw and coal and extremely high for sewage sludge.

Table 2.2: Typical Elemental Composition of Several Different Biomass Types and Coal on a dry basis[d.b.][6].

Fuel	C (%)	H (%)	O (%)	N (%)	S (%)	ASH (%)
Redwood	53.5	5.9	40.3	0.1	0	0.2
Rice Straw	39.2	5.1	35.8	0.6	0.1	19.2
Sewage sludge	29.2	3.8	19.9	4.1	0.7	42.1
PRB Coal	75	1.6	0.9	0.7	0.2	21.8

2.1.5. Performance of Biomass as a Fuel

The performance of chemical energy carriers can be assessed by comparing the quantities of their heating values. The heating value, or calorific value, describes the energy that is being released upon combustion of a specific amount of a fuel. The amount can either be expressed in mass, volume or mole. A distinction can be made between HHV and lower heating value [LHV] where the LHV does not take into account the energy that is needed for the evaporation of the water that is created during combustion. The LHV and HHV can be calculated interchangeably by with use of the hydrogen content as described by equation 2.5[12].

$$LHV^{\mathrm{db}} = HHV^{\mathrm{db}} - 2.4 \cdot 8.9 \cdot Y_{\mathrm{H}}^{\mathrm{db}} \tag{2.5}$$

Where 2.4 MJ$\cdot$kg^{-1} refers to the latent heat of vaporization of water and 8.9 kg water$\cdot$ kg^{-1} H equals the stoichiometric ratio between water produced upon combustion and hydrogen bound in the fuel structure. Y_{H} is the mass fraction of hydrogen in the fuel which commonly is around 6 wt % for biomass[12].

Besides an experimental determination of the higher heating value, the HVV can also be determined from the elemental composition by equation 2.5 [12]. The HHV considers the moisture and pyrolytic water to be present in the liquid phase in contrast to the LHV which considers the moisture and pyrolitic water to be present in the vapour phase. In equation 2.6 the HHV is expressed for dry basis biomass.

$$HHV^{\mathrm{db}} = 34.91 Y_{\mathrm{C}} + 117.83 Y_{\mathrm{H}} + 10.05 Y_{\mathrm{S}} - 1.51 Y_{\mathrm{N}} - 10.34 Y_{\mathrm{O}} - 2.11 Y_{\mathrm{ash}} \tag{2.6}$$

In order to compare the performance of biomass as an energy source, table 2.3 lists the heating values of biomass and most conventional chemical energy sources. It can be observed that all conventional fossil fuels and hydrogen have a higher gravimetric HHV compared to biomass. Hydrogen even has the highest gravimetric HHV which makes it very interesting as a possible sustainable fuel. The disadvantage of gaseous hydrogen is that it has a low volumetric HHV, the lowest of the fuels in table 2.3 to be precise.

Table 2.3: HHV for Several Conventional Energy Carriers. Values with Respect to Mass and Volume[64].

	HHV [MJ·kg^{-1}]	HHV [kJ·m^{-3}]
Biomass	16.2	20.25*
Gasoline	46.4	34200
Diesel	45.6	38600
Natural Gas	52.5	40.6
Coal	29.6	148*
Hydrogen	141.7	12.7

*calculated with an assumed bulk density of 200 kg·m^{-3} for charcoal and 800 kg·m^{-3} for biomass.

In order to transport and store hydrogen as a liquid of compressed gas, high pressures and low temperatures are required. When comparing the volumetric HHV of the fuels, it can be observed that the liquid fossil fuels are superior. It is easy to store and transport these energy carriers and for that reason, fossil fuels are still highly in demand.

The Van-Krevelen diagram in figure 2.4 shows a spread in the chemical composition and heating value of biomass and other fuels. The diagonal lines in the graph represent fuel compositions with the same value for HHV. As can be observed, a lower oxygen content contributes significantly to an increase in higher heating value. Biomass has a relatively high oxygen content when compared to lignite or coal.
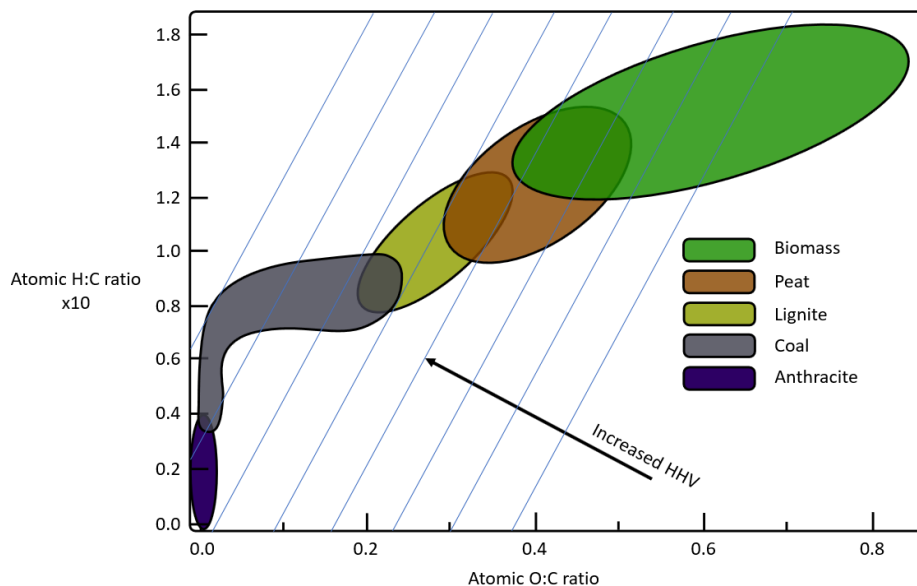
Figure 2.4: Van-Krevelen Diagram. Indicating Higher Heating Value by the Diagonal Lines as Function of Elemental Composition for Biomass, Peat, Lignite, Coal and Anthracite[12].

Table 2.3 and figure 2.4 show that biomass has a relatively low gravimetric and volumetric HHV. In order to make biomass more efficient to handle during storage, transportation and energy conversion it is possible to process the biomass and increase its HHV. Section 2.2 will explain several biomass conversion routes aimed at increasing the HHV.

2.2. Biomass Processing

Several biomass conversion processes exist for the conversion of biomass directly into energy or a wide variety of chemical energy carriers. Figure 2.5 illustrates different pathways for biomass to be converted. The most suitable conversion method can be found depending on the composition of the biomass input and the desired products that result from the conversion. As mentioned in chapter 1, in The Netherlands, the majority of woody biomass is combusted directly for electricity and heat production[20]. Other conversion technologies can generally be divided in thermochemical and biochemical conversion processes.
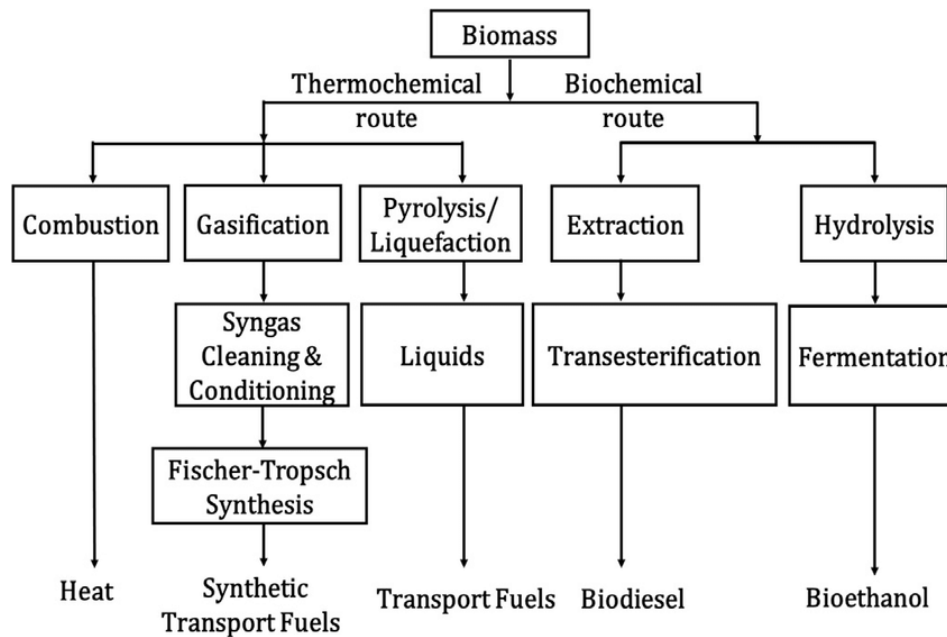
Figure 2.5: Processing Routes for Biomass Conversion[53].

Several process conditions for each of the conversion methods can be found in table 2.4.

Table 2.4: Comparison Between Several Biomass Conversion Routes Based on their Process Conditions[6].

Process	Temperature [C]	Pressure [MPa]	Catalyst	Drying
Liquifaction	250-300	5-20	Essential	Not required
Pyrolysis	380-530	0.1-0.5	Not Required	Necessary
Combustion	700-1400	>0.1	Not Required	Not Essential
Gasification	500-1300	>0.1	Not Essential	Necessary
Fermentation	30-50	0.1	Organic	Not required
Digestion	35-55	0.1	Not Required	Not required

In order to make a qualitative comparison, the performance of the processes have been rated for the categories: Energy Consumption, Economically Attractive, Process Duration and how established the method is in current industrial application. Table 2.5 gives the results. It can be observed that gasification is a fast and economically viable process. The process, however is highly energy intensive compared to other conversion methods. The biochemical processes proceed slower and in the case of digestion, it is not an economically feasible process for the production of chemical energy carriers.

Table 2.5: An Indication of the Advantages and Disadvantages of Several Biomass Conversion Routes[12][2].

Process	Energy Consumption	Economically Attractive	Process Duration	Established Energy Production Method
Gasification	-	+	+	+
Liquefaction	-	+-	+-	-
Digestion	+	-	-	-
Fermentation	+	+	-	+

2.3. Biomass Gasification Process

When biomass enters a gasifier, the matter is heated rapidly. Several process stages exist upon heating the biomass:

- Drying. During this process step, moisture leaves the biomass particle as steam

- Pyrolysis. Biomass thermally degrades into a solid, liquid and gaseous fraction. This process takes place in the absence of a reactant or with a limited supply of an oxidizer.

- Gasification. The pyrolysis products react with each other and with the gasification agent during this process step

- Gas Upgrading. The gasification products can be cleaned and upgraded in order to produce a highly selective gaseous product.

2.3.1. Biomass Pyrolysis

Pyrolysis (devolatilization) is a thermochemical decomposition of biomass into a range of useful products, either in the total absence of oxidizing agents or with limited supply that does not permit gasification to an acceptable extend. During Pyrolysis, large complex hydrocarbon molecules break down into smaller and simpler molecules of gas, liquid and char[6].

The gaseous fraction mainly consists out of CO, H_2, CO_2, CH_4 and a small amount of light hydrocarbons such as ethylene C_2H_4[12][6]. The liquid fraction is referred to as pyrolysis oil or bio-oil and contains the moisture, pyrolytic water and tars. Tars are hydrocarbon molecules consisting out of at least seven carbon atoms. Neeft et al[39] describes tars as all organic contaminants with a molecular weight higher than 78, which is the molecular weight of benzene[6]. The solid fraction that remains consists out of a small fraction of ash and char. For most studies char is modelled as pure carbon. In reality, a small fraction of oxygen and hydrogen are likely to be present in the char[6].

The first step in the pyrolysis process is the vaporization of the moisture, starting at 100°C. Increasing the temperature will initiate thermal degradation of the biomass. Its main compounds, cellulose, hemi-cellulose and lignin, will degrade over slightly different temperature ranges within 150°C to 500°C[6]. At a temperature of 500°C it is safe to estimate that all primary pyrolysis products have been formed. The primary products will mainly yield a carbon rich, solid product while the fraction of liquids and gasses is relatively low[66].

Secondary pyrolysis products are products that are formed from reactions between primary pyrolysis products. These products are formed at temperatures in a range of 300°C to 1000°C depending on the reaction mechanism[6]. Examples of these reactions are; tar cracking, oxidation, reforming, dehydration, condensation, polymerization and gasification. For this work, it is important to know that these reactions yield secondary pyrolysis products with either a higher liquid yield, or a higher gas yield. This is achieved by tar cracking into lighter tars, light hydrocarbons and permanent gasses. In addition, primary char will further react to permanent gas and secondary char.

2.3.2. Pyrolysis Parameters

The products that are being formed and their quantities are highly dependent on the process conditions. This section lists the most important parameters. These parameters will eventually play a significant role in pyrolysis modelling for the IHBFBSR.

Temperature

As stated in subsection 2.3.1, the pyrolysis temperature has a large influence on the product yield. For low temperatures a larger carbon rich solid fraction is formed while at higher temperatures the secondary pyrolysis reactions have a larger influence. In that case the product yields larger liquid or gas fractions[6]. The effect of the pyrolysis temperature is illustrated in figure 2.6.

Heating Rate and Residence Time

Pyrolysis can generally be divided into fast or slow pyrolysis depending on the average heating rate of the

biomass and the residence time. The heating rate is defined as the fraction of the final pyrolysis temperature T_{pyr} over the heating time $t_{heating}$. Equation 2.7 gives the relation[6].

$$R_{heating} = \frac{T_{pyr}}{t_{heating}} \qquad (2.7)$$

For slow pyrolysis, the heating time of the biomass is less than the characteristic pyrolysis reaction time. The converted primary products and formed secondary products remain present in the pyrolysis zone for several minutes. This process is mainly used for char production. In fast pyrolysis, the heating time is lower than the characteristic pyrolysis reaction time. The residence time is of the order of seconds to milliseconds. In that case, highly effective mass transport will shift the secondary reactions to producing more liquid and gaseous products. The effect of the pyrolysis heating rate is illustrated in figure 2.7[6].
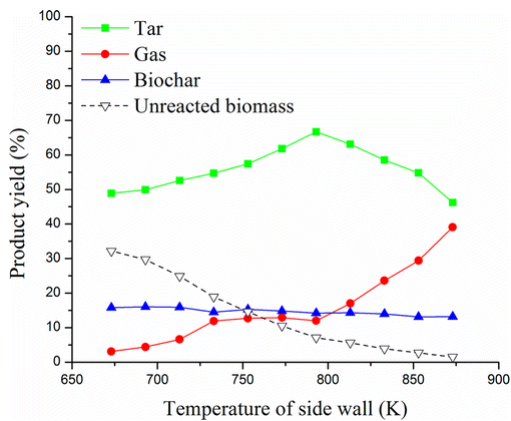
Figure 2.6: Gas-, Tar- and Gas Yield as Function of (Fast) Pyrolysis Temperature [66].
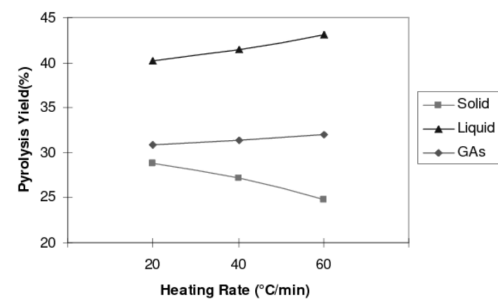
Figure 2.7: Gas-, Tar- and Gas Yield as Function of Heating rate[56].

Particle Size

The particle size and amount of biomass fuel that enters the pyrolysis zone affect the heat and mass transport to and from the particle. As the intra-particle temperature dictates the yields of locally produced products and reaction rates of the secondary reactions, it is obvious that the particle size has a large effect on the pyrolysis products. The effect of the biomass particle size is illustrated in figure 2.8 The amount of fuel is related to heat and mass transport between the bulk mixture of biomass particles and pyrolysis products in the inert gaseous environment. The effect of the biomass feed rate on the pyrolysis product yield is illustrated in figure 2.9.

Figure 2.8: Gas-, Tar- and Gas Yield as Function of Biomass Particle Size[66].

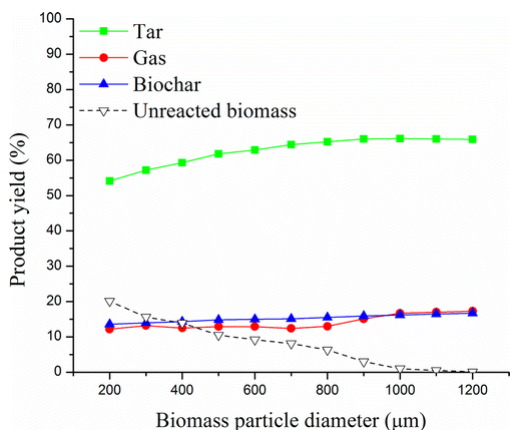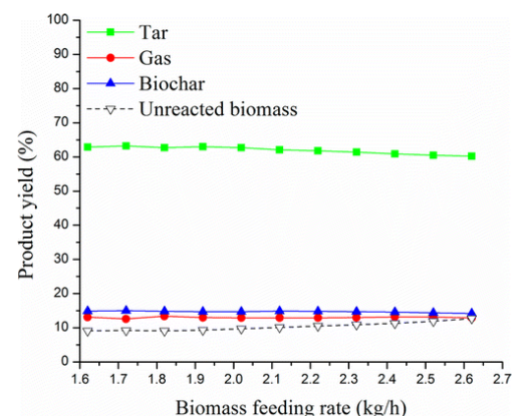Figure 2.9: Gas-, Tar- and Gas Yield as Function of Biomass Feed Rate[66].

Biomass Type
Finally, the type of biomass also affects the product yields as the fraction of lignin, hemi-cellulose and cellulose will be different for each biomass type. This is also the case for biomasses with a different proximate and ultimate analysis. A wide range in other biomass specific parameters that affect mass transport, heat transport and reaction kinetics such as pore density, conductivity and cell structure make it difficult to create a model that will be compatible with multiple types of biomass.

2.3.3. Gasification of Pyrolysis Products
The pyrolysis products are now entering the gasification step of the process. In this step, pyrolysis products react with each other and with the gasifying agent. Gasifying agents that can be used are air, pure oxygen, carbon dioxide and steam. In the case of air, the presence of oxygen will partially combust a fraction of the biomass. This process will beneficially add heat to the gasification process. Note that not enough oxygen is present during gasification in order to fully combust the biomass. When steam is used as agent, the product gas will yield higher concentrations of hydrogen.

The gasification product is known as producer gas. Its main constituents are hydrogen, carbon monoxide, carbon dioxide, steam, nitrogen and methane. Other gaseous products that will be present in the producer gas are light hydrocarbons such as ethylene. Also, the non-reacted gasifying agent will leave the gasifier mixed with the producer gas. After a cleaning and upgrading step, producer gas can be conversed into syn-gas. Syn-gas is a mixture of carbon monoxide and hydrogen and can be used for product synthesis such as Fischer-Tropsch synthesis. Through bio refineries it is possible to produce various hydrocarbon products[12].

Typical gasification reactions have been summarized in table 2.6. When air is used as gasifying agent, partial oxidation reactions R3 to R9 take place. The moisture and pyrolitic water will participate in the reforming reactions R10 to R14. When steam is used as gasifying agent, these reforming reactions play a significantly larger role in the gasification process.

Table 2.6: Typical Reactions Occurring during Gasification

Reaction Nr	Reaction Name	Reaction Equation	Source
R1	Boudouard	$C + CO_2 \longrightarrow 2CO$	[33]
R2	Water Gas Shift	$CO + H_2O \longrightarrow CO_2 + H_2$	[36],[43]
Oxidation			
R3	H_2 Oxidation	$\alpha C + O_2 \longrightarrow 2(\alpha-1)CO + (2-\alpha)CO_2$	[36],[43]
R4	H_2 Oxidation	$H_2 + 0.5O_2 \longrightarrow H_2O$	[18],[36]
R5	CO Oxidation	$CO + 0.5O_2 \longrightarrow CO_2$	[18]
R6	CH_4 Oxidation	$CH_4 + 0.5O_2 \longrightarrow CO + 2H_2$	[18]
R7	C_6H_6 Oxidation	$C_6H_6 + 3O_2 \longrightarrow 6CO + 3H_2$	[36]
R8	C_7H_8 Oxidation	$C_7H_8 + 3.5O_2 \longrightarrow 7CO + 4H_2$	[54]
R9	$C_{10}H_8$ Oxidation	$C_{10}H_8 + 7O_2 \longrightarrow 10CO + 4H_2O$	[18]
Reforming			
R10	Water Gas	$C + 1.2H_2O \longrightarrow 0.8CO + 0.2CO_2 + 1.2H_2$	[36],[43]
R11	CH_4 Reforming	$CH_4 + H_2O \longleftrightarrow CO + 3H_2$	[43]
R12	C_6H_6 Reforming	$C_6H_6 + 2H_2O \longrightarrow 1.5C + 2.5CH_4 + 2CO$	[54]
R13	Tar Reforming	$C_nH_x + nH_2O \longrightarrow (n+x/2)H_2 + nCO$	[6]

The reaction rates of the heterogeneous char reactions are mainly dependent on the reactivity of the char and gasifying medium. Oxygen is the most reactive agent. The rate of char-steam reactions is in the order of three to five orders lower with respect to the char-oxygen reaction. The Boudouard reaction is six to seven orders slower. Char hydrogen reactions are known for having the lowest reaction rate of these examples[6].

2.3.4. Gasification Parameters

One of the most important process parameters in gasification is the ratio between the biomass feed and the gasifying agent. In the case of air or pure oxygen as medium, this ratio is indicated as the equivalent ratio λ. In the case of steam gasification, the ratio is indicated as the steam to biomass [SB] ratio. Other important parameters that influence the gasification product composition are temperature, residence time, presence of catalysts, fluidization regime, bed material and char particle size.

Equivalent Ratio

The equivalent ratio or lambda value of a gasification process indicates the ratio between the supplied air to fuel ratio and the stoichimetric air to fuel ratio. The parameter can be calculated by equation 2.8[12]. The expressions in equation 2.8 are on a d.a.f. basis.

$$\lambda = \frac{\text{supplied O}_2 \text{ / fuel ratio (daf)}}{\text{stoichiometric O}_2 \text{ / fuel ratio (daf)}} \tag{2.8}$$

The value of the equivalent ratio indicates if reactions take place at a combustion, gasification or pyrolysis process. The corresponding values can be found in table 2.7. In the case of pyrolysis, no oxygen is present. In the case of gasification, sufficient oxygen is present in order to allow partial oxidation. The amount of oxygen is however lower than the stoichiometric oxygen to fuel ratio which is needed for combustion. Typical values for λ applied on biomass gasification range between 0.1 and 0.4[6].

Table 2.7: Processes for different lambda values

$\lambda[-]$	Process
$\lambda > 1$	Combustion
$0 < \lambda < 1$	Gasification
$\lambda = 0$	Pyrolysis

Figure 2.10 illustrates the effect of the equivalent ratio on the gasification products. In this example, gasification takes place at $T = 850°C$ and $P = 2\,\text{MPa}$. It can be observed that an equivalent ratio of 1 yields high concentrations of H_2O and CO_2 which are general combustion products. When the equivalent ratio is decreased, the yield of H_2O and CO_2 also decrease while the yield of H_2 and CO increase. At a certain point. Not enough oxygen is present in order to convert all char into gaseous products. This is called the carbon limit. For an equivalent ratio below the carbon limit, the concentration of CO remains more or less constant and the amount of solid carbon increases.
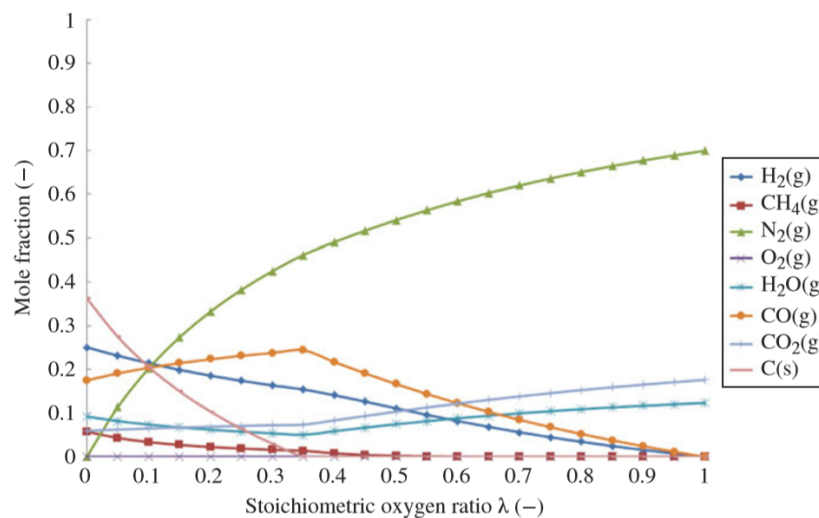

Figure 2.10: Effect of the Equivalent Ratio on the Gasification Products from Experimental Data at $T = 850°C$ and $P = 2\,\text{MPa}$[12].

Steam to Biomass Ratio

When steam is used as gasification agent, the stream-to-biomass [SB] ratio plays an important role in determining the final gas composition. The formula of SB can be found in equation 2.9 and 2.10[12].

$$SB = \frac{\dot{m}_{\text{steam}}}{\dot{m}_{\text{Biomass}}} \tag{2.9}$$

$$SB^* = \frac{\dot{m}_{\text{steam}} + \dot{m}_{\text{fuel moisture}}}{\dot{m}_{\text{Biomass}}} \tag{2.10}$$

Where, $\dot{m}$ is the mass flow of the component in $[\text{kg} \cdot \text{h}^{-1}]$.

2.4. Biomass Gasification Technologies

Gasification is a multi-phase process including a reacting gas and solid phase. Multiple reactor types qualify for these heterogeneous gasification reactions[12][6]. The three considered technologies are:

- Fixed Bed and Moving Bed Gasifiers

- Fluidized bed Gasifiers

- Entrained Flow Gasifiers

For each reactor type the production capacities are different. Their capacity is expressed in the amount of thermal input that is required by the reactor. An overview of the production capacities for several types of reactors is visualized in figure 2.11. Fixed and moving bed reactors are used for small-scale gasification between 10 kW and 1MW. Fluidized bed gasifiers are a large scale gasification technology ranging from 1MW to 100 MW. Entrained flow [EF] is applied at even a larger capacity between 50MW and 1000MW.[6]
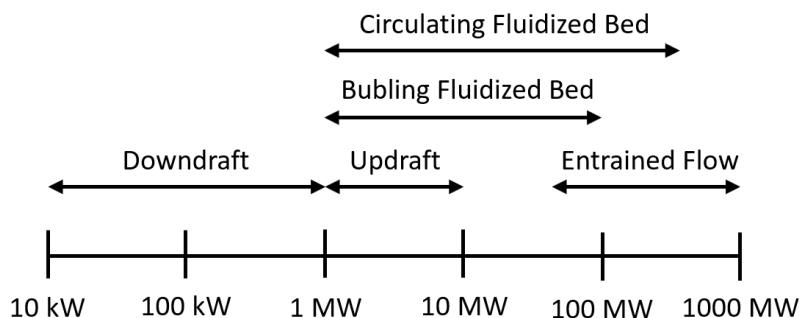
Figure 2.11: Conventional Biomass Gasification Technologies and their Corresponding Production Scale[6].

2.4.1. Fixed and Moving Bed Gasifiers

Fixed bed gasifiers operate on small scale ranging from 10 kW to 1 MW. One of their main advantages is that they can be build relatively inexpensively. For this reason many small scale gasifiers are being used world wide.[6]. Three basic configuration types exist:

- Updraft

- Downdraft

- Cross-draft

A visualization of the three configurations can be found in figure 2.12. For these examples, an air-blown gasifier has been used.
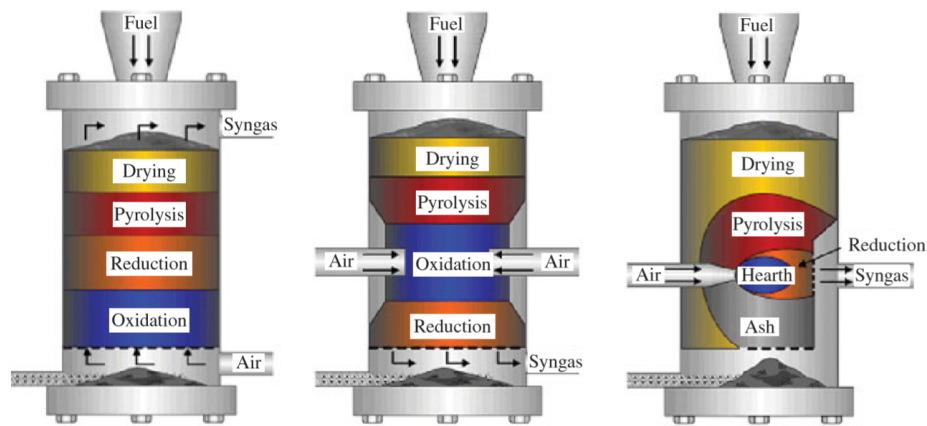
Figure 2.12: Updraft(left), Downdraft(mid) and Cross-draft(right) Configurations of Fixed/Moving Bed Gasifiers[12].

Fixed bed gasifiers host multiple zones in which the concentration of species is significantly different[12]. The drying and pyrolysis zone hosts a relative high amount of fuel and less gasification agent. The oxidation zone is oxygen rich and its location is different for each configuration. The reduction zone is an oxygen poor environment where much gasification agent an pyrolysis products are present. The heat from combustion in the oxidation zone facilitates the temperatures for drying, pyrolysis and gasification reactions.

2.4.2. Fluidization in Fluidized Bed Gasifiers

Fluidized Bed [FB] Gasifiers are commonly used for the large scale gasification of biomass. An inert or catalytic bed material consisting out of small solid particles is used in order to facilitate a well mixed environment for heterogeneous reactions. The turbulent flow of the gas phase and dispersed solids in the bedzone is the driver for efficient heat and mass transfer. Operating temperatures vary between 700 and 900 °C and operating pressures between 0 and 7.0 MPa[12]. Three main configurations exist for fluidized bed reactors[6]:

- Bubbling Fluidized Bed

- Circulating Fluidized Bed

- Twin Bed

Most commonly used are bubbling and circulating fluidized bed gasifiers[6]. In a FB gasifier, a gaseous agent is introduced at the bottom of the bedzone distributed evenly by a distributor plate. The gas phase exerts a drag force on the bed material. The gas velocity determines the fluidization behaviour of the bed. An overview of the fluidization regimes is visualized in figure 2.13.

For low gas velocities this drag force is less than the gravitational force acting on the bed. In that case, fluidization is not reached and the bed is referred to as packed bed or fixed bed. The volume of the gas phase in the bedzone equals the voidage of the bed material at rest.

When the gas velocity is increased in order for the drag force to be equals to the gravitational force on the bed, minimum fluidization is reached. The bed has expanded increasing the volume of the gas phase in the bedzone. Further increasing the gas velocity will introduce gaseous bubbles in the bedzone. The size of the bubbles increases for increasing gas velocity. At a certain stage, the bubbles will become of the same order of size as the diameter of the reactor. This characterizes the transition between the bubbling and slugging regime.

Increasing the gas velocity even further will result in a turbulent regime. Here, the drag force on the bed material is significantly larger than the gravitational force. The next regime is the fast fluidization regime. The velocity is high enough for the formation of gaseous bypass channels in which no bed material is present. When increasing the velocity to reach the last regime one speaks of pneumatic transport of the bed material.
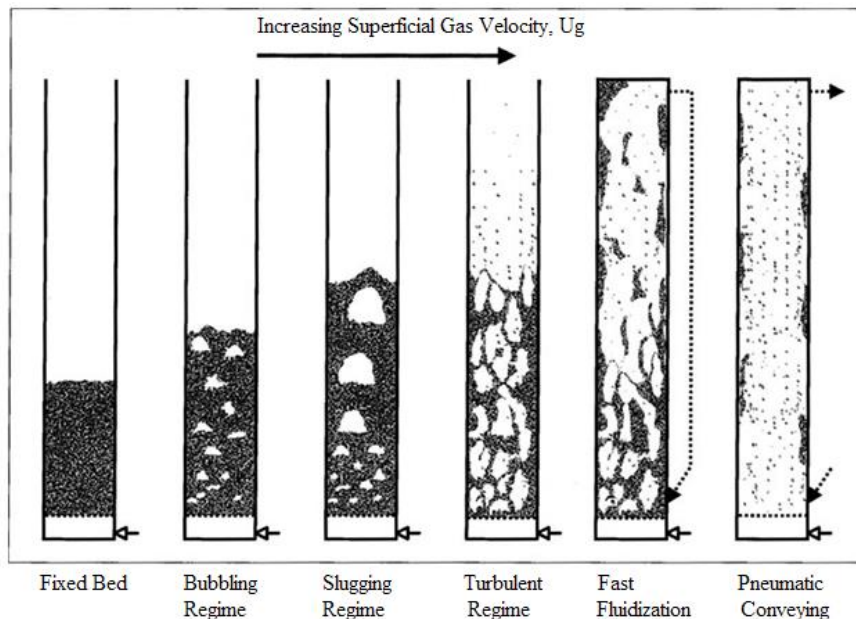
Figure 2.13: Fluidization Regimes for Bubbling Fluidized Bed Reactors[29].

Particle size and density of the bed material affect minimum fluidization and fluidization regimes strongly. Their relation can be found on the Geldart chart shown in figure 2.14. Four Geldart types, A,B,C and D are mentioned by Kunii and Levenspiel [29] in order to describe the effect of particle size and density on the fluidization behaviour.

- **Geldart A** particles is an aeratable bed material characterized by small particle sizes and/or low particle density. The bed expands considerably before fluidization is reached. Gross circulation of solids are occurring for even low amounts of bubbles.

- **Geldart B** particles are sand-like materials with either a high density and small particle size or large particle size and low density, including moderate compromises. The size of gas bubbles increases more or less linearly as function of height above the distributor plate. Geldart B particles are favourable for BFB reactors.

- **Geldart C** particles are cohesive particles with both a low density and small particle size. Fluidization is extremely difficult for this type of particles. Examples of Geldart C particles are wheat flour or starch.

- **Geldart D** particles are spoutable particles with both a high density and large particle size. Deep beds of Geldart D particles are difficult to fluidize. They give rise to large bubbles and channeling.

2.4.3. Bubbling Fluidized Bed Gasifiers

Figure 2.15 is a visualization of a typical bubbling fluidized bed reactor [BFB] reactor. In a BFB reactor, a gaseous agent is introduced at the bottom of the reactor and distributed by a distributor plate. The bed, when fluidized will facilitate effective heat and mass transfer throughout the bedzone. The biomass is introduced in the BFB reactor just above the distributor plate. Particle sizes of the biomass are typically lower than 10 mm [6]. The products leave the top of the reactor. Generally, some air is introduced for the partial oxidation of mainly biomass and char in order to supply heat to the reduction reactions. The flue gasses will leave the BFB at the top mixed with the product gas. The BFB can operate at atmospheric and elevated pressure. Char particles, ash and bed material can occasionally leave the reactor at the top as well. For this reason, a dust separator or cyclone is placed directly after the gas take-off.
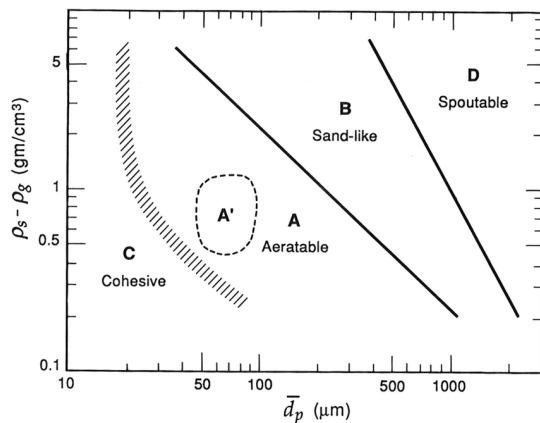
Figure 2.14: Geldart Chart Describing the Physical Properties of Several Bed Material Types Depending on their Size and Density[29].
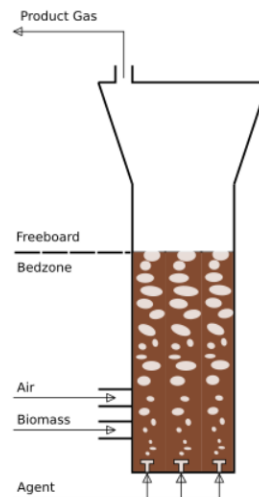
Figure 2.15: Visualization of the Working Principle of a Bubbling Fluidized Bed Reactor [BFB]

2.4.4. Circulating Fluidized Bed Gasifiers

Figure 2.16 (left) is a visualization of a typical circulating fluidized bed [CFB] reactor. A CFB is not very different from a BFB with solid recycle except for a its significantly different fluid dynamics behaviour. The fluidization velocity for CFB is higher (3.5-5.5 m/s) than that in BFB reactors (0.5-1.0 m/s)[12]. A CFB reactor consists of a tall riser in which biomass and the gasification agent are introduced. Both gas and a significant amount of solids leave the riser and are separated by a cyclone. The solids are reintroduced in the riser while the product gas leaves the system for further upgrading. Many commercial gasifiers of this type have been installed in various countries[6].

2.4.5. Twin Bed Gasifiers

Figure 2.16 (right) is a visualization of a typical twin bed [TB] reactor. A TB gasifier is an interesting example of an allothermal gasification process. For twin beds, the combustor and gasifier are separated volumes. Steam and biomass enter the gasifier. The clean product gas leaves at the top while solids leave at the bottom, but above the distributor plate. This solid fraction is a mix of bed material, unreacted biomass, char and ash. The solid fraction enters at the bottom of the combustor and char is combusted with air. Flue gasses leave at the top and the solid fraction is separated and fed back into the gasifier. The heat from the combustor can be used for the production of electricity and the heat supply to the gasification process[6].
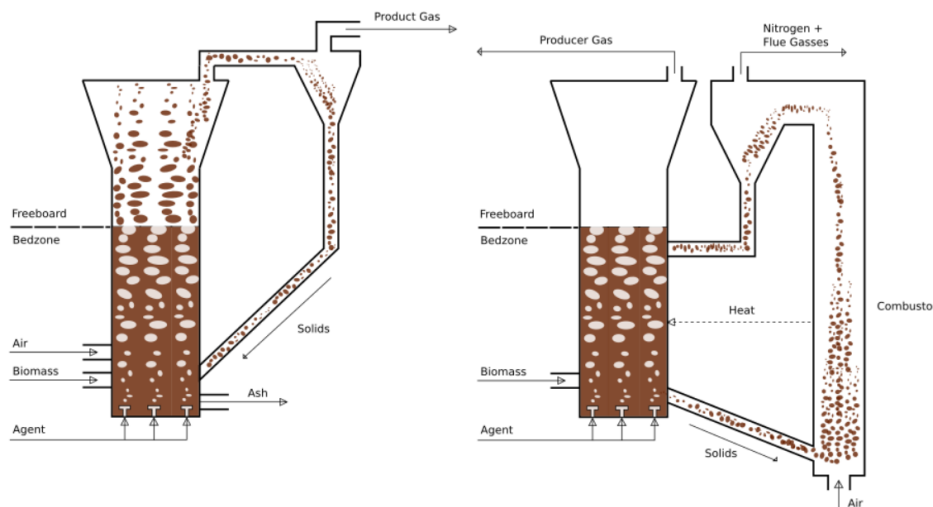
Figure 2.16: Visualization of the Working Principle of a Circulating Fluidized Bed Reactor[CFD](left) and Twin Bed Reactor [TB](right)

2.4.6. Entrained Flow Gasifiers

Entrained flow [EF] gasifiers are the most successful and widely used gasifier type for commercial gasification of coal, petroleum coke and refinery residues[6]. Operating temperatures in EF gasifiers vary between 1200 and 1500 °C. An advantage of these high temperatures is a low tar fraction present in the product. A disadvantage is that the reactor walls will have to withstand these temperatures for long periods of time during continuous operation. Often, the solid feed is introduced as powder or slurry. This means that biomass cannot be introduced as a pellet, but should be pre-treated to enter[12]. Either a mechanical sizing process grinds the biomass in order to enter as small particles, or a pyrolysis step is used in order to introduce a gaseous, oil and coke fraction to the EF gasifier. Examples of large scale EF gasifiers are the Koppers-Totzek gasifier (atmospheric pressure) and later developed PRENFLO (Spain) and Shell Coal Gasification Process (SCGP, The Netherlands) operating at elevated pressure (3.0-4.0 MPa)[12].

The fuel is inserted in the EF reactor. A burner near the fuel inlet introduces a oxygen rich zone in which combustion of a fraction of the fuel will take place. Further along the fuel's path an oxygen-poor environment creates a gasification zone. A separation zone separates the solid residue from the gaseous products.

2.4.7. Comparison between Conventional Gasifiers

The previous subsections have introduced several technologies for biomass gasification. Table 2.8 provides a list of advantages and disadvantages for each technology. This research is based on a gasifier set-up with a bubbling fluidized bed reactor. As can be observed from table 2.8, there are many advantages for the application of BFB technology. The gasification capacity is between 1-100 MW which makes it attractive for small commercial application. BFB reactors are an established reliable technology. In addition, heat and mass transfer is very efficient for BFB resulting in a Carbon Conversion[12].

Table 2.8: Advantages and Disadvantages of Various Conventional Reactor Types for Biomass Gasification

Technology	Advantages	Disadvantages
Updraft	- High CGE[6] - Effective combustion heat utilization [6]	- High tar content in product [12] - Low capacity [12]
Downdraft	- Relatively low tar content in product. [12] - Reliable, proven concept [12]	- Low capacity [12]
Crossdraft	- Short startup and response time [6] - Quick respond to engine load changes [6]	- High temperature endurance [12] - Low tar conversion [12]
Bubbling FB	- Excellent mass and heat mixing [6] - Reliable, proven concept [12] - High carbon conversion [12]	- Risk of tar condensation [12] - Risk of bed material sintering [29]
Circulating FB	- Long gas residence time [6] - Medium-large capacity application [6] - High carbon conversion [12]	- Relatively high dust content in producer gas [12]
Twin Bed	- Low nitrogen dilution of producer gas [6]	- Less char production for biomass compared to coal. [6] - Non-reacting steam consumes much energy and dilutes the producer gas [6]
Entrained Flow	- Commercially used for large capacity [12] - Low cost [12]	- Biomass pre-treatment required [12] - Biomass ash melting in alkali environment [6]

2.5. Allothermal Gasification Technologies

As mentioned at the beginning of this chapter, a distinction can be made between autothermal and allothermal gasifiers. The IHBFBSR set-up at the TU Delft is a novel allothermal gasifier. Two radiant tube facilitates heat transfer from the combustion to the reaction chamber. Next to the IHBFBSR, multiple allothermal projects exist. Although they are all indirectly biomass gasifiers, these projects have some fundamental differences. The considered similar projects are:

- MILENA (NL)

- Heat Pipe Reformer [HPR] (GER)

- Fast Internally Circulating Fluidized Bed [FICFB] (A)

- SilvaGas (US)

This section will give a brief description of the working principles of these technologies. Subsection 2.5.5 will compare each of the allothermal gasifiers with each other and with the IHBFBSR project. An overview of process conditions, working principles, project development, advantages and disadvantages will be provided.

2.5.1. MILENA Allothermal Gasifier (NL)

Research institute ECN has recently fused with research institute TNO, both based in the Netherlands. ECN of TNO has started their research on gasification in 1987[34]. The first design of the MILENA indirectly heated gasifier has been made in 1999. MILENA works according to the outside to inside direction which refers to the direction of heat flow to the gasification process. Biomass enters from the bottom with steam as gasification agent. Char and unreacted biomass leave the riser and enter the combustion chamber. This chamber is present around the reactor volume of the reformer. In the combustion chamber, the solids are combusted in order to provide heat to the reformer section. Solids that are not fully combusted and heated bed material re-enter the steam reformer for a second run at the bottom. For this reason, MILENA works according to the circulating fluidized bed reactor type. The working principle has been visualized in figure 2.17.

Figure 2.17: Visualization of the Working Principle of MILENA, ECN (NL)

The temperature in the reformer section can vary between 650 and 950 degrees. Carbon conversion can be maximized to 100% and a cold gas efficiency of 80% (including tar removal and combustion) is reached[15][35]. The producer gas that leaves the reformer has a high tar content. The tar is separated from the producer gas according to the OLGA process. The tar is combusted in order to provide extra heat to the process and increase its overall efficiency[15].

ECN started with a 30 kW lab-scale plant. In 2008, a pilot plant of 800kW has been launched. The MILENA allothermal configuration has been used for a bio-methane production plant in Alkmaar (NL) and for a 1 MWe capacity gasifier in India[46].

2.5.2. Heat Pipe Reformer Allothermal Gasifier (GER)

The Heat Pipe Reformer [HPR] has been developed at the TU Münich in Germany, starting with two pilot plants of 100 kW each[27]. The HPR as a separate reformer and combustion chamber, just like MILENA. The main difference is that instead of heating the bed material in the combustion chamber, a mix of biomass and char is combusted and the combustion heat is transferred to the reformer section by heat pipes. Heat pipes are closed tubes filled with a small amount of liquid. They ensure a high heat transfer coefficient between the two reaction chambers. This reduces the required heat transfer area significantly. It also enables complete separation of the reforming and combustor sections. The fact that unconverted char from the reformer is used increases its carbon conversion[27]. A visual representation of the HPR is given in figure 2.18.
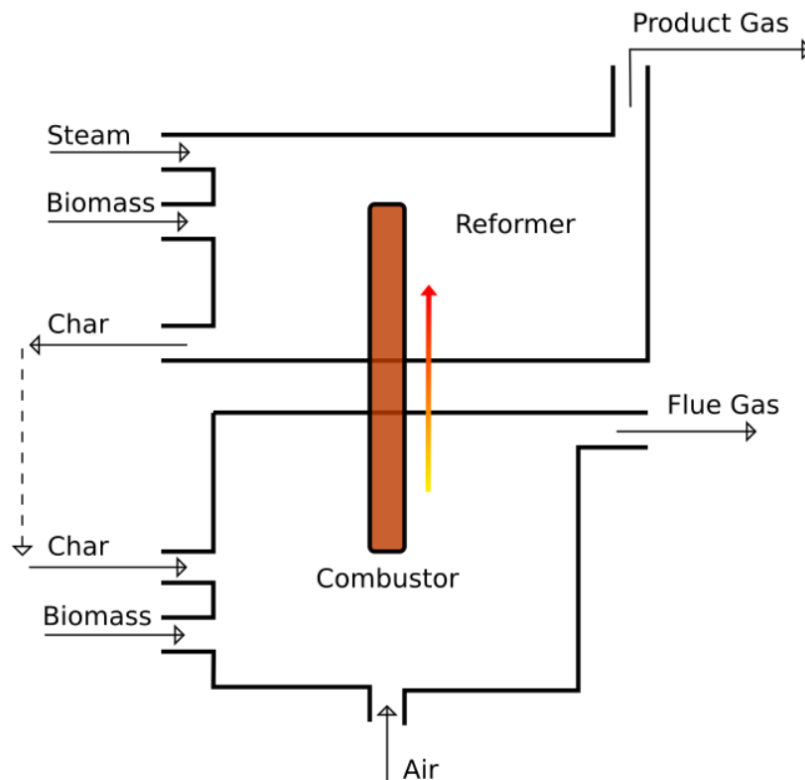
Figure 2.18: Visualization of the Working Principle of the Heat Pipe Reformer, TU Münich (GER)

The temperature in the reformer section can vary between 700 and 800 °C. Carbon conversion can be maximized to 85% and a cold gas efficiency of 75% is reached. The reformer operates at elevated pressure between 2 and 10 bar[27].

After the two 100 kW pilots, a 500 kW demo plant has been build in Pfaffenhofen, Germany. The Heat Pipe Reformer technology has been applied commercially on a 1MW scale in Grassau, Germany and on a 1MW scale in South Tyrol, Italy[27].

Besides the advantage of effective heat transfer from the combustor to the reformer there are a few drawbacks. Hydrogen, produced in the reformer, tends to diffuse into the heat pipe material. Another drawback is that the heat pipes are subject to erosion[27].

2.5.3. FICFB Allothermal Gasifier (A)

The FICFB is a Circulating Fluidized Bed reactor with a similar configuration compared to MILENA. Instead of an integrated system, the reformer and combustor have their own separated riser[48]. The reformer is fluidized by steam and the combustor with air. The bed material from the reformer is transfered to the combustor and is after being heated released back into the reformer. Just like the other allothermal technologies, flue gas and nitrogen from the combustor do not mix with the producer gas.

A visualization of the FICFB can be found in figure 2.19. It can be noticed that the reactor configuration is according to the twin bed technology, a special design of CFB technology.
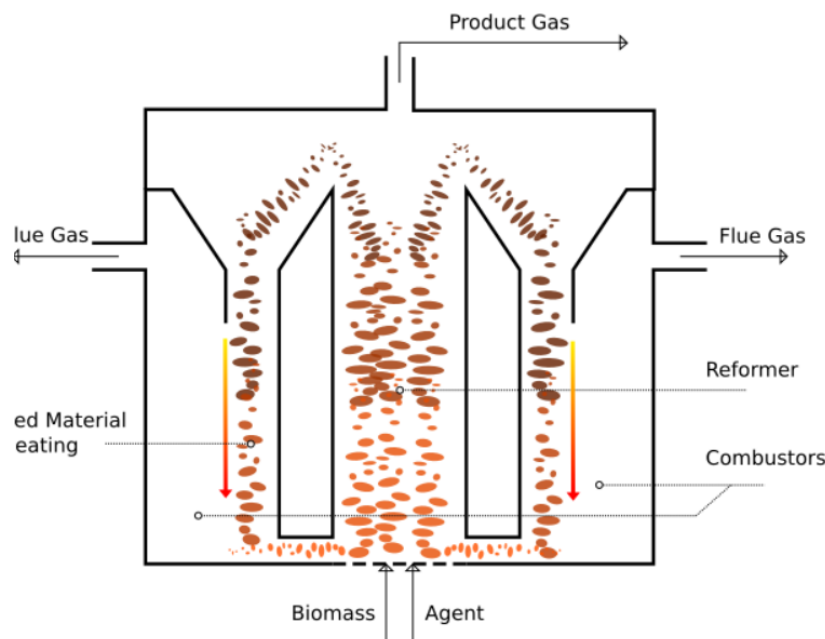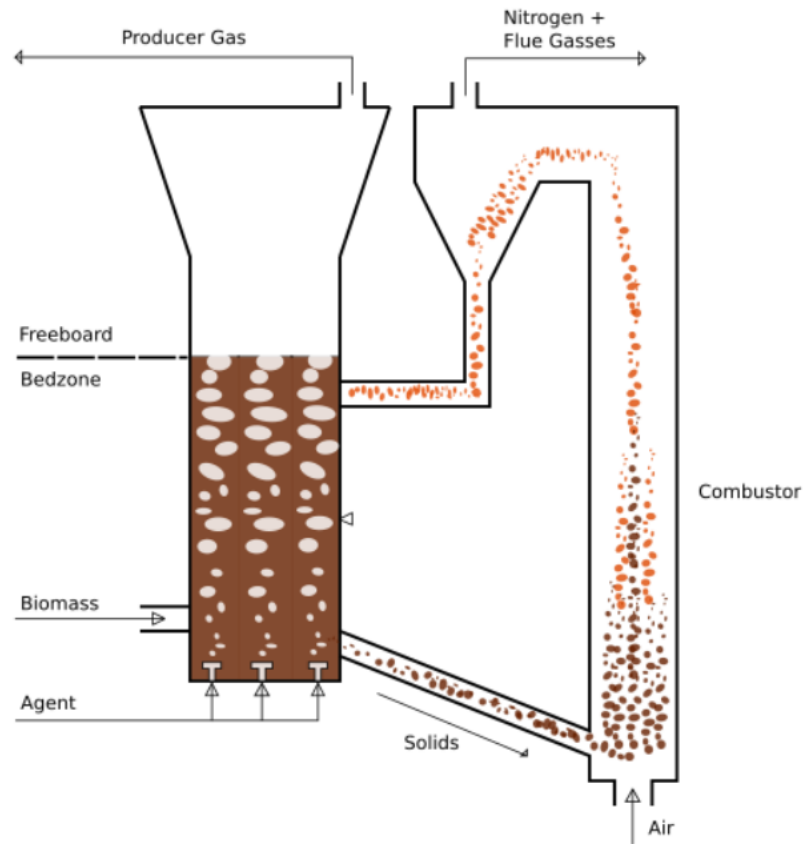

Figure 2.19: Visualization of the Working Principle of FICFB, Guessing, Austia

The temperature in the reformer section can vary between 700 and 900 °C. Carbon conversion can be maximized to 100% and a cold gas efficiency of 80% is reached. The reformer operates at atmospheric pressure[48].

After the 100 kW pilot at the TU Vienna, a 8 MW plant has been build in Guessing, Austria. The dual fluidized bed technology has been applied commercially on a 20MW scale for the production of bio-SNG in Göteborg, Sweden and a 30MW scale plant is planned to be designed in Vienna, Austria, for the production of electricity[48].

2.5.4. SilvaGas Allothermal Gasifier (US)

The Future Energy Resources Corporation (FERCO) has commissioned their large scale allothermal gasifier in Burlington, Vermont (US) to work continuously from April 2000[42]. The gasifier processes a biomass feed of 285 ton/day and it is connected to a McNeil power station which has a capacity to supply the electricity demand of 6000 households. The biomass gasification process was developed at the Battelle Memorial Institute in Columbus, Ohio (US). The SilvaGas is a twin bed process which can be compared with the MILENA and FICFB. A visualization of the gasifier can be found in figure 2.20. The main difference between SilvaGas and the other dual fluidized bed reactors is that only the bed material that exits the reformer at the top is separated from the product gas and transported to the combustor. The bed material is heated by the combustion of unreacted char and biomass. A cyclone separates the flue gasses from the heated bed material at the top of the combustor. The heated bed material is re-introduced in the reformer[42].
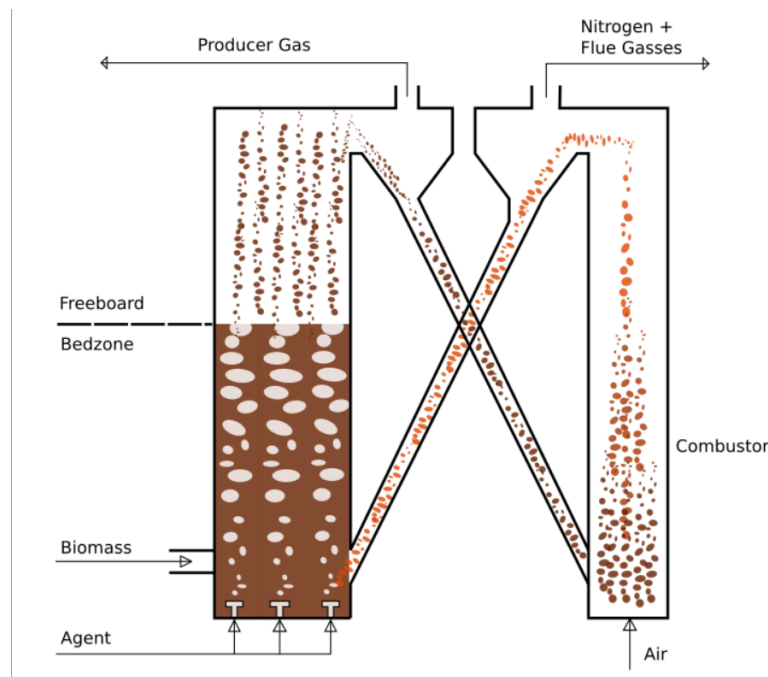
Figure 2.20: Visualization of the Working Principle of SilvaGas Burlington, Vermont (US)

2.5.5. Comparison between Allothermal Gasifiers

The past few subsections provided information of the working principles of several similar allothermal gasification technologies. This section will compare each of the allothermal gasifiers with each other and with the IHBFBSR project. An overview of process conditions, working principles, project development, advantages and disadvantages will be provided.

Table 2.9 gives the process conditions, working principles, project status and development and performance. The carbon conversion and cold gas efficiency are used in order to quantify their performances. It should be noticed that the conversion of fuel, other than biomass, for the heat generation needs to be taken into account for the calculation of the cold gas efficiency.

Table 2.10 summarizes the advantages and disadvantages of each technology. It can be observed that the FICFB and SilvaGas processes are the only processes with a continuous large scale operating plant. It must be noted that the FICFB's economic viability is dependent on local biomass supply and beneficially high feed-in tariffs for renewable energy as dictated by the Austrian government. The IHBFBSR and Heat Pipe Reformer are the only two technologies for which the combustion chamber and reformer are completely separated. This maximizes the quality of the producer gas.

The advantage that the producer gas is not diluted by the nitrogen from the combustion air applies to all allothermal technologies. The technologies discussed are economically more attractive than implementing char combustion with pure oxygen as alternative solution to producer gas dilution. For an assessment of which technology is superior, all technologies should be applied on industrial scale. Costs, efficiency, carbon conversion and cold gas efficiency will be the key performing indicators to evaluate the processes.

Table 2.9: Process Comparison for Multiple Allothermal gasification technologies similar to the IHBFBSR at the TU Delft

Process (cond.)	MILENA [34][15][35][46] (NL)	Heat Pipe Reformer [27] (GER)	FICFB (A) [48]	Ferco's SilvaGas (US)[42]	IHBFBSR (NL)
Reactor Type Gasifier	CFB	Pressurized FB	BFB	TB	BFB
Agent	Steam	Steam	Steam	Steam	Steam (+ Air)
Combustor	BFB	Combustion Chamber FB	CFB	CFB	Radient Tube Burner
Lab Scale	30 kW ECN (NL) 2004	Two Pilots 100 kW TU Münich (GER)	Pilot plant 100kW TU Vienna (A) 1991		50 kW TU Delft NL
Pilot Plant	800 kW ECN (NL) 2008	500 kW output Pfaffenhofen, (GER)	8MW fuel Guessing (A) 2001		
Demo Plant	4MW biomethane Alkmaar (NL)	1 MW Grassau (GER)	20MW BioSNG Goteborg, (S)		
Scale Up	1MWe India	1MW South Tyrol (IT)	30MWe Vienna (A) -Planned	200ton/day feed Vermont (US) -Designed	
Temperature	650-950	700-800	700-900	650-850	650-850
Pressure	atm	2-10 bar	atm	atm	atm
Carbon Conversion	100%	85%	100%	100%	76 %
CCE	80 %	75 %	80%	80 %	69.7% (from model)

Table 2.10: Advantages and Disadvantages of the Discussed Allothermal Biomass Gasification Projects.

Gasifier	Advantages	Disadvantages
MILENA	- OLGA Tar removal for tar combustion	- Substantial heat loss as a result of the "from outside to inside" heat transfer direction
Heat Pipe Reformer	- Low required heat transfer area	- Hydrogen diffusion from the reformer into the heat pipes - Erosion of the heat pipes
FICFB	- Low char content in fly ash. As a result, fly ash can be processed similarly to ash from the combustor - Proven concept. Continuous operation	- Economic viability is dependent on a local supply of biomass
SilvaGas	- Large production capacity - Economical viability is proven - Process stability	- No disadvantages or challenges mentioned in publications
IHBFBSR	- Effective temperature control by external heat source - Complete separation of combustion and reforming	- Bed removal limitation

3

Experimental Study

The Indirectly Heated Bubbling Fluidized Bed Steam Reformer [IHBFBSR] set-up at the TU Delft is a collaboration between the Dutch company Petrogas Gas-Systems and the TU Delft. The IHBFBSR is a 50 kW bubbling fluidized bed gasifier. The IHBFBSR is operated at atmospheric pressure: $p_r = 1$ [atm] and at a temperature of T_r[°C] which usually varies between 800 and 850 [°C]. This chapter describes the IHBFBSR set-up at the TU Delft in detail. Section 3.1 gives information on the biomasses used. Section 3.2 describes the properties of the bed materials used. Section 3.3 describes the five stages of the set-up. These five stages are the feeder section, the agent section, the reactor section, the burners and the gas analysis section.

3.1. Biomass Used for the IHBFBSR Set-Up

For the experiments, three different biomasses are used. The biomasses are characterized by their origin, a proximate and ultimate analysis and their heating value. For the initial tests two types of A-class wood will be used with a low moisture content and low ash content. The following set of experiments have been carried out with Miscanthus.

The A-class wood types, excellent red (RB) and premium green (GB), have been supplied by Labee group and arrive at the TU Delft in pellet shapes with a diameter of 6mm and a length between approximately 50mm and 250 mm. The wood originates from secondary and tertiary forestry biomass from the Netherlands. A-class refers to the low level of contaminants in the wood as well as to the removal of screws, nails or additional timber materials.

Miscanthus is a straw species that is cultivated specifically for the energy industry and is therefore classified as energy crop. It is attractive as an energy crop due to its fast growing property and its high energy density. This means that a relatively high energy content can be cultivated on a relatively small amount of land. The miscanthus used for the experiments originates from Munich, Germany. After harvest, the Miscanthus is dried and pelletized. The specifications of the A-class woods and Miscanthus are summarized in table 3.1.

The biomass arrives in a range of sizes. A large fraction of biomass pellets enters the gasifier as a pellet with a diameter of 6 mm and a variable length. Due to to transportation and handling, the pellets might brake, producing smaller pellets and individual biomass fibres and dust. In addition, the screw feeder of the IHBFBSR also damages the biomass pellets before they enter the reaction. The fraction and size of the individual fibres and dust has been determined by sieving the biomass after it has passed through the screw feeder of the IHBFBSR. The full report on determining the particle size distribution can be found in appendix B. The particle size distribution is visualized in figure 3.1. For each biomass type, three experiments have been conducted. Figure 3.2 gives the fraction of individual biomass particles compared to the amount of intact biomass pellets.

Table 3.1: Composition and Properties of RB and GB Wood Types and Miscanthus.

Component	RB	GB	Misc	Unit
Ultimate Analysis				
C	47.88 ± 0.08	48.41 ± 0.02	45.12 ± 0.02	wt % (daf)
H	6.44 ± 0.07	6.02 ± 0.02	6.19 ± 0.02	wt % (daf)
O	45.62 ± 0.02	45.26 ± 0.02	44.03 ± 0.02	wt % (daf)
N	0.06 ± 0.01	0.30 ± 0.03	0.49 ± 0.03	wt % (daf)
S	0.010 ± 0.001	0.010 ± 0.001	0.070 ± 0.001	wt % (daf)
Proximate Analysis				
Moisture	5.57 ± 0.11	5.08 ± 0.05	6.70 ± 0.05	wt % (ar)
VM	79.90 ± 0.81	75.22 ± 0.47	78.00 ± 0.47	wt % (ar)
FC	14.07	19.00	17.90	wt % (ar)
Ash	0.46 ± 0.12	0.69 ± 0.03	4.1 ± 0.03	wt % (ar)
Property	**RB**	**GB**	**Misc**	**Unit**
Bulk density	616 ± 7	625 ± 5	-	$[kg \cdot m^{-3}]$
HHV experimental	19.50 ± 0.02	18.89 ± 0.10	-	$[MJ \cdot kg^{-1}]$

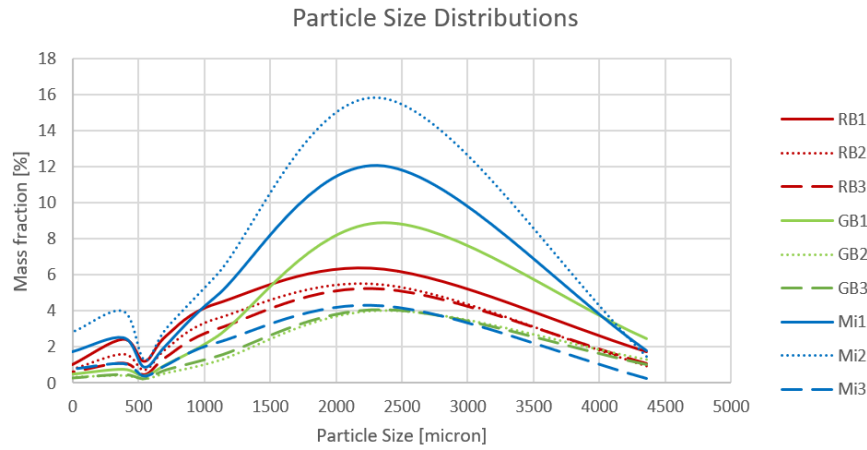
Figure 3.1: Visualization of the Particle Size Distribution of Three Separate Experiments for Each Biomass Type used in the IHBFBSR
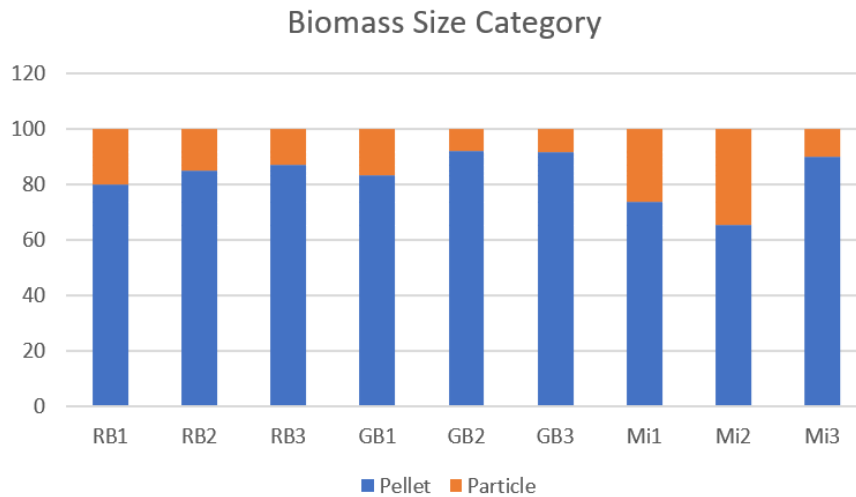

Figure 3.2: Fraction of Biomass Particles Compared to Intact Pellets for Each Biomass Type used in the IHBFBSR.

3.2. Bed Material

As bed material corundum is used which is an aluminum oxide with the formula: Al_2O_3. Corundum is a hard material with a classification of 9 on the Mohs scale of mineral hardness. The real density of the material is 3950 $[kg \cdot m^{-3}]$ and its bulk density is dependent on the voidage, and therefore, the bed material particle size. For the experiments with the IHBFBSR, three different bed sizes of corundum are used. Their specifications have been summarized in table 3.2

Table 3.2: Overview of Bed Material Size, Real Density and Bulk Density for Three Different Bed Material Sizes used at Experiments with the IHBFBSR

Bed Material	$d_p[\mu m]$	$\rho_{real}[kg \cdot m^{-3}]$	$\rho_{bulk}[kg \cdot m^{-3}]$
F046	500	3950	1636
F054	400	3950	1665
F060	300	3950	1871

In reality, the particle size of the bed material shows a range. For this study, it is assumed that the bed particles are spherical and that each particle has the same diameter.

3.3. Specifications of the Gasifier Set-up at TU Delft

The set-up can be divided into five sections: the feeding section, agent section, reactor section, burners and gas analysis section.

The feeding section consists of two bunkers, one for biomass pellets and one for the additives. The additives must be filled before each experiment. The biomass bunker can be filled during operation as it makes use of an intermediate bunker. After turning switch 1, the biomass proceeds to the intermediate bunker. When switch 1 is closed, the entrance to the intermediate bunker is resealed. With turning the second switch the biomass is slightly pressurized by nitrogen. This also makes sure to maintain inert feeding conditions. The mixture of biomass, nitrogen and additives is fed into the reactor by a volumetric feeder. In order to check the feeding section for blockages it must be assured that the fan of the volumetric feeder is turning and that the biomass is making a sound as it falls into the mixing section.

The heating section preheats the steam before it enters the gasifier. Steam is produced at 8 barg and 180[°C]. The steam is first depressurized to 5 barg by a pressure regulator. Next, it passes through a 6kW electrical heater where it is heated up to 650[°C] at 0.4 barg. If air, or a mixture of steam and air, is chosen as gasifying agent, the gasses are mixed before entering the pre-heater.

The reaction section receives the super heated steam in the windbox and passes it through a distributor plate. The distributor plate consists of 50 tuyeres with two orifices for each bubble cap. The bedzone consists of a reaction chamber with the c-100 burner in the middle as shown in figure 3.3. The agent is introduced at the bottom of the bedzone. The biomass is introduced slightly above the distributor plate. The range of steam to biomass ratios for which the IHBFBSR will be operated is $0.9 < SB < 1.5$. The equivalent ratio for which the IHBFBSR will be operated is $0.15 < \lambda < 0.4$. These equivalent ratios and steam to biomass ratios are achieved by setting the flow of the agent and vary the biomass feed flow. The reason for doing so is that similar fluidization properties can be expected for all values of λ and SB since the agent velocity is kept constant.

For any of the bed materials, 100 kg is inserted in the bedzone before the experiment. The height of the bedzone, without any agent passing through, depends on the particle size of the bed material. Six thermocouples are present in the bedzone spaced equally apart in the height direction of the reactor.

Above the bedzone, the freeboard can be found. The diameter of the freeboard increases at a certain point from 346 to 447 mm. Both the tip of the bottom radiant tube and the entire bottom radiant tube are present in the freeboard as indicated in figure 3.3. Four thermocouples are present in the freeboard spaced equally apart in the height direction of the reactor.

The diameter of both bedzone and freeboard have been summarized in table 3.3. The blueprints for the reactor with correct dimensions can be found in appendix C.
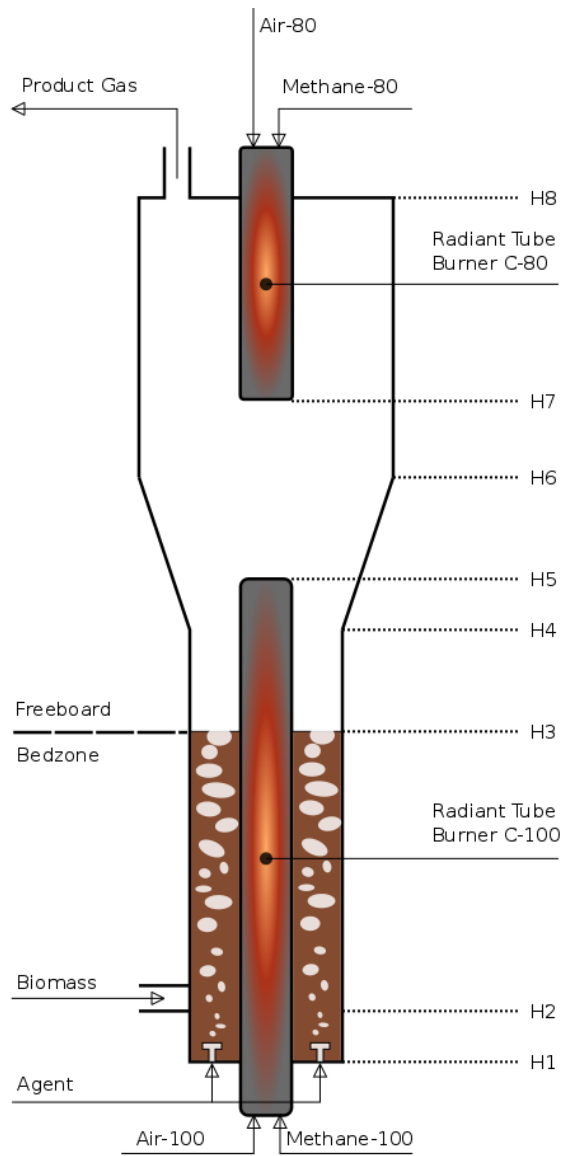
Figure 3.3: Geometry of the IHBFBSR (not at scale) with the Indication of Several Diameters as Function of Height.

Table 3.3: Diameter of the IHBFBSR as Function of Height as Indicated by Figure 3.3.

Reactor Section	Height Name	Height [m]	d_{out}[mm]	d_{burn}[mm]
Bedzone	H1	0.00	346	150
	H2	0.2	346	150
	H3	0.84-0.96	346	150
Freeboard	H4	1.068	346	150
	H5	1.206	382.2	150
	H5'	1.206	382.3	0
	H6	1.453	447	0
	H7	1.704	447	0
	H7'	1.704	447	100
	H8	2.454	447	100

Other dimensions of the reactor have been summarized in table 3.4.

Table 3.4: Reactor Dimensions of the IHBFBSR.

Parameter	Symbol	Value	Unit
Reactor wall material	-	AISI310S	-
Wall thickness	$D_i - d_i$	4.78	mm
Outside diameter windbox	D_{wb}	355.6	mm
Length windbox	L_{wb}	421	mm

Radiant Tube Burners use natural gas as a fuel. The air is pre-heated in counter current with the flue gasses that exit the burner to 60% of combustion temperature. The heat is spread evenly over the radiant tube surface by the circulating combustion gasses inside. The burners have been supplied by the company WS GmbH. They are self recuperative ceramic burners made of steel which work at a temperature of 1250[°C]. The burner placed in the bed zone (bottom) is a REKUMAT C100 and has a maximum capacity of $P_{rt,bottom}^{max}$ = 25 [kW]. The burner placed in the free board (top) is a REKUMAT C80 and has a maximum capacity of $P_{rt,top}^{max}$ = 15 [kW] Radiant tubes that have been considered are those of silicon carbonide (SiSiC). It is however mentioned that alkali components in the reformer can melt, agglomerate and therefore destroy them. Metal tubes, with a lower heat flux, are therefore preferred.

The nominal power from the c-80 and c-100 are 12 kW and 20 kW, respectively. The amount of methane that is needed for this power production has been calculated. The technical supplementary of both burners can be found in appendix D.

The Analysis Section is used in order to analyse the gasification products. The products that leave the gasifier pass through two cyclones. Their aim is to separate ash and unconverted char from the product gas stream. In order to analyse the product gas, a small sample is taken from the product gas pipe. The rest of the product gas that will not be analyzed is combusted by a flare and its combustion products are released in the atmosphere. The sample line passes through a heated filter first in order to separate small solids from the gas. The sample line from the product gas is separated into two parallel streams. One is used for the tar analysis and the other one is used for the gravimetric analysis.

The gaseous species that remain after the gravimetric analysis are also analysed. An overview of the analysis section is given in figure 3.4.
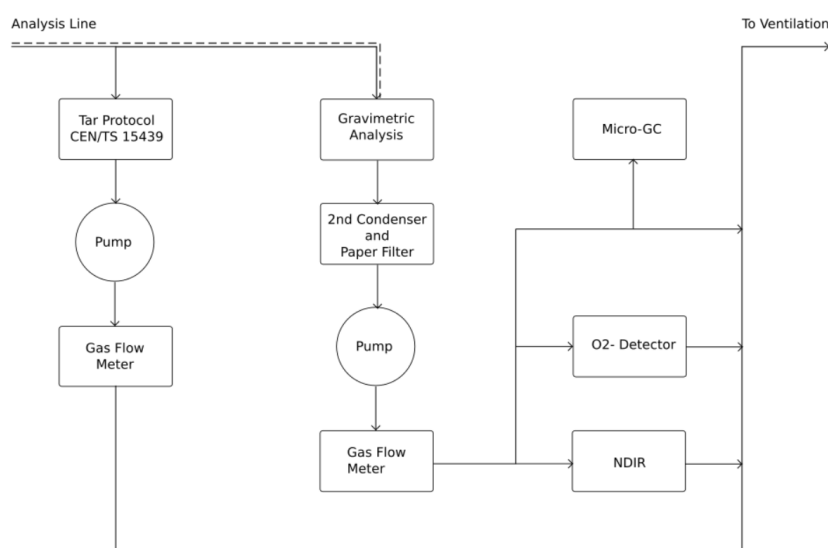

Figure 3.4: Visualization of the Gas Analysis Line Including the Tar Protocol and Gravimetric Analysis.

The tar analysis makes use of tar protocol CEN/TS 15439. The line that is used for the tar analysis is connected to a series of six bottles of which the first five contain 10 mL of iso-propanol each and the last one is empty and functions as a condenser. Bottle 2,4,5 and 6 have glass frits in the bottle that act as a filter. Bottles 1,2 and 3 are kept at a temperature between 35 and 40 °C while bottles 4,5 and 6 are kept at a temperature between -20 and -15 °C by an salt and ice bath. Tars and water in the product gas tend to dissolve in the iso-propanol. The residual gasses proceed to the ventilation. The extracted tars can be identified and quantified by high-performance liquid chromatography [HPLC].

The line that is used for the gravimetric analysis is traced at 400 °C in order to prevent the tars from condensing. Two empty bottles on a mass scale act as condenser in which water, and some tars, will condense. The weight scale has an accuracy of 0.001 g. The residual species after condensation will pass through a second condenser set-up. Two bottles, of which the first one is filled with silica gel, are aimed at removing all leftover tars and water that has been able to pass through the first condenser. Next, the species pass through a paper filter. It is now safe to assume that the residual species only consist out of permanent gasses. The permanent gasses pass through a pump and gas flow meter go towards several analysis equipment ventilation. A fraction passes through a gas flow meter and enters the NDIR. The NDIR measures the volume fraction of CO and CO_2 in the sample. The NDIR is from the brand Hartmann & Braun and type URAS10P. Another fraction of the permanent gasses passes through a gas flow meter and enter the O_2-detector. This equipment gives te volume fraction of oxygen in the sample. The O_2-detector is also of the brand Hartmann & Braun, type MAGNOS6G. The advantage of using the NDIR and O_2-detector is that this equipment give a continuous data output. The O_2-detector indicated if the gasifier is used for combustion of gasification and is used to identify the start time of an experiment. A third line goes to the ventilation. Before entering the ventilation, the μ-GC takes a sample of gas for analysis. The μ-GC is used in order to determine the permanent gas components with a specific interest in CO, CO_2, H_2 and CH_4. The amount of nitrogen which dilutes the product gas, is measured as well. This is particularly important when air is used as gasification agent. The μ-GC takes samples of the gas and outputs its results every five minutes. Therefore, there is a discrete data flow.

3.4. Experimental Results and Discussion

The experiments have only been carried out for air-gasification of green biomass [GB]. The intention had been to perform experiments with steam, but due to technical challenges, these experiments had not been possible during this research. The mass flow of air is kept constant at $\dot{m}_{air} = 19 \text{kg} \cdot \text{hr}^{-1}$. The temperature of the bedzone is kept constant at $T_{bedzone} = 840°C$. The measurements only include the molar fractions of CO, CO_2, H_2 and CH_4 in the product gas. The tars that have been produced during the experiments are still to be analyzed. A measurement for char production has been taken from another experiment. The results for the molar fractions of CO, CO_2, H_2 and CH_4 are visualized in figure 3.5.
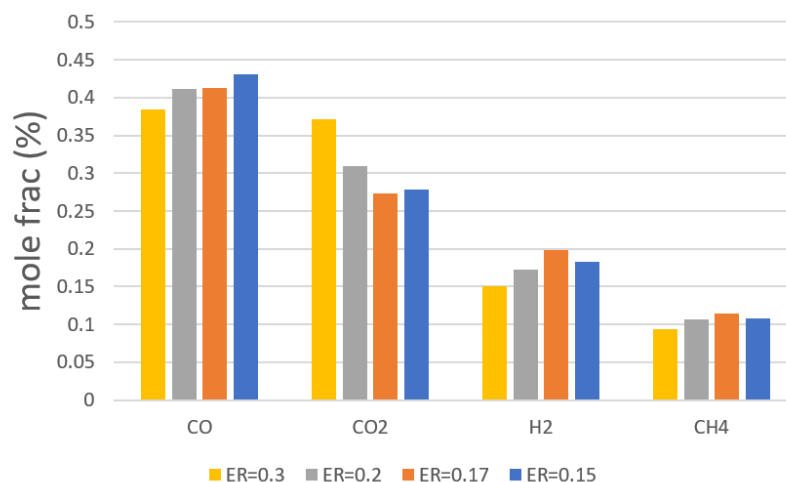
Figure 3.5: Molar Fractions of CO, CO_2, H_2 and CH_4 Measured by μ-GC from Experiments with the IHBFBSR Set-Up. The measurements are taken for Four Different Values of the Equivalent Ratio: 0.3, 0.2, 0.17 and 0.15

From figure 3.5 can be concluded that the most abundant gas, besides nitrogen, is carbon monoxide. Next is carbon dioxide followed by hydrogen and methane. It can be observed that for a decreasing equivalent ratio, the carbon monoxide fraction is increasing as well as the fraction of hydrogen and methane. However, this is not the case for the equivalent ratio of 0.15. The molar fraction of carbon dioxide is decreasing for a decreasing equivalent ratio. These results are in line with the expectations visualized in figure 2.10, except for the fact that the carbon monoxide fraction was expected to decrease with decreasing equivalent ratio. One of the possible explanations is that the results from figure 2.10 have been produced for a reactor pressure of 2 MPa instead of atmospheric conditions. Another likely explanation is that lower values of the equivalent ratio yield larger fractions of unreacted biomass in the IHBFBSR. Therefore, less carbon can be made available for gasification reactions that produce the carbon monoxide.

4

Process Modelling

This chapter focuses on gasification process modelling. Section 4.1 discusses various modelling options for fluidized bed gasifiers. Section 4.2 contains an analysis of mass and heat transfer phenomena in the IHBFBSR. When mass and/or heat transfer are rate limiting, they should be taken into account in the model. Section 4.3 discusses what kind of model is designed for the IHBFBSR. Section 4.4 discusses the pyrolysis model, section 4.5 discusses the equilibrium model and section 4.6 discusses the kinetic model.

4.1. Principles of Gasification Modelling

In general there are two different approaches when it comes to modelling a gasification process. The first approach is an Equilibrium Model [EM]. An equilibrium model predicts the composition of the gasification products under the assumption that all reactants and products are ideally mixed and full chemical equilibrium is reached after an infinite amount of time[5]. The equilibrium model can give an insight in a theoretically optimal product yield. EM's are discussed in subsection 4.1.1. The second approach is kinetic modelling. A kinetic model is used to predict the gasification product composition at a given time and location in the reactor.[5] In order to provide this prediction, a kinetic 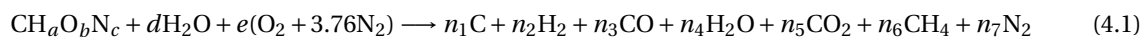model contains two crucial components or sub-models. First a description of fluid dynamics and second a model that describes chemical conversion. Section 4.1.2 will provide information about the various kinetic modelling options.

4.1.1. Equilibrium Models

Thermodynamic equilibrium models [EM] predict the maximum achievable yield of a desired product from a reacting system[31]. This means that full equilibrium is reached between all species in the reactor. The model is independent of reactor geometry and only takes the chemical reactions into account. Chemical equilibrium is either determined by the equilibrium constant of stoichiometric reactions or by minimizing the Gibbs free energy of all components that are present in the reactor. In an EM, the process is considered to be zero-dimensional.

Stoichiometric equilibrium models are models that solve the thermodynamic equilibrium with use of the equilibrium constants of significantly contributing reactions. These reactions are between species containing the elements C,H and O in the reactor. Biomass, an unconventional compound which is modelled as $CH_aO_bN_c$, is reacting to char, hydrogen, carbon monoxide, carbon dioxide, methane and water in the presence of a gasifying agent. This agent can either be air, steam or a combination of both. The reaction equation is given by equation 4.1[31][6].

$$CH_aO_bN_c + dH_2O + e(O_2 + 3.76N_2) \longrightarrow n_1C + n_2H_2 + n_3CO + n_4H_2O + n_5CO_2 + n_6CH_4 + n_7N_2 \qquad (4.1)$$

Where N_1 to n_7 are the stoichiometric coefficients and a, b, c are the hydrogen, oxygen and nitrogen content respectively of the biomass with respect to the carbon content of the biomass. The parameters a,b and c are obtained from the ultimate analysis of the biomass. The seven stoichiometric coefficients are subject to the four elemental balances of C, H, O and N. The balances are given by equation 4.2 to 4.5[6].

$$C : n_1 + n_3 + n_5 + n_6 = 1 \tag{4.2}$$

$$H : 2n_2 + 2n_4 + 4n_6 = a + 2d \tag{4.3}$$

$$O : n_3 + n_4 + 2n_5 = b + d + 2e \tag{4.4}$$

$$N : n_7 = c + 7.52e \tag{4.5}$$

These four balances count seven unknown variables: n_1 to n_7. The biomass composition a, b, c and gasifying agent inputs, d, e are considered to be known. The system can be solved for the seven unknown variables by including at least three reaction equations that consider their equilibrium constant[6]. When other species, such as tars and sulfur species, are added to the equation it is important that corresponding reaction equations and equilibrium constants are known in order to solve the system of equations.

For Non-stoichiometric EM, the reaction mechanism is not known. The method is based on minimizing the Gibbs free energy of the system. At this minimum, the system will be in equilibrium. The Gibbs free energy for the system is given as function of the quantity of all compounds (i = 1...N) present in the reactor by equation 4.6[6].

$$G_{\text{total}} = \sum_{i=1}^{N} n_i \Delta G_{\text{f},i}^0 + \sum_{i=1}^{N} n_i R_{\text{g}} T \ln\left(\frac{n_i}{\sum n_i}\right) \tag{4.6}$$

In this equation, $\Delta G_{\text{f},i}^0$ is the Gibbs free energy of formation of species i at standard pressure of 1 atm and standard temperature of 298 °K. n_i quantifies the amount of species i present in the reactor at equilibrium and is subject to the overall elemental balances described by equation 4.7.

$$\sum_{i=1}^{N} a_{i,j} n_i = A_j \tag{4.7}$$

Where $a_{i,j}$ is the number of atoms of the j-th element in species i. where j can either be C, H, O or N. A_j is the total number of atoms of element j present in the reactor. This information is available from the composition of the gasifying agent and the ultimate analysis of the biomass. The Lagrange multiplier method is used for minimizing the Gibbs free energy[6].

An advantage to EM is that the influence of fuel properties, chemical additives or pollutants and the influence of process parameters on the product composition can be studied[6]. The design of an EM is relatively simple and an EM will have a short computational time. An EM is more effective for gasification at higher temperatures (T>1500 K)[6]. The reaction rates at these temperatures are relatively high and therefore, full equilibrium of the species can be approximated before the products exit the reactor. For lower temperatures, it is not to be expected that equilibrium will be reached within the residence time of the species in the gasifier. In that case a kinetic model can provide the required information[6].

4.1.2. Kinetic Models

A kinetic model is a method that quantifies the amount of products from a reacting system after a finite time and at a specific location in the reactor system by taking into account a.o. reaction kinetics, hydrodynamics, particle residence time, and reactor geometry. For modelling biomass gasification in a bubbling fluidized bed reactor, often a kinetic model is used. Due to short residence times of the reactants and relatively low chemical conversion rates for low-medium gasification temperatures, a full equilibrium between reactants and products is often not achieved[6]. The gasification products exit the BFB gasifier before equilibrium is reached. Only a kinetic model can make an accurate prediction of the product composition. A Kinetic model consists of two sub model components:

- Chemical Conversion Model

- Fluid Dynamics Model

Both components must be solved simultaneously in order to obtain a time and location dependent composition solution. The considered fluid dynamics models in this study can be divided into three main groups[18]:

- Computational Fluid Dynamics Models [CFD]

- Fluidization Models [FM]

- Black Box Models [BBM]

CFD models describe fluid dynamics by simultaneously solving balances for mass, momentum and species over a discrete region of the gasifier[5]. Fluidization models make use of multiple phases in the bedzone. These phases differ from the thermodynamic definition of phase for the reason that they simply indicate a discrete pre-defined region with similar properties such as particle concentration, velocity state of gas or gas/solid mixing[18]. The flow patterns are often described by semi-empirical relations. Black box models work with overall balances over the reactor.

For modelling the chemical conversion in the reactor, also different mechanisms are used. The pyrolysis step marks the conversion of a non-conventional biomass into conventional components that can become subject to stoichiometric gasification reactions. For modelling the pyrolysis step, three model variations exist[13]:

- One Component Model

- Multi-Component Model

- Distributed Activation Energy Model [DAE]

The pyrolysis products will be subject to multiple predefined gasification reactions. The gasification reactions can be divided into homogeneous gas phase reactions and heterogeneous char particle reactions. For the latter, multiple solid-gas reaction mechanisms exist. The considered options for solid-gas reaction kinetics are:

- Uniform Conversion Model [UCM]

- Shrinking Unreacted Particle Model [SUPM]

- Shrinking Unreacted Core Model [SUCM]

- Progressive Model with Shrinking (Reacting) Core [PMSC]

A full overview of all kinetic models, sub models and model variations considered in this study has been visualized in figure 4.1.
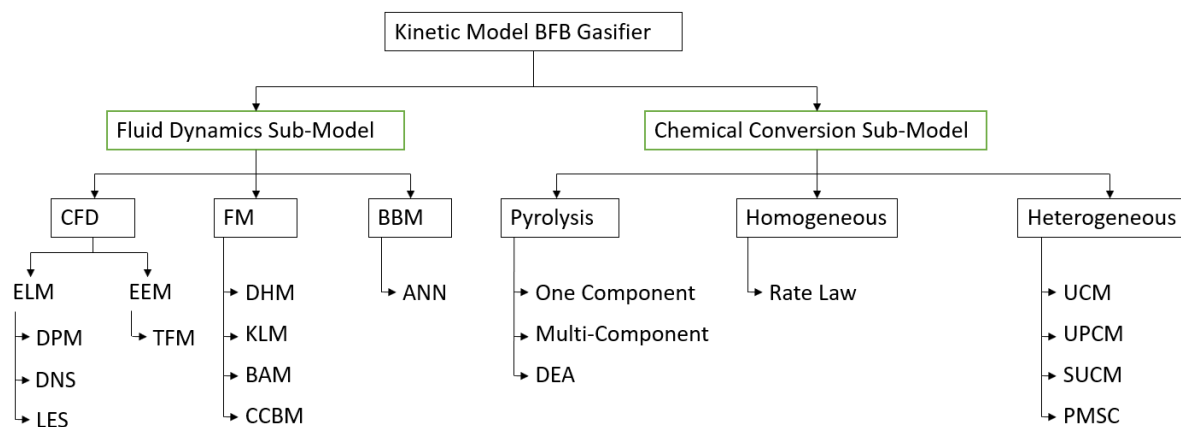

Figure 4.1: Visualization of the Kinetic modelling Options for Fluidized Bed Gasifiers

Various options for fluid dynamics submodels and chemical conversion submodels have been analyzed. More information on these submodels can be found in Appendix F.

4.2. Heat and Mass Transfer in the IHBFBSR

This section discusses heat and mass transfer phenomena in the IHBFBSR. Generally, two transfer steps are of interest in biomass gasification: heat transfer limitation in the pyrolysis step and mass transfer in the heterogeneous char particle reactions. Both transfer limitations are discussed in section 4.2.1 and 4.2.2, respectively.

4.2.1. Heat Transfer Limitations in the Pyrolysis Process

Heat and mass transfer limitations in the pyrolysis process can be evaluated best when observing the pyrolysis of a single biomass particle. In the process, several steps are considered:

- External heat transfer towards the biomass particle

- Internal heat transfer from the surface of the biomass particle towards its center

- Formation of pyrolysis products at $T_{pyr}(r)$, which can vary over the particle's radius

- Internal mass transfer of the devolatilization products towards the surface of the particle

- External mass transfer of the devolatilization products from the particle towards the bulk

The mass transfer from the pyrolysis products away from the particle reduces convective heat transfer from the bulk towards the particle. In other words: external mass transfer reduces external heat transfer[58].

Biomass particle conversion in the pyrolysis process can be explained best by using the Shrinking Density model. Pyrolysis products leave the biomass particle and porous char with a lower density compared to the initial biomass is left. The biomass conversion process can be described by partial differential equations of energy conservation, in equation 4.8, and the mass conservation of gas species i in equation 4.9[58].

$$\frac{\partial}{\partial t}(\rho_s \cdot C_{p,b} \cdot T) = r^{-n}\frac{\partial}{\partial r}\left[r^n \cdot k_{b,eff} \cdot \frac{\partial T}{\partial r} - r^n \cdot u_g \cdot \rho_g \cdot C_{p,g} T\right] + H\dot{m}''' \tag{4.8}$$

$$\frac{\partial}{\partial t}(v_g \cdot \rho_g \cdot Y_i) = r^{-n}\frac{\partial}{\partial r}\left[r^n \cdot D_{i,eff} \cdot \rho_g \cdot \frac{\partial Y_i}{\partial r} - r^n \cdot u_g \cdot \rho_g \cdot C_{p,g} Y_i\right] + \dot{m}''' \tag{4.9}$$

On the left hand side, the equation describes the change in energy or mass given a certain location as a function of time. The first term on the right hand side of the equation represents the internal transport of energy and mass, respectively. The second term represents external energy and mass transport. Finally, the third term indicated the change in energy or mass as result of physical and thermochemical conversion. Because the biomass is inserted as a cylindrical pellet, it is chosen to consider $n = 1$.

At the surface of the particle ($r = r_0$), the internal and external transfer terms need to be equal due to a continuity constraint. The remaining balances at the particle's surface are described by equation 4.10 for energy conservation and 4.11 for gas species conservation[58].

$$-k_{b,eff} \cdot \frac{\partial T}{\partial r}\bigg|_{r_0} = h_{eff} \cdot (T_{r_0} - T_\infty) \tag{4.10}$$

$$-D_{i,eff} \cdot \frac{\partial Y_i}{\partial r}\bigg|_{r_0} = h_m \cdot (Y_{i,r_0} - Y_{i,\infty}) \tag{4.11}$$

Equation 4.10 and 4.11 imply that internal energy transport is described by Fouriers Law and internal mass transport is described by Fick's law[58]. On the right hand side of these equations the external energy and mass transport are described by Newton's Law for external heat and mass transfer.

In equation 4.10, $k_{b,eff}$ is the effective thermal conductivity of the biomass particle expressed in $[W \cdot m^{-1} \cdot K^{-1}]$. T is the local temperature in K at radial position r in [m], where r_0 is the radius of the particle and $r = 0$ represents the centre of the particle. h_{eff} is the effective external heat transfer coefficient expressed in $[W \cdot m^{-2} \cdot K^{-1}]$. This coefficient consists out of the contribution of both convective heat transfer and radiative heat transfer from the bulk to the particle's surface. T_{r_0} is the temperature at the particle's surface and T_∞ is the temperature of the bulk, both in $[K]$[58].

In equation 4.11, $D_{i,\text{eff}}$ is the effective molecular diffusivity of gas species i inside the biomass particle in $[\text{m}^2 \cdot \text{s}^{-1}]$. Y_i is the concentration of gas species i at radial position r. h_m is the effective external mass transfer coefficient. Y_{i,r_0} is the concentration of species i at the particle's surface and $Y_{i,\infty}$ is the concentration of species i in the bulk.

Considering the five pyrolysis process steps listed at the beginning of this section, It is desired to predict which process step limits the rate of pyrolysis. In order to answer this question, several dimensionless numbers are introduced. These numbers calculate the ratio between the rate of one process step compared to another process.

The Pyrolysis Number [Py] describes the ratio between the rate of internal heat transport and the thermochemical rate. The Pyrolysis number is calculated by equation 4.12[12].

$$Py = \frac{k_{\text{b,eff}}}{k \cdot \rho_\text{b} \cdot C_{p,\text{b}} \cdot r^2} \tag{4.12}$$

In this equation, ρ_b is the particle density of the biomass in $[\text{kg} \cdot \text{m}^{-3}]$ and $C_{p,\text{b}}$ is the specific heat of the biomass particle in $[\text{W} \cdot \text{kg}^{-1} \cdot \text{K}^{-1}]$. k respresents the rate coefficient of the pyrolysis reaction in

The Pyrolysis' Number [Py'] describes the ratio between the rate of external heat transport and the thermochemical rate. The Pyrolysis' number is calculated by equation 4.13[12].

$$Py' = \frac{h_\text{eff}}{k \cdot \rho_\text{b} \cdot C_{p,\text{b}} \cdot r} \tag{4.13}$$

A third dimensionless number: the thermal Biot number $[Bi_\text{t}]$ describes the ratio between the rate of external heat transport compared to the rate of internal heat transport. The thermal Biot number is calculated by equation 4.14[12].

$$Bi_\text{t} = r \cdot \frac{h_\text{eff}}{k_{\text{b,eff}}} \tag{4.14}$$

Pyle and Zaror (1984)[45] describes three regimes depending on the values of the two Pyrolysis numbers and the Biot number. The three regimes are described as listed below. The corresponding values of the dimensionless numbers are listed in table 4.1[12].

1. No heat transfer limitation. The pyrolysis process is rate limited by the thermochemical process.

2. The pyrolysis process is limited by external heat transport. The temperature of the particle is uniform over its radius but the particle heats slowly.

3. The pyrolysis process is limited by internal heat transport. There is a temperature gradient over the biomass particle. The temperature gradient is likely to cause a variation in the locally produced pyrolysis products, produced at $T_\text{pyr}(r)$.

Table 4.1: Values for the Pyrolysis numbers and Biot Number for Each of the Regimes Stated by Pyle and Zaror(1984)[45]

Regime	Py	Py'	Thermal Bi
1	Py ≈ 0-10	Py' > 10	Bi < 1
2	Py > 1	Py' > 1	Bi < 1
3	Py < 10^{-3}	Py' « 1	Bi > 50

From the dimensionless numbers, it can be concluded that the pyrolysis temperature and size of the biomass particles influence the rate limiting property of the pyrolysis. The effect of particle size and temperature is illustrated in figure 4.2. The IHBFBSR will be operated in a temperature range of $T_\text{pyr}(r) = 800 - 850°C$. For a temperature of 850 °C, the pyrolysis rate is limited by the thermochemical reaction rate for small particles ($d_\text{p} < 0.1$ mm) and rate limited by heat transport for large particles ($d_\text{p} > 3$ mm). In the intermediate regime, the chemical rate and heat transport rate are more or less equal[18].
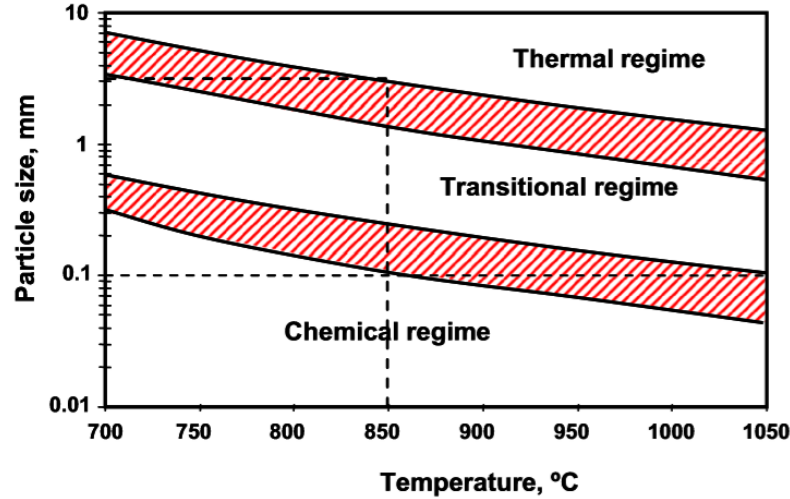
Figure 4.2: Pyrolysis Regimes Depending on Temperature and Particle Size[18].

The parameters that are used in equation 4.12 to 4.14 describe several physical properties of the biomass particle and quantify the heat transfer to the biomass particle. Values for these parameters which are representative for the process conditions in the IHBFBSR have been found in literature. It would however be more accurate to experimentally determine these parameters through own conducted experiments that match the exact pyrolysis conditions. The values of each of the parameters will be stated with its corresponding reference. At the end of this subsection, the dimensionless numbers have been calculated. The translation of these results in either an external, internal or chemical rate limitation will be motivated.

A model for the determination of the thermal conductivity of wood is well described by Thunman et al.[58]. A distinction can be made between the parallel and perpendicular thermal conductivity of wood. Perpendicular thermal conductivity refers to the thermal conductivity perpendicular to the fiber structure of the wood and parallel thermal conductivity parallel to the fibre structure. The conductive resistance over the boundaries of these fibres is larger compared to the conductive resistance parallel to the fibre direction, therefore the thermal conductivity in perpendicular direction is lower. Thunman et al. state that the effective thermal conductivity of wood can be estimated as 1.2 times the perpendicular thermal conductivity (equation 4.15)[58].

$$k_{b,eff} = 1.2 \cdot k_{b,per} \tag{4.15}$$

Thunman's model is based on the determination of thermal conductivity of wood at room temperature as described by MacLean(1941)[32]. MacLean's model determines the thermal conductivity in perpendicular direction as function of bulk density and moisture content as described by equation 4.16[32]. This relation holds for a moisture content on an ar basis that is less 30 wt%.

$$k_{b,per} = 23.7 \cdot 10^{-3} + 0.2 \cdot 10^{-3} \cdot \rho_b \cdot \left[1 + \frac{2 \cdot Y_{moisture}^{ar}}{1 - Y_{moisture}^{ar}} \right] \tag{4.16}$$

It is chosen to calculate the parameters based on the properties the Green Biomass GB used on the IHBFBSR. The main reason for this choice is that most experiments are conducted using GB biomass. The properties of RB and GB are very similar and it is expected that these two biomasses will experience similar rate limitations. The particle radius of GB biomass pellets equals:

$r = 0.003 [m]$

The moisture content of GB is:

$Y_{moisture}^{ar} = 5.08$ wt%

The bulk density is equal to:

$\rho_b = 616 [kg \cdot m^{-3}]$

These values have also been used for the calculation of Py and Py'according to equation 4.12 and 4.13. The corresponding value of the perpendicular thermal conductivity according to MacLean's model is:

$k_{b,per} = 0.16$ [W·m^{-1}·K^{-1}]

The effective thermal conductivity is calculated according to equation 4.15 and is equal to:

$k_{b,eff} = 0.192$ [W·m^{-1}·K^{-1}]

Pyle et al. uses a similar value for the thermal conductivity equal to:

$k_{b,eff} = 0.126$ [W·m^{-1}·K^{-1}][45]

The slightly lower value can be explained by the lower bulk density of wood of 450-550 [kg·m^{-3}] as considered by Pyle et al.[45]. Pyle's thermal conductivity value will not be used for further calculations, but is validates the order of magnitude of the output from MacLean's model.

The specific heat of wood is described by Jenkins et al. according to equation 4.17[6][25]. For an assumed pyrolysis temperature of $T_{pyr} = 850[°C] = 1123.15[K]$, the specific heat of the biomass is equal to:

$c_{p,b} = 1240.4$ [J·kg^{-1}·K^{-1}].

$$c_{p,b} = 1.16 \cdot T \text{ [K]} + 266 \text{ [J·kg}^{-1}\text{·K}^{-1}\text{]} \tag{4.17}$$

Pyle et al. uses a similar but higher specific heat for a temperature of $T_{pyr} = 623 - 780[°C] = 896 - 1053[K]$:

$c_{p,b} = 1670$ [J·kg^{-1}·K^{-1}]

The specific heat by Pyle et al. is a factor 1.35 higher compared to the result of Thunman's model. It is chosen to use Jenkins' model, for the reason that this model is valid for pyrolysis temperatures equal to the pyrolysis temperature of the IHBFBSR.

Blasi et al.[13], states that radiation is the dominant mechanism for external heat transport in pyrolysis. The corresponding radiative heat transfer coefficient is in the range of $h_{rad} = 80 - 230$ [W·m^{-2}·K^{-1}][13]. Convective heat transfer coefficients are much lower and are in the order of $h_{conv} = 5$ [W·m^{-2}·K^{-1}][13]. The effective external heat transfer coefficient equals the sum of the convective and radiative heat transfer coefficients[58] as described by equation 4.18.

$$h_{eff} = h_{rad} + h_{conv} \tag{4.18}$$

The radiative heat transfer coefficient at $T_{pyr} = 850[°C] = 1123.15[K]$ is expected to be at the top of its range. The effective heat transfer coefficient is therefore assumed to be equal to:

$h_{eff} = 235$ [W·m^{-2}·K^{-1}]

Blasi et al.[13], describes several studies that express the chemical rate of pyrolysis for a one-compound model. Only three studies report rates for experiments conducted at similar pyrolysis temperatures as for the IHBFBSR. Nunn et al.[41], gives the rate constant as described by equation 4.19.

$$k = 33.38 \cdot 10^4 \text{ [s}^{-1}\text{] exp}^{\frac{-69000 \text{ [kJ·kmol}^{-1}]}{R_g \cdot T_{pyr}}} \tag{4.19}$$

The corresponding rate at $T_{pyr} = 850[°C] = 1123.15[K]$ equals:

k = 206.24

The unit of the rate constant depends on the rate kinetic expression.

Reina et al.[49], gives the rate constant as described by equation 4.20.

$$k = 6.33 \cdot 10^2 \text{ [s}^{-1}\text{] exp}^{\frac{-91530 \text{ [kJ·kmol}^{-1}]}{R_g \cdot T_{pyr}}} \tag{4.20}$$

The corresponding rate at $T_{pyr} = 850[°C] = 1123.15[K]$ equals:

k = 0.035

This is a substantially different result compared to the result by Nunn et al. . Pyle et al.[45], gives the rate constant as described by equation 4.21.

$$k = 2.5 \cdot 10^3 \, [\text{s}^{-1}] \, \exp^{\frac{-67500 \, [\text{kJ} \cdot \text{kmol}^{-1}]}{R_g \cdot T_{\text{pyr}}}} \tag{4.21}$$

The corresponding rate at $T_{\text{pyr}} = 850[°\text{C}] = 1123.15[\text{K}]$ equals:

k = 1.815

This rate finds itself between the results from Nunn et al.[41] and Reina et al.[49]. It is chosen to calculate the dimensionless numbers for all three kinetic rates. It is recommended to find a more accurate expression for the kinetic pyrolysis rate which relates to the physical process in the IHBFBSR.

The results for the three dimensionless numbers are summarized in table 4.2. A set of all dimensionless numbers has been calculated for each of the kinetic rates. From the table can be concluded that the difference

Table 4.2: Values for the Pyrolysis numbers and Biot Number for Each of the chemical rates Stated by Nunn[41], Reina[49] and Pyle and Zaror(1984)[45].

Kinetic Rate	Source	Py	Py'	Thermal Bi
206.24	[41]	$Py = 1.354 \cdot 10^{-4}$	$Py' = 4.972 \cdot 10^{-4}$	$Bi_t = 3.672$
0.035	[49]	$Py = 0.798$	$Py' = 2.930$	$Bi_t = 3.672$
1.81	[45]	$Py = 1.543 \cdot 10^{-2}$	$Py' = 5.666 \cdot 10^{-2}$	$Bi_t = 3.672$

in the kinetic rates influences the Pyrolysis numbers significantly. For a kinetic rate of 206.24, Py and Py' are both well below 1. This is also the case for the kinetic rate of 1.81. This means that the rate of heat transfer is less compared to the chemical rate and indicates a heat transfer limitation. The Biot number indicates that the external heat transfer rate is higher compared to the internal heat transfer rate. The pyrolysis process is rate limited by internal heat transfer for a chemical rate of 206.24 and 1.81. as described by Nunn et al.[41] and Pyle et al.[45]. For a chemical rate of 0.035[49], Py is in the range of 0.1-1. Py' is in the range of 1-10. This indicates that the rate of rate of heat transport is about equal to the chemical rate, although the process is slightly limited by internal heat transfer, not by external heat transfer. This result corresponds with the indicated heat transfer limitation in figure 4.2.

Overall can be concluded that it is likely that internal heat transfer limitation can occur during pyrolysis of biomass in the IHBFBSR. The biomass particle is likely to have a temperature gradient over its radius.

4.2.2. Mass Transfer Limitations in Heterogeneous Char Reactions

Char that is created in the pyrolysis step is highly porous and has a significant specific surface area. The porosity and specific surface area are quantitatively influenced during the creation of the char particle in the pyrolysis step. The main controlling parameter is the heating rate. For high heating rates, gaseous pyrolysis products quickly leave the biomass particle leaving behind a char particle with high porosity. For slow heating rates, more time is available for secondary pyrolysis reactions. This results in more char formation and lower porosity[12].

Fundamental process steps involved in char-gas reactions have been described by de Jong et al.[12] as:

1. External mass and heat transfer from the bulk gas to the char's external surface layer

2. Internal mass and heat transfer through the ash layer and between char particles

3. Pore diffusion of gaseous reactants and products and heat conduction inside the char particle

4. Adsorption of the reactants on the surface of the char particle

5. Elemental chemical reaction at the surface of the char particle

The rate of heterogeneous reactions is either limited by the rate of the elemental reaction or mass transfer. In addition, a distinction can be made between internal and external transfer limitations. For the conversion of a char particle, the energy and mass balances as stated by equation 4.8 and 4.9 apply as well. Also in this case, the external and internal energy and mass transfer terms are equal at the surface of the char particle. Therefore, equation 4.10 and 4.11 hold as well for char conversion.

In order to assess the rate limitation of the heterogeneous reactions several dimensionless numbers are introduced concerning the heterogeneous char reactions.

The Thiele modulus [Th_n] is a dimensionless number that describes the ratio between the kinetic reaction rate and diffusion rate. The Thiele modulus can be calculated by equation 4.22[12]. In this equation, r is the char particle radius in [m] and k_n is the reaction rate coefficient for an n-th order heterogeneous reaction.

$$Th_n = r \cdot \sqrt{\frac{k_n \cdot a_{s,m} \cdot \rho_g \cdot C_i^{n-1}}{D_{eff}}} \tag{4.22}$$

D_{eff} is the effective diffusion coefficient of the gaseous reactants and products in the char particle in [$m^2 \cdot s^{-1}$]. This rate is a function of the binary diffusion coefficient $D_{i,j}$ and porosity ϵ of the char as described by equation 4.23[12].

$$D_{eff} = \epsilon^2 \cdot D_{i,j} \tag{4.23}$$

The value of the Thiele modulus determines if the reaction is limited by the reaction rate or internal mass transfer through pore diffusion. For a Thiele modulus » 1 the reaction is controlled by internal mass transfer. For a Thiele modulus « 1 the reaction is controlled by the chemical rate[12].

The mass Biot number [Bi_m] is a dimensionless number that describes the ratio between the external mass transport rate and internal mass transfer rate. The Biot number can be calculated by equation 4.24[12]. In this equation, h_m is the mass transfer coefficient of the gas phase in [$m \cdot s^{-1}$]. D_{eff} is the effective diffusion coefficient of the gaseous reactants and products in and to the char particle in [$m^2 \cdot s^{-1}$] as stated by equation 4.23.

$$Bi = r \cdot \frac{h_m}{D_{eff}} \tag{4.24}$$

For a Biot number » 1 the reaction is controlled by external mass transport. For a Biot number = 1 the reaction is controlled by internal mass transport[12].

Di Blasi (2009)[14] introduces three regimes that describe the rate limiting conditions of solid char particle reactions. These regimes are:

1. The kinetic reaction rate is dominant for low temperature reactions with small char particles. As time proceeds, the particle size remains more or less constant but a variation in particle density can be observed.

2. Internal mass transfer is rate limiting for larger particle sizes. Porosity is low and therefore reactions take mainly place at the char particle surface. As a result, the char particle decreases in size when there is no significant change in density.

3. External mass transfer is rate limiting. This occurs at high reaction temperatures and large char particles. In this regime, the reaction depends on the surface area of the char particle and is therefore dependent on its size.

Table 4.3 summarizes the values of the Thiele Modulus and Biot number for each of the regimes.

Table 4.3: Values for the Thiele Modulus and Biot Number for Each of the Regimes Stated by Di Blasi(2009)[14].

Regime	Thiele Modulus	Biot Number
1	Th = 1	Bi = 1
2	Th »1	Bi = 1
3	Th »1	Bi »1

In equation 4.23, ϵ is the porosity of the char particle. It is assumed that the char particle has a porosity of 50 %. Basu et al.[6] describes common char porosity to be around 40-50%. Due to the high heating rate in the IHBFBSR it is expected that the particle will have a relatively high porosity and for that reason, the outer end of the range has been chosen.

The kinetic rates of char oxidation, reforming and the Boudouard reaction are summarized in table 4.4

Table 4.4: Rate constants for Char Oxidation, Reforming and the Boudouard Reaction.

Reaction	Kinetic Rate Symbol	Pre-exp. Factor [s^{-1}]	Activation Energy [kJ · kmol^{-1}]	Kinetic Rate	Source
Char Oxidation	k_{Ox}	$5.957 \cdot 10^5 \cdot T^2$	149440	84054.6	[36][43]
Char Reforming	k_{Ref}	$2.9875 \cdot 10^6$	129000	2.9844	[36][43]
Boudouard	k_{CO_2}	$7.94628 \cdot 10^{11}$	268000	0.2717	[33]

The reaction rates in table 4.4 are already with respect to the reactor volume. Therefore, $a_{\text{s,m}}$ and ρ_{g} do not need to be calculated. The only parameter left to be calculated for the Thiele modulus is the effective diffusion coefficient D_{eff}. The relation is given equation 4.23[12].

The binary diffusion coefficient, or diffusivity, describes the diffusion of the reactants towards the char particle and of products away from the particle. Diffusive transport will only occur near the particle's surface and in the particle pores. To see if the reaction is mass transport limited, it is decided to calculate the diffusion coefficients for the reactants of the heterogeneous chemical system. Since experiments have only been performed with air as gasification agent, only the diffusion of species in air is studied.

For char oxidation, the binary diffusion coefficient for the diffusion of oxygen in nitrogen is taken into account[58]. The binary diffusion coefficient is given as a function of temperature as described by equation 4.25 according to Thunman et al.[58]

$$D_{\text{O}_2,\text{N}_2} = \exp\left[-15.2 + 3.34 \cdot (\ln T_{\text{r}}) - 0.221 \cdot (\ln T_{\text{r}})^2 + 0.0096 \cdot (\ln T_{\text{r}})^3\right] \tag{4.25}$$

The diffusivity of oxygen in nitrogen at $T_{\text{r}} = 1123$[K] is equal to:
    $D_{\text{O}_2,\text{N}_2} = 1.980 \cdot 10^{-4}[\text{m}^2 \cdot \text{s}^{-1}]$.

In the case of char reforming, the diffusion of steam in air needs to be taken into account. This will be approached by the diffusion of steam in nitrogen. The binary diffusion coefficient is given as a function of temperature as described by equation 4.26 according to Thunman et al.[58]

$$D_{\text{H}_2\text{O},\text{N}_2} = \exp\left[-20.3 + 5.17 \cdot (\ln T_{\text{r}}) - 0.430 \cdot (\ln T_{\text{r}})^2 + 0.0176 \cdot (\ln T_{\text{r}})^3\right] \tag{4.26}$$

The diffusivity of steam in nitrogen at $T_{\text{r}} = 1123$[K] is equal to:
    $D_{\text{H}_2\text{O},\text{N}_2} = 2.455 \cdot 10^{-4}[\text{m}^2 \cdot \text{s}^{-1}]$.

For the Boudouard, the diffusion of carbon dioxide in air needs to be taken into account. This will be approached by the diffusion of carbon dioxide in nitrogen. The binary diffusion coefficient is given as a function of temperature as described by equation 4.27 according to Thunman et al.[58]

$$D_{\text{CO}_2,\text{N}_2} = \exp\left[-17.8 + 4.22 \cdot (\ln T_{\text{r}}) - 0.327 \cdot (\ln T_{\text{r}})^2 + 0.0139 \cdot (\ln T_{\text{r}})^3\right] \tag{4.27}$$

The diffusivity of carbon dioxide in nitrogen at $T_{\text{r}} = 1123$[K] is equal to:
    $D_{\text{CO}_2,\text{N}_2} = 1.690 \cdot 10^{-4}[\text{m}^2 \cdot \text{s}^{-1}]$

Turns et al. gives a similar value of $1.15 \cdot 10^{-4}$ for the diffusion of carbon dioxide in air[59]. Therefore, taking the binary diffusion coefficient of carbon dioxide in nitrogen is acceptable in order to reflect on rate limiting transport phenomena.

In equation 4.24, the external mass transfer coefficient h_m is not easily described. Therefore, the mass Biot number given as a function of the Sherwood number [Sh] as described in deJong et al.[12]

$$Bi_m = \frac{Sh}{2 \cdot \epsilon^2} \tag{4.28}$$

The Sherwood number can be expressed as function of the Reinolds number [Re] and Schmidt number [Sc] as described in equation 4.29. This is done by both de Jong et al.[12] and Thunman et al.[58].

$$Sh = 2 + 0.6 \cdot Re^{\frac{1}{2}} \cdot Sc^{\frac{1}{3}} \tag{4.29}$$

The Reinolds number is expressed by equation 4.30 and the Schmidt number by equation 4.31.

$$Re = \frac{\sqrt{D_r^2 - D_{b,burner}^2} \cdot U_{bulk}}{\nu} \tag{4.30}$$

$$Sc = \frac{\nu}{D_{i,j}} \tag{4.31}$$

In equation 4.30 and 4.31, ν is the kinematic viscosity of the bulk. In the case of air gasification, the kinematic viscosity of air will be taken. The kinematic viscosity of air at $T_r = 1123[K]$ is equal to:
$\nu = 141.8 \cdot 10^{-6}[m^2 \cdot s^{-1}][59]$

The binary diffusion coefficients of the corresponding reactants have been mentioned for the calculation of the Thiele modulus. The bulk velocity is approximated by equation 4.32.

$$U_{bulk} = \frac{\dot{m}_{agent}}{\rho_{agent} \cdot A_{cross}} \tag{4.32}$$

The cross-sectional area of the bedzone can be calculated as function of its hydraulic diameter as given by equation 4.33.

$$A_{cross} = 0.25\pi \left[D_r^2 - D_{b,burner}^2 \right] \tag{4.33}$$

The density of air at $T_r = 1123[K]$ is equal to:
$\rho_{air} = 0.3166[kg \cdot m^{-3}][59]$

The cross-sectional area of the bedzone is equal to:
$0.076[m^2]$

For most experiments, the mass flow of gasification agent has been equal to:
$\dot{m}_{agent} = 19[kg \cdot hr^{-1}] = 5.278 \cdot 10^{-3}[kg \cdot s^{-1}]$

The value for the bulk velocity at that mass flow is equal to:
$U_{bulk} = 0.219[m \cdot s^{-1}]$

The corresponding value for the Reinolds number equals:
$Re = 481.5$

The results for the three heterogeneous reaction have been summarized in table 4.5.

Table 4.5: Values for the Thiele modulus and Mass Biot Number for Char Oxidation, Reforming and the Boudouard Reaction. Included are Corresponding Variables that are Used to Calculate the Dimensionless Numbers.

Reaction	Kinetic Rate	Reactant i	Diffusivity of i in nitrogen D_{i,N_2}	Thiele Modulus Th	Biot number Bi_m	Mass Transfer Limitation?
Char Oxidation	84054.6	O_2	$1.98 \cdot 10^{-4}$	123.62	27.56	Y
Char Reforming	2.9844	H_2O	$2.455 \cdot 10^{-4}$	0.6615	25.93	N
Boudouard	0.2717	CO_2	$1.69 \cdot 10^{-4}$	0.2406	28.83	N

It can be observed from the Thiele modulus that for char oxidation the chemical rate is higher compared to the internal mass transfer rate. This is not the case for the other two char-gas reactions. The mass Biot number indicates that the external mass transfer rate is higher than the internal heat transfer rate. It is therefore concluded that char oxidation is rate limited by diffusive mass transport of oxygen towards the char particle's surface and into the char particle's pores. The value of the Thiele modulus is not extremely high. This means that it is still expected that some oxygen will effectively diffuse into the char particle's pores. The normalized mass fraction of oxygen in the char particle is illustrated in figure 4.3.
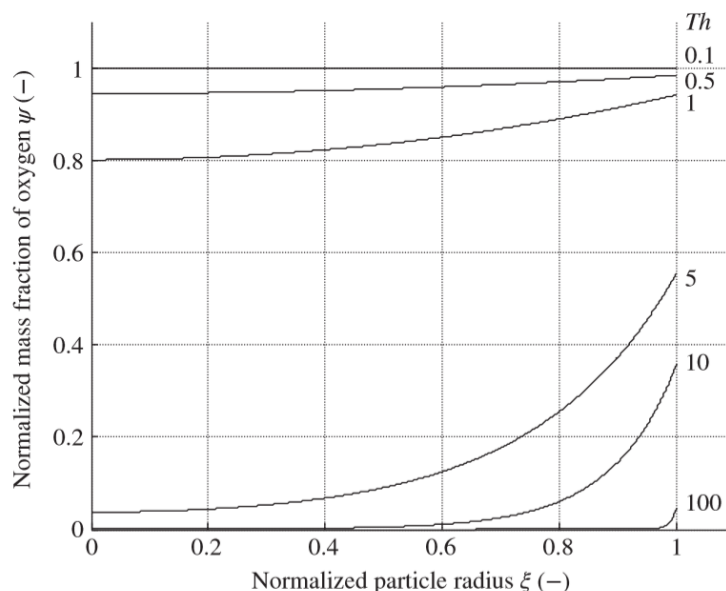
Figure 4.3: Visualization of the Influence of the Thiele Modulus on the Reactant Concentration in the Char Particle[12]. This Particular Graph Corresponds to a Biot Number of 5.

A shrinking particle model would best describe the conversion, although a shrinking density model is also allowed due to the presence of oxygen into the particle. In gasification, the oxygen supply is limited. Therefore, the char particle will soon find itself in an environment out of oxygen. The char reforming reaction and Boudouard reaction still proceed. These reactions are rate limited by their chemical reaction. It can also be concluded from figure 4.3 that for these reactions with a Th«1, a constant reactant concentration is expected throughout the particle. Therefore, a shrinking density model would best describe the conversion of char. This is important to take into account when steam is used as gasifying agent instead of air. In that case, The model should only include a shrinking particle model.

4.3. Model Design Choices for the IHBFBSR

It is decided to design a reactor model for the IHBFBSR biomass gasifier set-up at the TU Delft. Section 4.1 has shown that multiple modelling options exist for modelling a BFB reactor. This section explains the model design choices for the IHBFBSR model.

It is chosen to model the IHBFBSR with both an equilibrium model and a kinetic model. An equilibrium model is a useful tool to illustrate the commercial value of the process and its relevance for scale up. Nevertheless, an equilibrium model will not be sufficient for optimizing the reactor set-up and provide an accurate composition prediction of the product stream due to a lack of detail. A kinetic model is able to provide this information. The programming tool ASPEN Plus™is used for the kinetic modelling. The advantage is that ASPEN Plus™already has databases on the properties of various chemical species and that it can simulate a chemical reaction process given its kinetics.

For the EM, it is chosen to make a non-stoichiometric equilibrium model that is based on the reduction of Gibbs free energy of all components. This method is easily implemented in the simulation environment of ASPEN Plus™.

Section 4.1 has explained that a kinetic model is composed of two sub-models. For modelling the fluid dynamics in the IHBFBSR, it is chosen to use a limited fluidization model. A fluidization model provides enough detail on the fluid dynamics in the IHBFBSR in order to make an accurate prediction of carbon conversion and cold gas efficiency as well as the composition of the product stream. The other considered option, CFD modelling, would add more detail in the model, but this also leads to an increase in computational time and complexity. CFD modelling can be of interest in order to increase the accuracy of the model, but it is out of the scope of this study.

The chosen fluidization model is a zero-dimensional model. This means that the bedzone is modelled as a continuously stirred tank reactor [CSTR] assuming a well mixed single emulsion phase. The volume of the emulsion in the reactor is approached by assuming a constant bed expansion for all bed material sizes. The static bed height is different for each bed material size. In this way, the influence of the bed material size at fluidization is taken into account as well for the kinetic model. The freeboard of the IHBFBSR is modelled as a one-dimensional plug flow reactor [PFR]. It is chosen not to look into two- or three-dimensional models due to the fact that the product composition at the outlet of the IHBFBSR is of the most interest rather than a spatial description of species throughout the reactor.

For the chemical conversion model, it is chosen to decouple the pyrolysis process and the gasification process. For the pyrolysis model, a one-component pyrolysis model is used. This is because a multi-component pyrolysis model adds in complexity while an experimental determination of the multi-component fractions would still be required. The model describes the mass yields of the considered pyrolysis products as a function of temperature as measured during own performed pyro-probe experiments. The biomass particle converts into porous char according to the Shrinking Density Model.

Homogeneous gas phase reactions present in the bedzone and in the freeboard are modelled using a rate law expression. The kinetic parameters have been found from literature. For these parameters, it is observed if the process conditions of the semi-empirical relations match the process conditions of the IHBFBSR.

Heterogeneous reactions that take place in the emulsion phase of the IHBFBSR are modelled with LMHW kinetics. These kinetics assume that there are no mass- and heat transfer limitations and that the conversion takes place in isothermal conditions. The porous char oxidizes according to the Shrinking Particle Model for the reason that the oxygen supply to the reaction is mass transfer limited. After all oxygen has reacted, the heterogeneous reactions are dominated by the water gas reaction and Boudouard reaction. For these reactions, it has been calculated that there is no significant mass transfer limitation. The char particle converts according to the Shrinking Density Model after depletion of oxygen in the reactor. The Shrinking Density Model is chosen for the reason that char particles are very porous and the absence of mass transfer limitations.

Both the equilibrium and the kinetic model are developed in ASPEN Plus™. ASPEN Plus™is a software tool for chemical process design. The software integrates a level of fluid dynamics and information about the chemical components in order to produce a visual modelling environment. Each unit operation is modelled by a separate block which needs the process conditions and assumptions as an input. Material streams between the blocks are modelled by arrows. As soon as the software contains all the necessary information about the chemical process, the steam composition of all the streams can be given as an output. The software can also assist in an energy analysis, economic evaluation or sensitivity analysis for one of the process variables. These properties are used to reflect on the performance of the IHBFBSR.

4.4. Pyrolysis Model

Although section 4.2 has concluded an internal heat transport limitation, it is chosen to model the pyrolysis process as it is chemical rate limited. As result of this assumption, it is possible to use the experimental data from the pyroprobe experiments for modelling the pyrolysis in the IHBFBSR. A temperature gradient over the biomass particle during pyrolysis is expected to produce slightly different products on a local scale. This can however could be evaluated in the ASPEN Plus™model for the reason that a sensitivity analysis of the pyrolysis temperature can be performed.

The assumption for the pyrolysis model are itemized below.

- The biomass particle is a homogeneous material

- The biomass particle is heated instantly to $T_{\mathrm{pyr}}[\degree C]$ with a uniform temperature distribution over its radius.

- The devolatilization products form at the surface and in the pores of the biomass particle according to the yields as determined by the pyroprobe experiments.

- Gasseous products are transported away from the reaction zone and the process leaves a porous char structure with a lower density compared to the initial biomass particle. The size of the particle remains intact. This is according to the Shrinking Density Model.

- The devolatilization products do not react until the particle is fully pyrolyzed.

- The unreacted devolatilization products will proceed towards the gasification model, either the equilibrium model or the kinetic model. They consist out of permanent gasses, vapours, pyrolitic water, moisture and a solid char and ash fraction.

The pyrolysis model is based on experimentally determined mass yields. During the experiments a small amount of biomass is pyrolized in a pyroprobe. The experiments have a fast-pyrolysis characteristic, and are performed at a heating rate of $600\degree C \cdot s^{-1}$. The residence time of the biomass varies around 12 seconds. These measurements resemble the conditions in the IHBFBSR and are therefore a good approximation for modelling the pyrolysis step. The experiment is performed for pyrolysis temperatures of 600, 700, 800, 900 and 1000 $\degree C$. The experiments have been performed for Red Biomass (RB), Green Biomass (GB) and Miscanthus. The composition of the solid, liquid and gas phase of the pyrolysis products are visualized in figure 4.4. This figure also indicates which components are being measured and which yields will be calculated.
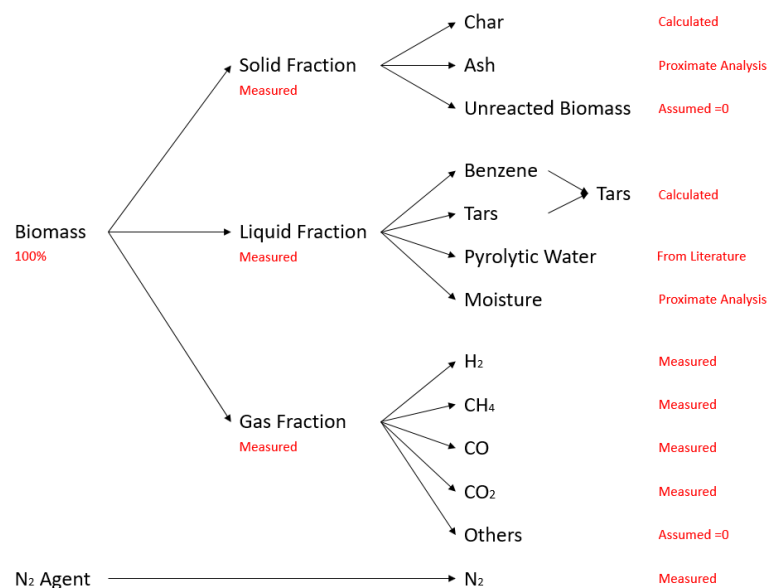

Figure 4.4: Pyrolysis Products from the Pyroprobe Experiments and their Determination Strategy.

The mass of the solid fraction, liquid fraction and gaseous fraction is measured after each pyrolysis experiment. The solid fraction consists of ash, char and unreacted biomass. It is assumed that all biomass has reacted. The mass yield of the char is calculated as the difference between the mass yield of the solid fraction minus the ash content from the proximate analysis on an a.r. basis according to equation 4.34.

$$Y_{\text{char}}^{\text{ar}} = Y_{\text{solid}}^{\text{ar}} - Y_{\text{ash}}^{\text{ar}} \tag{4.34}$$

When observing results of the pyroprobe experiments, it has been concluded that the mass balance does not close. For each experiment, 10-20% of mass is not accounted for. This deviation can be explained by the determination of the liquid fraction. First, all vapours are condensed. It is possible that not all vapours have condensed. Secondly, the condensed liquids are dissolved in iso-propanol. It is also possible that not all liquids have dissolved effectively. Similar deviation mechanisms are not likely to occur for the solid and gas yield measurements. Therefore, it is assumed that the mass deviation is a liquid substance. It is also assumed that the composition of this liquid is the same as the measured liquid fraction. The mass yield of the real liquid fraction is therefore equal to the sum of the measured liquid fraction and the mass deviation as stated by equation 4.35.

$$Y_{\text{liquid}}^{\text{ar}} = Y_{\text{liquid-measured}}^{\text{ar}} + Y_{\text{dMass}}^{\text{ar}} \tag{4.35}$$

The liquid fraction consists out of tars, benzene, pyrolitic water and moisture. The moisture content is known from the proximate analysis. In order to determine the amount of pyrolitic water, an existing model is used[1]. The formation of pyrolitic water is described as a function of the pyrolysis temperature as stated in equation 4.36.

$$Y_{\text{pyr-H}_2\text{O}}^{\text{ar}} = 5.157 \cdot 10^{-5} \cdot T^2 - 1.186 \cdot 10^{-1} \cdot T + 84.91 \tag{4.36}$$

The model from which the expression in equation 4.36 originates, has originally been composed for for a slow-pyrolysis process operating at similar pyrolysis temperature as the IHBFBSR. For the reason that the amount of pyrolytic water does not vary much for either slow or fast pyrolysis, it is assumed that the function of pyrolytic water also applies to the IHBFBSR fast pyrolysis set-up. The amount of water is calculated as the sum of the pyrolitic water and the moisture according to equation 4.37. The amount of tar and benzene is calculated as the liquid fraction minus the amount of water according to equation 4.38.

$$Y_{\text{H}_2\text{O}}^{\text{ar}} = Y_{\text{pyr-H}_2\text{O}}^{\text{ar}} + Y_{\text{moisture}}^{\text{ar}} \tag{4.37}$$

$$Y_{\text{tar}}^{\text{ar}} = Y_{\text{liquid}}^{\text{ar}} - Y_{\text{H}_2\text{O}}^{\text{ar}} \tag{4.38}$$

For the gaseous fraction of the pyrolysis products of the pyroprobe experiment is assumed that it consists only of the gasses H_2, CO_2, CH_4, CO, N_2. Nitrogen is used as inert transportation agent during the experiment. It is assumed that other gasses such as ethylene, C_2H_4, have a mass yield of zero. The contribution of H_2, CO_2, CH_4 and CO are measured and are normalized to contribute as 100% of the mass of the gas sample.

4.4.1. Pyroprobe Results

The results of the pyroprobe experiments have been visualized in the graphs in figure 4.5 to 4.7. The experimental data of the individual experiments can be found in appendix D. From the results can be observed that the liquid yield is highest for low pyrolysis temperatures and decreases for increasing temperature. Also the solid yield decreases for increasing pyrolysis temperatures These two processes result in a higher gas yield for increasing temperature. These observations are in line with the predicted influence of the temperature on the pyrolysis products as described in figure 2.6. It can also be observed that the solid yield tends to stabilize for temperatures above approximately 850°C. This indicates that nearly all reactive char has been pyrolyzed to its fullest potential. Nevertheless, a complete stabilization is not observed which indicates that still some unreacted biomass is present. In that case a carbon conversion of less than 100% is achieved.

For the RB and GB biomass it can be observed that the liquid yield and gas yield also stabilize above approximately 900°C. For miscanthus, the yield gradient of liquid and gaseous products decreases significantly for temperatures above 900°C, but does not completely stabilize. This indicates that for temperatures above 900°C, the product yields are less temperature dependent and carbon conversion is close to maximal.

It is desired to yield a large gaseous fraction as feed to the gasification process. It is also desired to have low tar yields to prevent tar sticking in the reactor. It is important that the biomass is pyrolyzed to its fullest potential to maximize product yields. This is the case for the nearly stable char yields observed for temperatures above 850°C. The gas yields of H_2, CO_2, CH_4 and CO have been visualized in the graphs in figure 4.8 to 4.10.
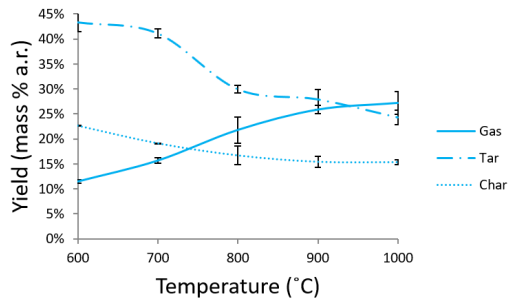
Figure 4.5: Gas-, Tar- and Solid Yield as function of (Fast) Pyrolysis Temperature for Miscanthus From the pyroprobe Experiment
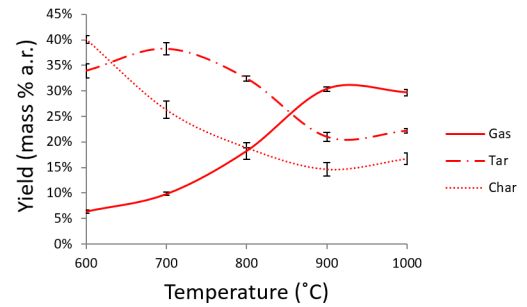
Figure 4.6: Gas-, Tar- and Solid Yield as function of (Fast) Pyrolysis Temperature for RB From the pyroprobe Experiment
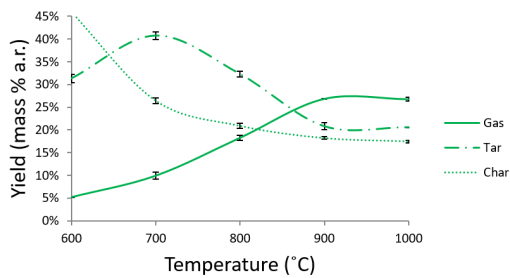
Figure 4.7: Gas-, Tar- and Solid Yield as function of (Fast) Pyrolysis Temperature for GB From the pyroprobe Experiment
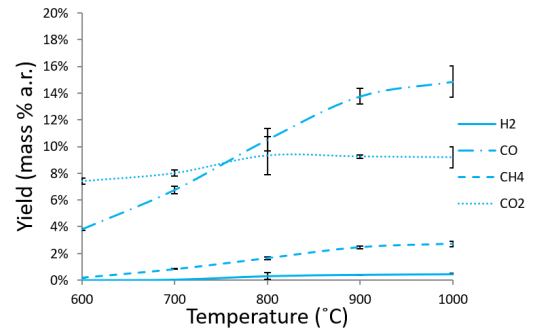
Figure 4.8: pyroprobe Yields for the Devolatilization Gasses of Miscanthus For a Temperature Range of 600-1000 °C
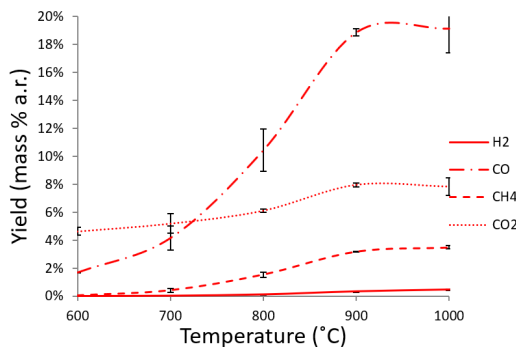
Figure 4.9: pyroprobe Yields for the Devolatilization Gasses of RB For a Temperature Range of 600-1000 °C
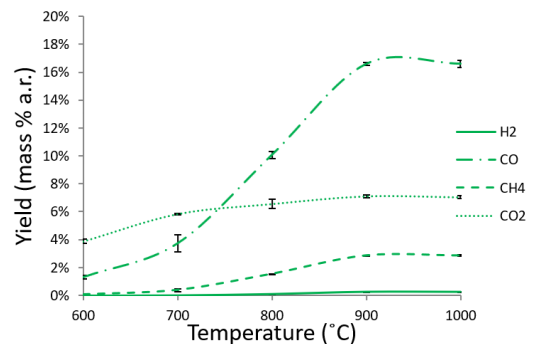
Figure 4.10: pyroprobe Yields for the Devolatilization Gasses of GB For a Temperature Range of 600-1000 °C

It can be observed for all three biomasses, that low temperatures yield more carbon dioxide and high temperatures yield more carbon monoxide and methane. The hydrogen yield increases as well as function of temperature but is much lower than the yields of carbon monoxide and methane due to its low molecular mass.

4.4.2. Lumped Tars Model

As described in section 2.3, multiple different tars are formed as the result of devolatilization. For the reason that there are no kinetics available for the oxidation and gasification reactions of each of the tars it is decided to lump the tars together into groups. In this study, it has been chosen to design four lumped tar groups. For these four tars, gasification kinetics are known. Most other studies of biomass gasifiers use one lumped tar group. Adding more tar groups than four is not expected to contribute significantly to improving the accuracy of the model results.

The composition of tar from biomass devolatilization is described by Basu as summarized in table 4.6[6]. Note that benzene will be present in the liquid fraction of the pyrolysis products but is actually not a tar.

Table 4.6: Typical Composition of Tar[6].

Component	Enthalpy of formation	Weight Yield
	$\Delta H_{f_0}[kJ\,mol^{-1}]\,T = 298.15K$	%
Benzene	100.41	37.9
Toluene	73.476	14.3
Other 1-ring aromatic hydrocarbons		13.9
Naphthalene	174.276	9.6
Other 2-ring aromatic hydrocarbons		7.8
Other 3-ring aromatic hydrocarbons		3.6
Other 4-ring aromatic hydrocarbons		0.8
Phenolic compounds	-58.807	4.6
Heterocyclic compounds		6.5
Others		1.1

Based on this table, it is possible to make four lumped tar groups. The first group is benzene with a weight share of 37.9 % of the tar mass, a molecular formula C_6H_6 and an enthalpy of formation of $\Delta H_{f_0} = 100.41[kJ \cdot mol^{-1}]$. The second group is toluene including other 1-ring aromatic hydrocarbons. This group represents 28.2% of the tar mass, has the molecular formula C_7H_8 and an enthalpy of formation of $\Delta H_{f_0} = 73.476[kJ \cdot mol^{-1}]$. The third group is naphthalene including other 2,3 and 4-ring aromatic hydrocarbons. This group represents 21.8% of the tar mass, has the molecular formula $C_{10}H_8$ and an enthalpy of formation of $\Delta H_{f_0} = 73.476[kJ \cdot mol^{-1}]$. The fourth and last group consists out of phenolic compounds, heterocyclic compounds and others. This group is modelled as phenol with a weight share of 12.2% of the tar mass, a molecular formula C_6H_5OH and an enthalpy of formation of $\Delta H_{f_0} = -58.807[kJ \cdot mol^{-1}]$.

4.4.3. Devolatilization Curves

The pyrolysis model will consist of yield curves as a function of the pyrolysis temperature. Each biomass type has its own curve. The curves have been constructed on the average result of 3 experiments for pyrolysis temperatures of 600, 700, 800, 900 and 1000 $°C$ for each of the biomass types. The best fit is obtained when the curves are approximated by a 4-th degree polynomial. Table 2 in Appendix G, shows the coefficients of each of the polynomials. They relate to the fourth degree polynomial described in equation 4.39 where i is the chemical component for which the yield is calculated. For completeness, the coefficients of the pyrolytic water model have been included in the table as well[1].

$$Y_i = aT^4 + bT^3 + cT^3 + dT + e \tag{4.39}$$

The curves have been generated by use of the fourth degree polynomial function: polyfit(4) from Matlab™.

4.4.4. Sulfur, Chlorine and Nitrogen Compounds

From the ultimate analysis of the biomass as described in section 3.1 it can be observed that small amounts of sulfur, chlorine and nitrogen compounds are present in the biomass. For the equilibrium and kinetic model it is assumed that sulfur reacts to H_2S, chlorine reacts to HCl and nitrogen reacts to NH_3. These components are present in the reactor during gasification. It is assumed that they will not react during the process as it is

not the focus of this study. This section, however, reflects on the influence that H_2S, HCl and NH_3 can have on the reactor performance.

H_2S can cause corrosion of the gasifier and pipes. H_2S can also cause poisoning of catalysts which are often used in gasifiers[36]. In addition, a reaction of H_2S and NH_3 can cause the formation of ammonium(poly)sulfide which solidifies for temperatures below 150 °C[12].

On contact with water, HCl becomes corrosive hydrochloric acid. Besides its corrosive properties, the fumes of HCl can cause severe reportorial problems. With chlorine compounds in the product gas, there is also the risk of formation of fouling species that solidify at low temperatures. An example is NH_4Cl which solidifies at temperatures between 250-280°C [12].

In the presence of oxygen, NH_3 can be converted into NO_x gasses. NO_x is difficult to remove and is highly undesirable as it is an air pollutant. The formation potential of N_2O is very low, but it should be mentioned for the reason that its effect of global warming is 36 times as severe as the effect of CO_2[12].

The reactions in order to form H_2S, HCl and NH_3 have been described by equation 4.40 to 4.42. The reactions are modelled in ASPEN Plus ™with a stoichiometric reactor and the reactions proceed until all sulfur, chlorine and nitrogen compounds have been fully converted. The conversion takes place at atmospheric pressure and at a temperature equal to the pyrolysis temperature.

$$H_2 + S \longrightarrow H_2S \tag{4.40}$$

$$H_2 + 2Cl \longrightarrow 2HCl \tag{4.41}$$

$$3H_2 + 2N \longrightarrow 2NH_3 \tag{4.42}$$

4.4.5. Pyrolysis Model in ASPEN Plus™

In the ASPEN Plus™ model, it is design such that it is possible to select one of the three biomasses as input for the pyrolysis models. The biomass is defined by its proximate and ultimate analysis. The biomass enters a yield reactor "RYIELD" in which it is converted to the pyrolysis products as described in section 4.4 with use of the mass yields described in subsection 4.4.3. The calculator block "YDEVO" is implemented in the model to calculate the mass yields that correspond to the chosen pyrolysis temperature. The calculations have been coded in FORTRAN. The code inputs the pyrolysis temperature from the RYIELD block and outputs the mass yields to the RYIELD block. An overview of the FORTRAN code has been added to this study in appendix E. The Pyrolysis model in ASPEN Plus™, is visualized in figure 4.11.
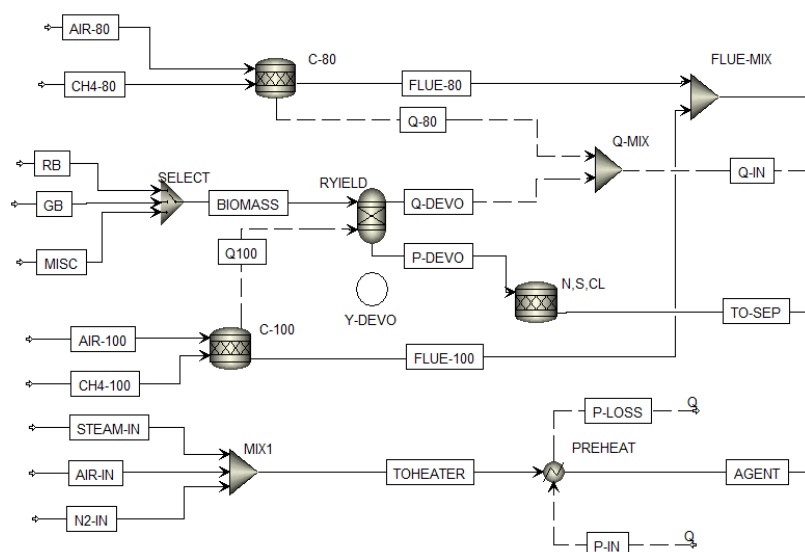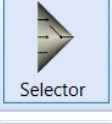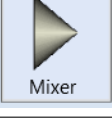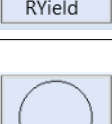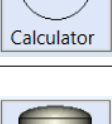
Figure 4.11: Visualization of the Pyrolysis Model in ASPEN Plus™, including the blocks: SELECTOR, RYIELD, YDEVO and N,S,Cl

Both stoichiometric reactors C-80 and C-100 represent the burners in which methane is combusted. The heat from the bottom burner is added to the yield reactor to supply heat to the pyrolysis process. The heat from the top burner combined with the left over heat from pyrolysis will proceed to the gasification model. A summary of all the reactor blocks is given in table 4.7.

Table 4.7: Summary of all Reactor Blocks in the Pyrolysis Model of the IHBFBSR in ASPEN Plus™

Blockname	Block ID	Pictogram	Description
RStoic	C-80	RStoic	Model of the top burner: Combustion of methane with air to deliver 12 kW of heat to the CSTR.
RStoic	C-100	RStoic	Model of the bottom burner: Combustion of methane with air to deliver 20 kW of heat to the Yield Reactor for the pyrolysis process.
Selector	SELECT	Selector	Selector that allows to choose between three different biomass input sources: RB, GB and Miscanthus.
Mixer	MIX1	Mixer	Mixes steam, air and nitrogen that can enter the as gasifying agent. The right agent flow is obtained by adjusting the mass flow for each of the individual steams.
RYIELD	RYIELD	RYield	Yield reactor in which pyrolysis of the biomass takes place. The mass yields for all pyrolysis products are calculated by the calculator block Y-DEVO. The yield reactor will output only conventional species since all biomass is converted. For most experiments, the pyrolysis temperature is 850 degrees Celsius. Pressure equals atmospheric pressure.
Calculator	Y-DEVO	Calculator	The calculator block Y-DEVO is used to calculate the mass yields of the pyrolysis products in [%wt] as function of the pyrolysis temperature and biomass type. The calculator block also sets the temperature of the gasifier equal to the chosen pyrolysis temperature as specified in RYIELD.
RStoic	N,S,CL	RStoic	In this stoichiometric reactor, nitrogen, sulfur and chlorine components are fully converted to H2S, NH3 and HCl. These reactions will involve a small amount of the hydrogen from the pyrolysis products as reactant. The formed species are assumed to be inert.
Heater	PREHEAT	Heater	This heater pre-heats the gasifying agent to 650 degrees Celsius.
Mixer	FLUE-MIX	Mixer	This mixer combines the flue gasses from the two burners C-80 and C-100 into one outlet.
Mixer	Q-MIX	Mixer	This mixer combines the heat from the pyrolysis zone and the heat from the top burner as the heat that will enter the bedzone.

4.5. Equilibrium Model

The non-stoichiometric EM makes use of the Gibbs reactor block in ASPEN Plus™. This reactor block considers the reactants at the input and outputs the amount of products by minimizing the Gibbs free energy of the chemical system. The Gibbs reactor is operated at a temperature equal to pyrolysis temperature T_{pyr}[°C]. The temperature of the pyrolysis model, RYIELD, and the temperature of the Gibbs reactor are automatically linked by FORTRAN code in the calculator block YDEVO. Therefore, it is only necessary to variate the temperatue of RYIELD in order to variate the temperature of the whole reactor system. The pressure in the reactor equals $p_{Gibbs} = 1$[atm]. The EM including the pyrolysis model is visualized in figure 4.12.
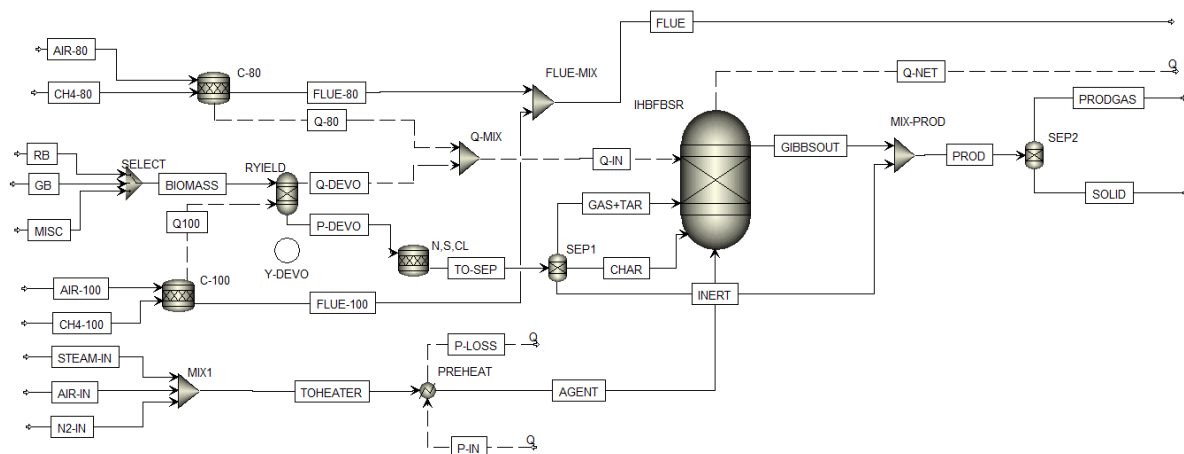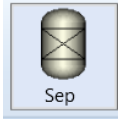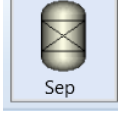
Figure 4.12: Equilibrium Model of the IHBFBSR in ASPEN Plus™

The ASPEN Plus™blocks that have been added to the pyrolysis model to obtain the EM, are explained in table 4.8.

Table 4.8: Summary of all reactor blocks in the ASPEN Plus™model of the IHBFBSR

Blockname	Block ID	Pictogram	Description
Separator	SEP1	Sep	This separator block splits the pyrolysis products into three groups: vapor phase components [Gas+Tar], solid components [CHAR] and inert components [INERT]. It is chosen to separate The inerts are modelled not to enter the reactors.
RGIBBS	IHBFBSR	RGibbs	This reactor models the gasification zone of the IHBFBSR. The reactor The temperature in the reactor equals the pyrolysis temperature in RYIELD. The pressure equals 1 atm.
Separator	SEP2	Sep	This separator models the two cyclones that are present in the IHBFBSR set-up. The solids, char and ash, are removed from the product gas. This model assumes that all solids and gasses are completely separated.
Mixer	MIX-PROD	Mixer	This mixer combines the product output from the Gibbs reactor with the inert stream that originates from separator SEP1. The combined stream is a model for the product gas (solids included) that exits the IHBFBSR at the top.

On the left, three biomasses are introduced and fully defined by ultimate and proximate analysis. A selector block is used in order to choose a biomass type. The gasification agent is a mixture of steam, air and nitrogen. The mass flows of each of the streams can be entered manually. The agent is pre-heated to 650 [°C] by a pre-heater block.

The pyrolysis products enter a stoichiometric reactor for the conversion of sulfur, chlorine and nitrogen compounds as described in section 4.4.4. The products then enter the gasification zone which consists of a Gibbs reactor named IHBFBSR. The gasification products pass through a separator in which the solid and gas phase are separated. This ideal separator models the two cylcones of the IHBFBSR.

Results of the equilibrium model describe the composition of the products form the Gibbs reactor in molar flow in [kmol·hr^{-1}]. These results have been generated for the process parameters as summarized in table 4.9. The reactor temperature equals $T_r = 850$[°C]. The reactor temperature is equal to the pyrolysis temperature for the reason that steady state is assumed.

Table 4.9: Process Conditions for the EM Corresponding to the Model Results Given in this Chapter.

Parameter	Symbol	Value	Unit
Pyrolysis Temperature	T_{pyr}	850	[°C]
Biomass Type	-	GB	-
Biomass Mass Flow	$\dot{m}_{Biomass}$	17.4	[kg·hr^{-1}]
Air Agent Mass Flow	$\dot{m}_{Air}$	19	[kg·hr^{-1}]
N$_2$ Agent Mass Flow	$\dot{m}_{N_2}$	4	[kg·hr^{-1}]
Steam Agent Mass Flow	$\dot{m}_{Steam}$	0	[kg·hr^{-1}]
Equivalent Ratio	λ	0.2	-
Steam to Biomass Ratio	SB	-	-

The stream composition of "PROD", just after the mixer "PROD-MIX" is given in table 4.10. The gas composition relative to the total product gas composition is calculated according to equation 4.43.

$$\gamma_i = \frac{\dot{F}_i}{\sum_{i=1}^{4} \dot{F}_i} \tag{4.43}$$

With i = H$_2$, CO, CO$_2$ or CH$_4$.

The relative gas fractions γ_i have been visualized in figure 4.13.
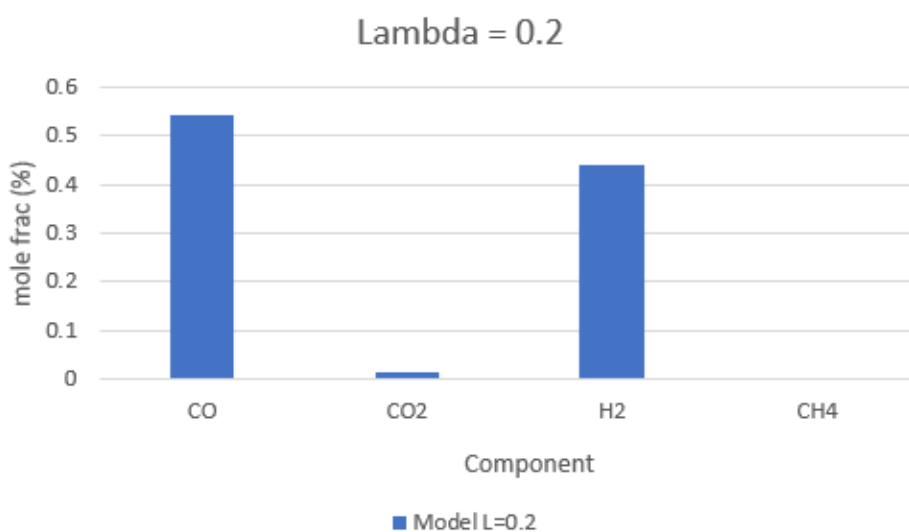
Figure 4.13: Results of the Equilibrium Model of the IHBFBSR in ASPEN Plus™at an Equivalent Ratio Equal to 0.2.

Table 4.10: Results for the EM under the Process Conditions as Described in Table 4.9.

Species	PROD [kmol/h]	MM	PROD [kg/h]	frac (mass)	frac (mol)
CO	0.595	28.01	16.66595	0.414495549	0.29252704
CO_2	0.014	44.01	0.61614	0.015323896	0.006882989
H_2	0.483	2.01	0.97083	0.024145321	0.237463127
CH_4	0.004	16.04	0.06416	0.001595711	0.001966568
BENZENE	0	78.11	0	0	0
TOLUENE	0	92.14	0	0	0
NAPHTHA	0	128.17	0	0	0
PHENOL	0	94.11	0	0	0
H_2O	0.012	18.01	0.21612	0.005375078	0.005899705
O_2	0	32	0	0	0
N_2	0.663	28	18.564	0.461701576	0.325958702
CHAR	0.259	12.01	3.11059	0.077362869	0.1273353
S	0		0	0	0
NH_3	0.004				0.001966568
HCL	0				0
H_2S	0				0
CL_2	0				0

For the equilibrium model, it is observed that carbon conversion is extremely low. After pyrolysis, the molar flow of char entering the gasification reactions equals:

$$\dot{F}_{char}^{in} = 0.272 \text{kmol} \cdot \text{hr}^{-1}$$

The molar flow of char that exits the gibbs reactor equals:

$$\dot{F}_{char}^{out} = 0.259 \text{kmol} \cdot \text{hr}^{-1}$$

It is calculated that the EM yields a low carbon conversion of 62.8%. This carbon conversion mainly takes place in pyrolysis. The char conversion in gasification is only 8.5%. The corresponding CGE for these process conditions equals 64.3%. The contributors to the CGE are carbon monoxide and hydrogen. It can be observed that all tar species have been converted in carbon monoxide and hydrogen. The char that remains after gasification can also be used as fuel, nevertheless, the gasifier is aimed at producing gaseous energy carriers. When the energy of the produced char is accounted for, the process at chemical equilibrium converts biomass into other fuels with an efficiency of 92.3%. A sensitivity analysis of the equivalent ratio and its effect on the product gas is illustrated in figure 4.14 and 4.15.
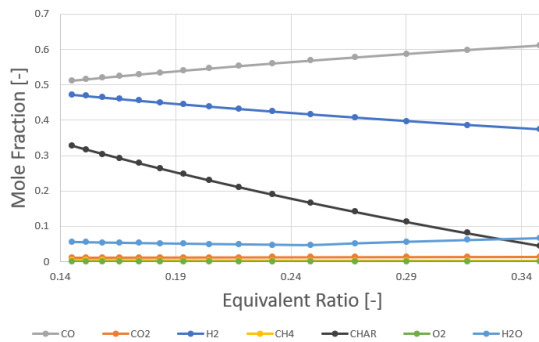
Figure 4.14: Molar fractions of CO, H_2, CO_2, CH_4 for an Equivalent Ratio between 0.14 and 0.35 for [GB] at a Temperature of 850°C and at atmospheric pressure
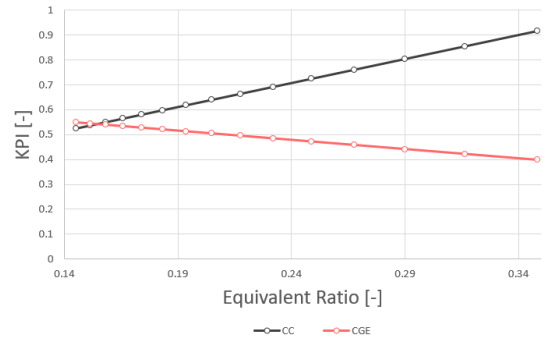
Figure 4.15: CC and CGE for an Equivalent Ratio between 0.14 and 0.35 for [GB] at a Temperature of 850°C and at atmospheric pressure

4.6. Kinetic Model

The kinetic model consists out of a chemical conversion submodel and a fluidization model. The chemical conversion of species is discussed in subsection 4.6.1. It is chosen to model the bedzone and freeboard separately due to its substantial difference in fluid dynamics. A simplified fluidization model has been design for the bedzone. This topic is discussed in subsection 4.6.2. Subsection 4.6.3 discusses the model of the freeboard. Finally, the complete kinetic model of the IHBFBSR is discussed and visualized in subsection 4.6.4.

4.6.1. Gasification Reactions

For the reason that both steam and air can be used in gasification experiments with the IHBFBSR, it is chosen to model all (partial) oxidation reactions and reforming reactions of the devolatilization products. These include the heterogeneous oxidation and reforming reactions of char and homogeneous oxidation and reforming reactions of CO, H_2, the four defined tars (benzene, toluene, naphthalene and phenol). In addition, two important reactions in gasification are the Boudouard and water gas shift reaction. Boudouard describes the reaction between char and CO_2 and the water gas shift is an equilibrium reaction between CO and H_2O as reactants and CO_2 and H_2 as products. The considered reactions have been summarized in table 3.

Table 4.11: Typical Reactions Occurring during Gasification

Reaction Nr	Reaction Name	Reaction Equation	Source
R1	Boudouard	$C + CO_2 \longrightarrow 2CO$	[33]
R2	Water Gas Shift	$CO + H_2O \longrightarrow CO_2 + H_2$	[18],[43]
Oxidation			
R3	Char Oxidation	$\alpha C + O_2 \longrightarrow 2(\alpha - 1)CO + (2 - \alpha)CO_2$	[18],[43]
R4	H_2 Oxidation	$H_2 + 0.5O_2 \longrightarrow H_2O$	[18],[36]
R5	CO Oxidation	$CO + 0.5O_2 \longrightarrow CO_2$	[18]
R6	CH_4 Oxidation	$CH_4 + 0.5O_2 \longrightarrow CO + 2H_2$	[18]
R7	C_6H_6 Oxidation	$C_6H_6 + 3O_2 \longrightarrow 6CO + 3H_2$	[36]
R8	C_7H_8 Oxidation	$C_7H_8 + 3.5O_2 \longrightarrow 7CO + 4H_2$	[54]
R9	$C_{10}H_8$ Oxidation	$C_{10}H_8 + 7O_2 \longrightarrow 10CO + 4H_2O$	[18]
Reforming			
R10	Water Gas	$C + 1.2H_2O \longrightarrow 0.8CO + 0.2CO_2 + 1.2H_2$	[18],[43]
R11	CH_4 Reforming	$CH_4 + H_2O \longleftrightarrow CO + 3H_2$	[43]
R12	C_6H_6 Reforming	$C_6H_6 + 2H_2O \longrightarrow 1.5C + 2.5CH_4 + 2CO$	[54]
R13	C_7H_8 Reforming	$C_7H_8 + 21H_2O \longrightarrow 7CO_2 + 29H_2 + 7CO$	[54]
R14	C_6H_5OH Reforming	$C_6H_5OH + 3H_2O \longrightarrow 2CO + CO_2 + 2.95CH_4 +$ $0.05C + 0.1H_2$	[54]

The kinetics for these reactions have been summarized in table 4 which can be found appendix H. For most homogeneous reactions, the reaction rate is expressed as a function of the concentration of the reactants according to the Rate Law equation. The reaction constant is described according to Arrhenius considering an Arrhenius constant and activation energy. The rate law equation is given by equation 4.44[38].

$$r_i = k_i [A]^a [B]^b \tag{4.44}$$

In the case of a simple reaction equation, such as:

$$aA + bB \longrightarrow cC + dD \tag{4.45}$$

With a rate constant described by Arrhenius' Law:

$$k_i = A_i \exp\left[\frac{-E_{a,i}}{R_g T}\right] \tag{4.46}$$

The heterogeneous char reactions are described by Langmuir Hinshelwood [LMHW] kinetics. In ordinary solid-gas reactions, the reaction can be divided into seven process steps[38]:

1. Mass transfer of the reactants from the gas phase to the film around the reacting particle

2. Pore diffusion inside the particle

3. Reactant adsorption onto the particle surface

4. Elemental reaction

5. Product desorption

6. Diffusion of products towards the film

7. Mass transfer of the products from the film to the gas phase

The process steps 1,2,6 and 7 depend on the hydrodynamics of the BFB reactor.

For using the LMHW kinetic expression, it is assumed that these mass transfer processes are not rate limiting. Another assumption that enables the use of LMHW kinetics is that reactions take place in isothermal conditions. The LMHW mechanism takes into account the adsorption of a gaseous reactant on the surface of a solid reactant as well as the chemical reaction rate. The reaction rate for LMHW kinetics is described by equation 4.47 and 4.48.

$$r_i = \frac{[\text{KineticTerm}][\text{DrivingForceTerm}]}{[\text{AdsorptionTerm}]} \tag{4.47}$$

$$r_i = \frac{k_i[\text{A}]^a}{1 + k_a[\text{A}]^a + k_c[\text{C}]^c + k_d[\text{D}]^d} \tag{4.48}$$

In the case of a simple reaction equation, such as:

$$a\text{A(g)} + b\text{B(s)} \longrightarrow c\text{C(g)} + d\text{D(g)} \tag{4.49}$$

With a reaction constant, and adsorption constants described by Arrhenius' Law as in equation 4.46.

4.6.2. Bedzone Model

It is chosen to model the bedzone and freeboard of the IHBFBSR separately in ASPEN Plus™due to their different behaviour in fluid dynamics. The bedzone is well mixed and has a nearly uniform temperature distribution. The residence time is relatively long compared to the residence time of species in the freeboard due to this effective mixing. The freeboard mainly hosts a gaseous phase and axial mixing is limited in the reactor. Residence time of the gasses are relatively short.

The bedzone of the reactor is modelled as a CSTR reactor in ASPEN Plus™. Arguments for selecting a CSTR are:

- Solid and gas phase present

- Well mixed volume

- Long residence time compared to freeboard

- Steady state process

- Continuous feed and product stream

All reactions, R1 to R14 are taken into account in the bedzone. After the introduction of pyrolysis products at the bottom of the bedzone, the pyrolysis products will be subject to the gasification agent. In the case of air-gasification, partial oxidation reactions R3 to R9 will play a role in parallel with reforming reactions R10-R14. Reforming occurs with the steam that is created from pyrolysis and is the sum of moisture and pyrolytic water content. In the case of steam gasification, the reaction rates of the oxidation reactions will be zero as the result of their dependency on the oxygen concentration in the bedzone. The reforming reactions will play a large role due to the abundance of steam in the bedzone. The Boudouard reaction and water gas shift reaction are also taken into account in the bedzone.

The CSTR is assumed to operate in isothermal conditions at steady state. The temperature is equal to the isothermal reactor temperature. In most experiments, this temperature ranges between 800 and 900 °C. The pressure is equal to atmospheric pressure.

The reactor volume of the CSTR is assumed to be equal to the volume of the vapour phase present in the bedzone. This volume equals the volume of the bedzone at fluidization minus the volume of the bed material. The size of the bed material has an influence on the reactor volume of the CSTR. It is chosen to variate the reactor volume in order to take into account the effect of the bed material particle size on the gasification process. The hydraulic diameter of the bedzone is constant over the height of the fluidized bed and is described by equation 4.50.

$$D_{Hyd} = \sqrt{d_{in}^2 - d_{burn}^2} \tag{4.50}$$

The inside diameter of the bedzone equals $d_{in} = 346 mm$ and the diameter of the bottom radiant tube burner equals $d_{burn} = 150 mm$. The hydraulic diameter of the bedzone equals $D_{Hyd} = 311.8 mm$. A total mass of 100 kg of bed material is present in the bedzone of the IHBFBSR. As described in chapter 3 the real density and bulk density of each of the bed materials is known. When there is no agent introduced in the bedzone, the bed is in the fixed bed regime and its height can be calculated by equation 4.51

$$L_{Fixed} = \frac{M_{bed}}{\rho_{bulk} A_{Hyd}} \tag{4.51}$$

In which A_{Hyd} is the cross-sectional area of the reactor as calculated by equation 4.52

$$A_{Hyd} = 0.25\pi D_{Hyd}^2 \tag{4.52}$$

The voidage of the bed material in the fixed bed regime is described by equation 4.53. The meaning of the voidage can be expressed as [m^{3}gas · m^{-3}reactor].

$$\epsilon_{Fixed} = 1 - \frac{\rho_{bulk}}{\rho_{real}} \tag{4.53}$$

It is assumed that the expansion of the bed at minimum fluidization equals 0.2 with respect to the height in fixed bed configuration.[29] The particle size of the bed material has a limited effect on the expansion for agent velocities less than 3 m · s^{-1}[26]. The expansion of the volume is equal to the increase in bedzone height for the reason that the cross-sectional flow area does not change. The corresponding bedzone volume at fluidization is calculated by equation 4.54.

$$V_{Fluid} = 1.2 \cdot L_{Fixed} \cdot A_{Hyd} \tag{4.54}$$

When the volume of the bed particles is subtracted from the bedzone volume, the volume of the vapour phase is obtained. The volume of the bed material particles is described by equation 4.55. The volume of the solid and gas phase are calculated by equation 4.56. This is the volume that will be entered in the CSTR reactor model in ASPEN.

$$V_{bed} = \frac{M_b}{\rho_{real}} \tag{4.55}$$

$$V_{CSTR} = V_{fluid} - V_{bed} \tag{4.56}$$

An overview of the bed material size dependent properties is presented in table 4.12.

Table 4.12: Overview of the Different CSTR Properties for Different Bed Material Sizes used at Experiments with the IHBFBSR

Bed Material	$d_p[\mu m]$	ρ_{real}[kg · m^3]	ρ_{bulk}[kg · m^3]	$L_{fixed}[m]$	$L_{Fluid}[m]$	$V_{Fluid}[L]$	$V_{CSTR}[L]$
F046	500	3950	1636	0.800	0.961	73.3	48.0
F054	400	3950	1665	0.787	0.944	72.1	46.8
F060	300	3950	1871	0.700	0.840	64.1	38.8

4.6.3. Freeboard Model

The freeboard of the reactor is modelled as a PFR reactor in ASPEN Plus™. Arguments for selecting a PFR are:

- Mainly gas phase present

- Uniform velocity pattern

- No axial mixing

- Short residence time

- Steady state

- Continuous feed and product stream

The PFR is assumed to operate in isothermal conditions at a temperature equal to the pyrolysis temperature. This temperature ranges between 800 and 850 °C. The pressure is equal to atmospheric pressure.

The PFR has a variable diameter over its height. This is partly due to the geometry of the gasifier and partly by the fact that the burners are present in certain areas of the freeboard. The hydraulic diameter of the geometry is calculated for all heights indicated in figure 4.16. Figure 4.16 also shows the ASPEN Plus™implementation of the CSTR and PFR stack. The hydraulic diameter is calculated by equation 4.50.

The cross-sectional flow area is calculated as in equation 4.52. The dimensions have been summarized in table 4.13. It can be observed from the table that the height of the bedzone H3, and consequently also the height of the freeboard, varies. This variation is the effect of the bed material particle size. The corresponding relative height of H3 to H8 is automatically calculated by FORTRAN code in ASPEN Plus™ The calculation for L_{PFR} is given by equation 4.57. The code can be found in Appendix I.

$$L_{\text{PFR}} = 2.454 - L_{\text{CSTR}} \tag{4.57}$$
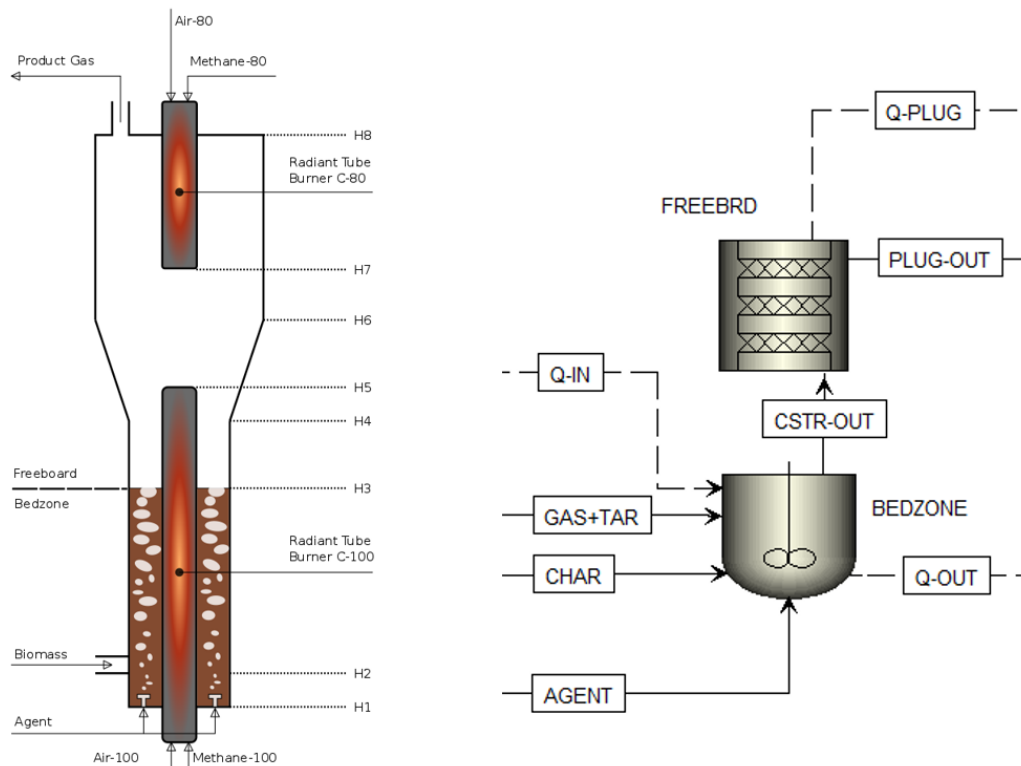
Figure 4.16: Geometry of the IHBFBSR (not at scale) with the Indication of Several Diameters as Function of Height.

Table 4.13: Diameter of the IHBFBSR as Function of Height

Reactor Section	Height Name	Height [m]	Relative Height w.r.t. the CSTR [%]	d_{in} [mm]	d_{burn} [mm]	D_{Hyd} [mm]
Bedzone	H1	0.00	0	346	150	311.8
	H2	0.2	$(0.2/L_{CSTR}) \cdot 100$	346	150	311.8
	H3	L_{CSTR}	1	346	150	311.8
Reactor Section	**Height Name**	**Height [m]**	**Relative Height w.r.t. the PFR [%]**	d_{in} [mm]	d_{burn} [mm]	D_{Hyd} [mm]
Freeboard	H3	L_{CSTR}	0	346	150	311.8
	H4	1.068	$(1.068-L_{CSTR})/L_{PFR}$	346	150	311.8
	H5	1.206	$(1.206-L_{CSTR})/L_{PFR}$	382.2	150	351.5
	H5'	1.206	$(1.206-L_{CSTR})/L_{PFR}$	382.3	0	382.3
	H6	1.453	$(1.453-L_{CSTR})/L_{PFR}$	447	0	447
	H7	1.704	$(1.704-L_{CSTR})/L_{PFR}$	447	0	447
	H7'	1.704	$(1.704-L_{CSTR})/L_{PFR}$	447	100	435.7
	H8	2.454	1	447	100	435.7

4.6.4. Gasification Model in ASPEN Plus™

Figure 4.17 visualizes the complete kinetic model of the IHBFBSR in ASPEN Plus™including the pyrolysis model. The biomasses, agent, pyrolysis model and modelled burners have been introduced in section 4.4 and 4.5. After the conversion of nitrogen, sulfur and chlorine species, the devolatilization products are separated into three streams. One stream contains all solids, the second contains all vapours and the third one contains all inerts. Amongst these inerts, the ash, H_2S, HCl and NH_3 can be found. The inert species do not enter the reactor section. The vapours and solids do enter the CSTR in the kinetic model. In the CSTR, partial oxidation takes place in the presence of air. The products and remaining reactants proceed to a PFR which models the freeboard. The reaction rates of the water gas reaction and the Boudouard reaction are different from the rates used in the CSTR for the reason that the density of the char particles has decreased according to the Shrinking Density Model. The change in kinetic rate can be found in appendix H.

For both the CSTR and PFR it can be quantified what the heat duty is of the reaction process. In order to do so, heat steams Q-PLUG and Q-OUT are introduced.

After the reactor section, the gasification products are mixed once again with the inert species. The resulting mix passes through two cyclones. The cyclones have been modeled by an ideal separator. For this separator, it is assumed that 100 % of the solids are separated from the product gas.
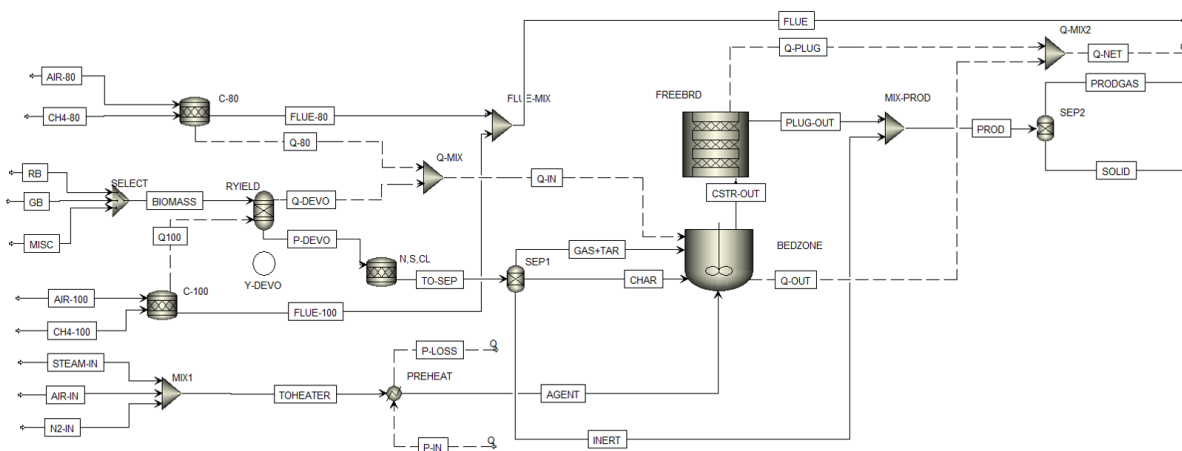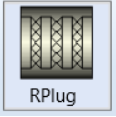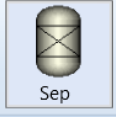
Figure 4.17: ASPEN Plus™Kinetic Model of the IHBFBSR

A summary of all the reactor blocks, that are added for the kinetic model, is given in table 4.14

Table 4.14: Summary of Additional Reactor Blocks in the ASPEN Plus™Kinetic Model of the IHBFBSR

Blockname	Block ID	Pictogram	Description
CSTR	BEDZONE	RCSTR	This CSTR models the bedzone of the IHBFBSR. The reactor volume depends on the particle size of the bed material and is between 38 and 48 L. The temperature in the bedzone equals the pyrolysis temperature in RYIELD. The pressure equals 1 atm. In the bedzone, both oxidation and reforming reactions take place.
PFR	FREEBRD	RPlug	This PFR models the freeboard of the IHBFBSR. The reactor height is defined as L=1.6m . The diameter varies as function of height and is given by table 4.13. The temperature in the freeboard equals the pyrolysis temperature in RYIELD. The pressure equals 1 atm. In the freeboard, mainly a gas phase is present and reforming reactions take place.
Separator	SEP2	Sep	This separator models the two cyclones that are present in the IHBFBSR set-up. The solids, char and ash, are removed from the product gas. This model assumes that all solids and gasses are completely separated.
Mixer	Q-MIX2	Mixer	This mixer combines the heat from the CSTR and the PFR in order to quantify the amount of heat that is transferred from the CSTR to the PFR.
Mixer	MIX-PROD	Mixer	This mixer combines the product output from the PFR with the inert stream that originates from separator SEP1. The combined stream is a model for the product gas (solids included) that exits the IHBFBSR at the top.

5

Results and Discussion

5.1. Model Validation

The experimental data set that is used for the model validation has been generated in February 2019. The gasification agent is air. Four different equivalent ratios have been selected:

$\lambda = 0.30, 0.20, 0.17$ and 0.15

The equivalent ratio has been adjusted by varying the feed rate of biomass. The agent flow is kept constant in order to assure fluidization at all equivalent ratios. Other constant process parameters are summarized in table 5.1.

Table 5.1: Process Conditions for the EM Corresponding to the Model Results Given in this Chapter.

Parameter	Symbol	Value	Unit
Reactor Temperature	T_r	840	[°C]
Biomass Type	-	GB	-
Biomass Mass Flow	$\dot{m}_{Biomass}$	11.6, 17.4, 20.5, 23.2	$[kg \cdot hr^{-1}]$
Air Agent Mass Flow	$\dot{m}_{Air}$	19	$[kg \cdot hr^{-1}]$
N$_2$ Agent Mass Flow	$\dot{m}_{N_2}$	4	$[kg \cdot hr^{-1}]$
Steam Agent Mass Flow	$\dot{m}_{Steam}$	0	$[kg \cdot hr^{-1}]$
Equivalent Ratio	λ	0.3, 0.2, 0.17, 0.15	-
Steam to Biomass Ratio	SB	-	-
Bedzone Material	-	F046	-
Bedzone Volume	V_{CSTR}	48	[L]

Key parameters that quantify the performance of the IHBFBSR are the carbon conversion and the cold gas efficiency. The values of these parameters have been measured as part of the experiment. For the carbon conversion, the char is removed after the experiment. The bed material is extracted from the reactor with a vacuum cleaner. The bed material is sieved to obtain the char that is left in the bed. The collected solids from the cyclones are combined in one vessel. Two samples of around 800 mL are collect and their masses are determined. The solids will be combusted for four hours. The weight difference indicated the mass of carbon present in the solids from the cyclones. The combustion process is repeated until there is no change of mass observed. The mass of carbon in the bed and carbon from the cyclones is considered to be the char residue.

A few assumptions have been made. First, The char consists only of solid carbon. Secondly, During start up of the reactor there is enough oxygen present for full combustion. It is assumed that no char is produced during start up. Another assumption states that the char mass is not reduced after the experiments and during cooling down of the reactor due to an absence of reactants. The values for carbon conversion of the experiments and of the model can be found in table 5.2.

Table 5.2: Values of the Carbon Conversion for the Four Evaluated Values of λ.

Equivalent Ratio λ	Mass Flow of Char $\dot{m}_{\mathrm{Char}}^{\mathrm{db}}$	Mass Flow of Biomass $\dot{m}_{\mathrm{Bio}}^{\mathrm{db}}$	Carbon Fraction in GB Biomass $Y_{\mathrm{C,Bio}}^{\mathrm{db}}$	Carbon Conversion CC
0.3	0.00	11.01	0.4841	1
0.2	0.540	16.52	0.4841	0.932
0.17	1.033	19.46	0.4841	0.89
0.15	1.477	22.02	0.4841	0.86

The cold gas efficiency is calculated with data on the heating value of all gasification products and with the product composition from the experiments and the model separately. The cold gas efficiency of the four experiments can be found in table 5.3. The heating values used in the calculations originate from IEA Bioenergy Agreement[64]. For the calculation of the CGE, it is important to take into account the fuel conversion in the burners as well. This is done by taking the power that is provided by the burners and multiply them by their efficiency. For these calculations a burner efficiency of 90 % has been assumed.

Table 5.3: Cold Gas Efficiency for the IHBFBSR for the Four Evaluated Values of λ.

Equivalent Ratio λ	$\dot{m}_i \cdot LHV_i$ [MJ·hr^{-1}]	$\dot{m}_{\mathrm{Bio}} \cdot LHV_{\mathrm{Bio}}$ [MJ·hr^{-1}]	Heat Produced $P_{\mathrm{burn}} \cdot \eta_{\mathrm{burn}}$ [MJ·hr^{-1}]	Cold Gas Efficiency CGE
0.3	253.14	241.86	128	0.52
0.2	404.90	362.79	128	0.71
0.17	488.90	427.4	128	0.77
0.15	555.92	483.72	128	0.78

The results from the experimental study are compared with the results from the model at the same process conditions. Only the yield of permanent gasses can be validated. It has not been able to gather data on the tar samples within the duration of this study. Without a tar analysis, it is not possible to determine the cold gas efficiency over the experiments. The data from the experiments and from the model is visualized in the graphs in figure 5.1 to 5.4. Each figure represents the results for a value of the equivalent ratio. From the figure can be concluded that the model predicts the gas composition relatively well.
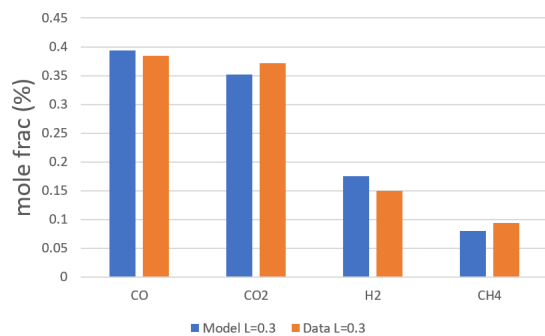
Figure 5.1: Gas Composition Data from the IHBFBSR (Blue) Compared to Model Output (Orange) for an Equivalent Ratio of $\lambda = 0.30$
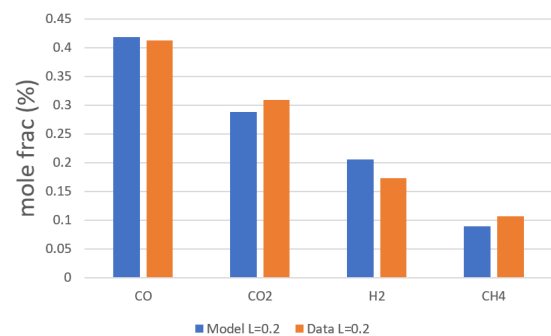
Figure 5.2: Gas Composition Data from the IHBFBSR (Blue) Compared to Model Output (Orange) for an Equivalent Ratio of $\lambda = 0.20$
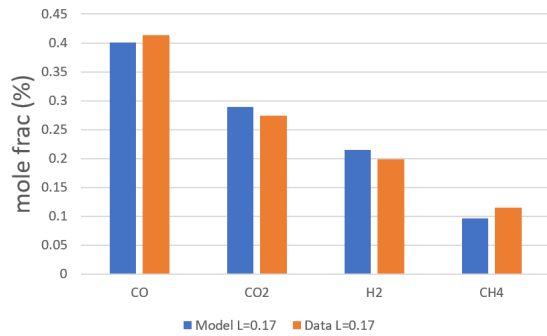
Figure 5.3: Gas Composition Data from the IHBFBSR (Blue) Compared to Model Output (Orange) for an Equivalent Ratio of $\lambda = 0.17$
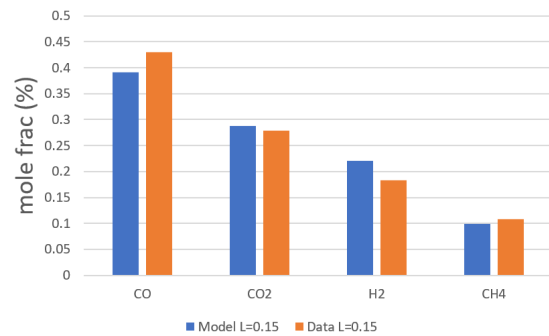
Figure 5.4: Gas Composition Data from the IHBFBSR (Blue) Compared to Model Output (Orange) for an Equivalent Ratio of $\lambda = 0.15$

The carbon conversion of the experiment ,with an equivalent ratio of $\lambda = 0.20$, is measured to be 76%. The model predicts a carbon conversion of 77.4%. The model and the experiments produce similar results. There are several mechanisms that can explain the small differences between the model outcome and experimental data. These mechanisms will be discussed in the following section.

5.2. Error between Experimental Data and Model Output

The results of the experiments and the model are not 100% the same. An error between the results can have various reasons. The absolute and relative error between the experimental data and the kinetic model can be found in table 5.4.

Table 5.4: Errors between the Mole Fractions of CO, CO_2, H_2 and CH4 from Experimental Data and from the Kinetic Model

Component X	Molar Fraction of X $\bar{Y}_X^{db}$ From Experimental Data	Molar Fraction of X $\bar{Y}_X^{db}$ From the Kinetic Model	Absolute Error Data-Model	Relative Error [Data-Model]/Data
$\lambda = 0.3$				
CO	0.385	0.357	0.028	0.072
CO_2	0.371	0.380	-0.009	-0.023
H_2	0.150	0.190	-0.040	-0.266
CH_4	0.094	0.073	0.021	0.220
$\lambda = 0.2$				
CO	0.412	0.408	0.004	-0.009
CO_2	0.309	0.281	0.028	0.091
H_2	0.173	0.235	-0.062	-0.359
CH_4	0.106	0.076	0.030	0.285
$\lambda = 0.17$				
CO	0.413	0.392	0.021	0.052
CO_2	0.274	0.282	-0.008	-0.029
H_2	0.198	0.245	-0.047	-0.237
CH_4	0.115	0.082	0.033	0.29
$\lambda = 0.15$				
CO	0.430	0.397	0.051	0.120
CO_2	0.278	0.285	-0.007	-0.025
H_2	0.183	0.0.250	-0.067	-0.365
CH_4	0.108	0.086	0.022	0.205

Considered causes for the error can be generally divided in errors or uncertainty in the model, or errors and uncertainty that origins from the experiment.

There are many reasons why the model can produce different results than what is physically happening. It is important to be aware of these limitations when the model is used for reactor optimization and design. Amongst other mechanisms, the error between the model and reality can be explained by the following mechanisms:

- The one-phase fluidization model is a very limited description of the fluid dynamics that are physically happening.

- The proximate and ultimate analysis that are used for the identification of the biomass can deviate from the real composition of the biomass. This can be due to measurement errors in the equipment that is used for these analysis' and by spread in composition over the biomass bulk compared to the analyzed sample.

- The pyrolysis model is based on a uniform temperature gradient over the biomass particle. It is also assumed that the particle is heated instantly to the pyrolysis temperature and that pyrolysis only takes place at this particular temperature. In reality it takes a finite amount of time to heat the biomass particle and a temperature gradient over the particle will be present. During the heating process, pyrolysis products will also be formed.

- It is assumed that the biomass particle pyrolyzes entirely before the pyrolysis products are subject to gasification reactions. In reality, there is an overlap between primary and secondary pyrolysis reactions as well as gasification reactions.

- The amount of pyrolytic water is described by an empirical relation found in literature. There will be an error between the actual amount of pyrolytic water produced and the model.

- The pyrolysis mass yields of the permanent gasses and the solids and liquids have been fitted on experimental data. There can be an error in the pyroprobe experiments due to measurement errors of a sample that is not representative for the biomass bulk. In addition, interpolation between the measurements for different temperatures will increase uncertainty.

- It is chosen to model only four convertional tar species. This is already more detailed compared to other kinetic gasifier models, but nevertheless the prediction will deviate from reality. In reality, many tar species are present in the reactor and all of the contribute to the gasification product composition, CC and CGE.

- It is assumed that the pyrolysis and gasification take place in isothermal conditions. In reality, there will be temperature gradients over the gasifier.

- The selected reactions for the gasification model are a collection of the most important reactions that contribute significantly to the product composition. In reality more reactions take place having a minor effect on the product composition.

- The reaction rates of the kinetics in the model have been found in literature. The rates have been determined by experiments and the process conditions of these experiments have been similar to those of the IHBFBSR, but not entirely equal. Differences in feed rates, temperature, reactor geometry and species present in the reactor will always lead to an error in the kinetic rates found in literature and the rates that describe the chemical conversion in the IHBFBFSR.

- It is assumed that reactants are spread out uniformly throughout the gasifier. In reality, local clusters of concentration excesses or deficits can cause a local change in reaction rate.

Besides the fact that the model deviates with respect to the physical system, data from the experiments can also deviate from what is happening in reality. Considered reasons are:

- Measurement errors in the sensors that operate the reactor (pressure sensors, temperature sensors ect.)

- A variance in the reactor temperature due to the control system, and inhomogeneous temperature distribution in the reactor.

- Measurement errors in the μ-GC, NDIR and O_2-detector.

- An error due to the fact that not 100% of the condensables are captured in the bottles.

- Errors due to the fact that measurements are taken at discrete time steps and are used to describe a continuous process.

- Char formation during start up of the reactor and char reduction during cooling down will affect the determination of the carbon conversion. The error of the measurement equipment and carbon handling when it is transported from the reactor to the measurement set-up will also affect the outcome.

- Operational errors of the valves that control feed rates for the gasification process.

- Deviation between the biomass sample has been analyzed and the biomass that is used for the experiment. Weeks or months of storage can cause a slight deviation in the composition of the pellets.

- Operational errors, and minor technical failures can slightly alter the process conditions in which the experiments take place.

When all these possible error mechanisms are taken into account it can be concluded that the model of the IHBFBSR resembles the data from experiments with air gasification in the IHBFBSR quite well.

5.3. Sensitivity Analysis

Within the time span of this project, it is only possible to conduct a limited amount of experiments. It is chosen to study the sensitivity of the parameters listed below. The steam to biomass ratio is an important process parameter for steam gasification. Unfortunately, the model has not been validated for steam gasification. Therefore, it is chosen not to include a sensitivity analysis of the SB. The influence of the bed material size can be modelled by a sensitivity analysis of the bezone volume. The sensitivity analysis will be discussed in subsections for each parameter.

- Equivalent Ratio

- Temperature

- Bed Material Size

5.3.1. Sensitivity of Equivalent Ratio

The equivalent ratio is described in section **??** as the ratio between supplied oxygen to biomass ratio and stoichiometric ratio of oxygen needed for full combustion of the fuel. A value of $\lambda = 1$ indicates full combustion. For values less then $\lambda = 1$, gasification takes place. The equivalent ratio is often varied between 0.1 and 0.4 is gasification. An optimal equivalent ratio is where the carbon conversion and cold gas efficiency are maximal. The sensitivity analysis on the product composition as function of the equivalent ratio is visualized in figure 5.5. The sensitivity analysis on the CC and CGE as function of the equivalent ratio is visualized in figure 5.6. The data has been produced by the kinetic model. The corresponding model result data can be found in appendix J. The process conditions for this analysis have been summarized in table 5.5.

Table 5.5: Process Conditions for the Kinetic Model Corresponding to the Sensitivity Analysis of the Equivalent Ratio

Variable	Symbol	Range	Unit
Equivalent Ratio	λ	$0.12 - 0.35$	-
Biomass Mass Flow	$\dot{m}_{\text{Biomass}}$	$10 - 24$	$[\text{kg} \cdot \text{hr}^{-1}]$
Parameter	**Symbol**	**Value**	**Unit**
Pyrolysis Temperature	T_{pyr}	840	$[°\text{C}]$
CSTR Temperature	T_{cstr}	840	$[°\text{C}]$
PFR Temperature	T_{pfr}	840	$[°\text{C}]$
Biomass Type	-	GB	-
Air Agent Mass Flow	$\dot{m}_{\text{Air}}$	19	$[\text{kg} \cdot \text{hr}^{-1}]$
N_2 Agent Mass Flow	$\dot{m}_{N_2}$	4	$[\text{kg} \cdot \text{hr}^{-1}]$
Steam to Biomass Ratio	SB	-	-
CSTR Volume	V_{CSTR}	48	$[\text{L}]$

From figure 5.5 can be observed that the fraction of solids is decreasing for increasing equivalent ratio until it reaches zero at approximately $\lambda = 0.25$. This point is referred to as the carbon limit. The gas fraction is increasing for increasing equivalent ratio until the carbon limit. Increasing the equivalent ratio beyond this point causes a decrease in the gas fraction of the gasification product. The condensable fraction contains the tars and water. This water includes the biomass' moisture and pyrolytic water. The tar fraction is more or less constant until the carbon limit and increases slightly beyond the carbon limit. Figure 5.6 clearly shows the carbon limit and corresponding values for CC and CGE.
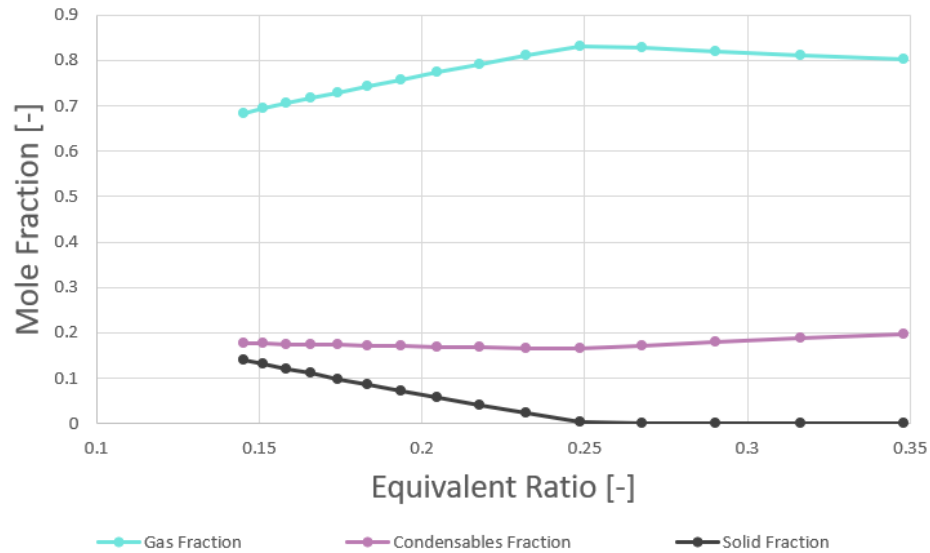
Figure 5.5: The Sensitivity Analysis on the Product Composition as Function of the Equivalent Ratio λ.
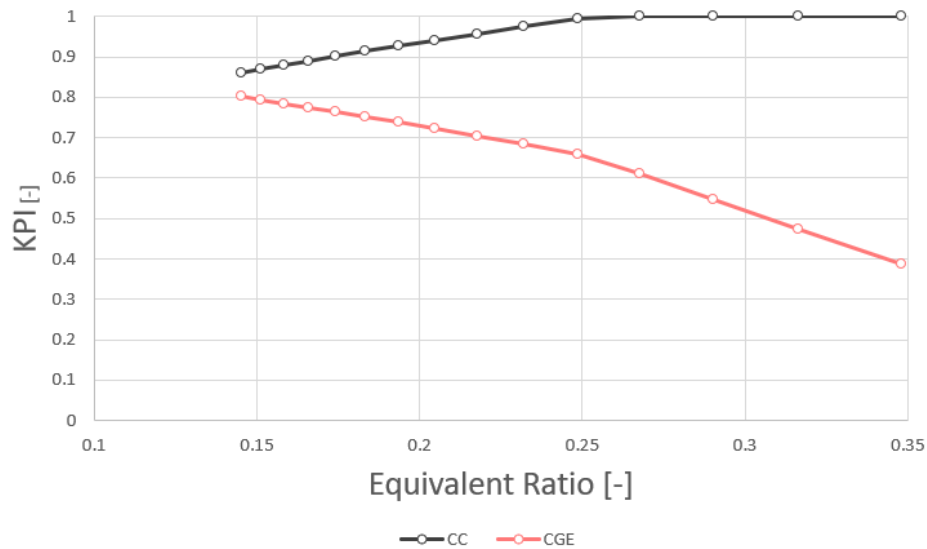
Figure 5.6: The Sensitivity Analysis on the CC and CGE as Function of the Equivalent Ratio λ.

The gas composition as function of ER as illustrated in figure 5.7 meets the expected result as described in section 2.3. For an ER 0.15, the char is not converted into products to its fullest potential. This means that in the model, a fraction of char leaves the gasifier unreacted. When the equivalent ratio is increased the amount of oxygen in the reactor increases. This leads to a decrease in the amount of char as the result of combustion. For an equivalent ratio of approximately 0.25, all char is converted into products. Further increasing the

equivalent ratio will increase the reaction rate of char oxidation as the result of a higher oxygen concentration in the bedzone. The oxidation of gaseous products will also increase The consequence is a lower yield of carbon monoxide and hydrogen and a higher yield of carbon dioxide. Increasing the equivalent ratio beyond 0.25 will lower the CGE as can be observed in figure 5.6. The theoretical optimum for this process is at an equivalent ratio of 0.25 where the carbon conversion equals unity and the CGE is maximal for full carbon conversion. The optimum will however shift as a result of varying other process conditions.
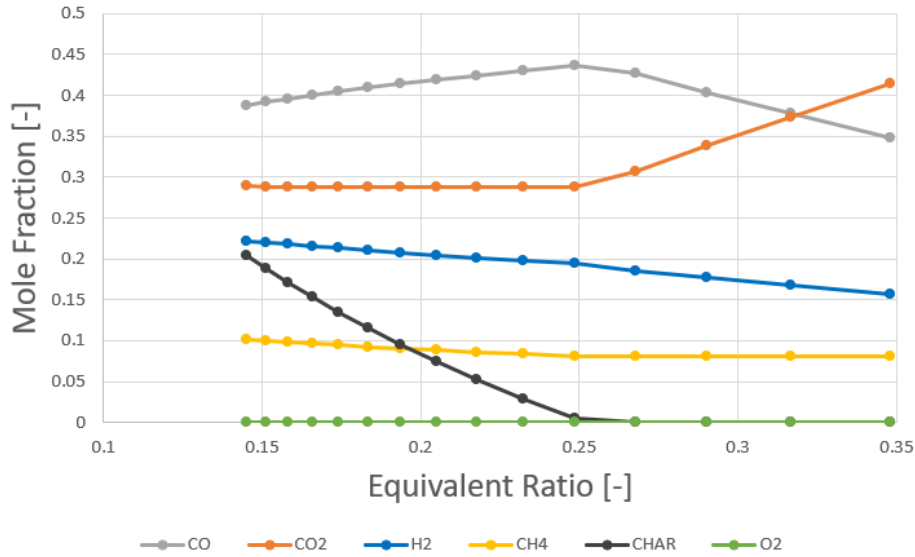
Figure 5.7: The Sensitivity Analysis on the Product Gas Composition as Function of the Equivalent Ratio λ.

The relative molar fractions of each of the tar groups and water with respect to the total molar flow of condensables is visualized in figure 5.8. Even though these results have not been validated yet with experimental data, it is interesting to see what the effect of the equivalent ratio is on the kinetics that have been taken into account for tar oxidation and reforming. Beyond the carbon limit, the water fraction increases, and therefore the relative fractions of the tars decrease. Besides an increase in the fraction of water, there is no significant increase or decrease in the tar species as function of the equivalent ratio.
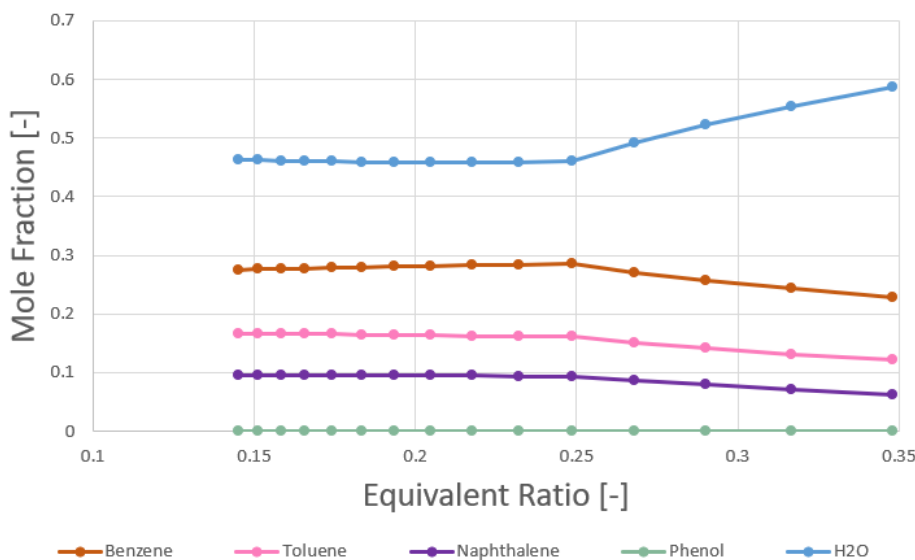
Figure 5.8: The Sensitivity Analysis on the Composition of the Condensable Fraction as Function of the Equivalent Ratio λ.

5.3.2. Sensitivity of Reactor Temperature

The temperature of the reactor is modelled to be constant for all pyrolysis and gasification reactions. The temperature influences the reaction rates and therefore the composition of the product. The temperature has been evaluated over a range between $T_r = 600 - 900 [°C]$. Within this range, the pyrolysis model interpolates on collected pyroprobe data. The sensitivity analysis on the product composition as function of the reactor temperature is visualized in figure 5.9. The sensitivity analysis on the CC and CGE as function of the reactor temperature is visualized in figure 5.10. The data has been produced by the kinetic model. The results have not yet been validated for the reason that the experimental set-up has not been able to collect this data. The corresponding model result data can be found in appendix J. The process conditions for this analysis have been summarized in table 5.6.

Table 5.6: Process Conditions for the Kinetic Model Corresponding to the Sensitivity Analysis of the Reactor Temperature

Variable	Symbol	Range	Unit
Pyrolysis Temperature	T_{pyr}	$600 - 900$	[°C]
CSTR Temperature	T_{cstr}	$600 - 900$	[°C]
PFR Temperature	T_{pfr}	$600 - 900$	[°C]
Parameter	**Symbol**	**Value**	**Unit**
Biomass Type	-	GB	-
Equivalent Ratio	λ	0.23	-
Biomass Mass Flow	$\dot{m}_{Biomass}$	15	$[kg \cdot hr^{-1}]$
Air Agent Mass Flow	$\dot{m}_{Air}$	19	$[kg \cdot hr^{-1}]$
N_2 Agent Mass Flow	$\dot{m}_{N_2}$	4	$[kg \cdot hr^{-1}]$
Steam Agent Mass Flow	$\dot{m}_{Steam}$	0	$[kg \cdot hr^{-1}]$
Steam to Biomass Ratio	SB	-	-
CSTR Volume	V_{CSTR}	48	[L]

Figure 5.9: The Sensitivity Analysis on the Product Composition as Function of the Reactor Temperature $T_r = T_{pyr}$.

From figure 5.9 can be concluded that the gas fraction increases for increasing temperature. The condensible fraction remains more or less constant and the solid fraction decreases for increasing temperatures. The carbon limit is reached for a temperature of 850 [°C] given that the experiment has been performed at an equivalent ratio of 0.23. The carbon limit will shift towards higher temperatures for lower values of the equivalent ratio and towards lower temperatures for higher values of the equivalent ratio.
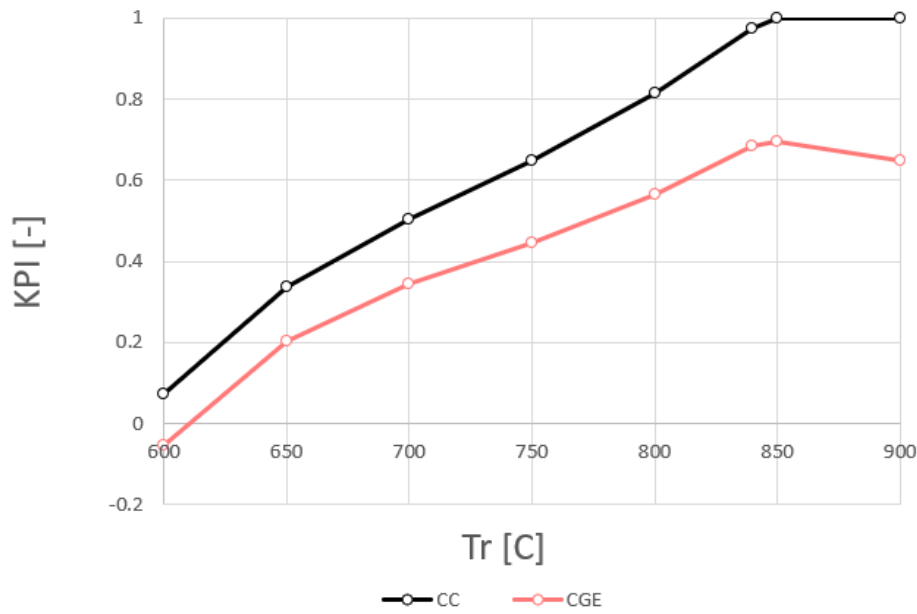
Figure 5.10: The Sensitivity Analysis on the CC and CGE as Function of the Reactor Temperature $T_r = T_{pyr}$.

Figure5.10 shows that the CGE is maximal at the carbon limit at approximately 850 [°C].
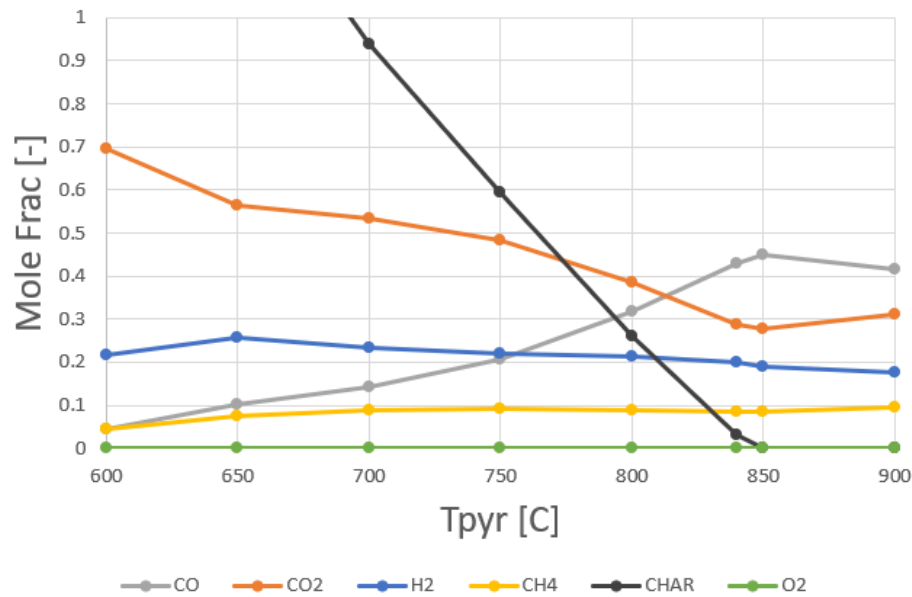
Figure 5.11: The Sensitivity Analysis on the Product Gas Composition as Function of the Reactor Temperature $T_r = T_{pyr}$.

From figure 5.11 can be observed that the fraction of carbon monoxide in the gas fraction is increasing for increasing temperatures below the carbon limit. This increase directly contribute to the increase in CGE as observed in figure 5.10. The fraction of carbon dioxide is decreasing for increasing temperatures below the carbon limit. Beyond the carbon limit, the opposite is valid. Carbon monoxide is decreasing and carbon dioxide increasing for increasing temperatures. For this reason, the CGE decreases beyond the carbon limit and reaches its maximum at the carbon limit.

Figure 5.12 shows the composition of the condensable products. The fraction of water decreases for increasing temperature below the carbon limit and increases for increasing temperature beyond the carbon limit.

The opposite is true for the tar species. It can be observed that the most abundant condensible hydrocarbon is benzene, followed by toluene, naphthalene and phenol. These fractions remain quite similar to the fractions of condensible hydrocarbons observed in the devolatilization products. This indicates that for an equivalent ratio of 0.23, the tar reactions have a relatively low impact on the product gas composition.
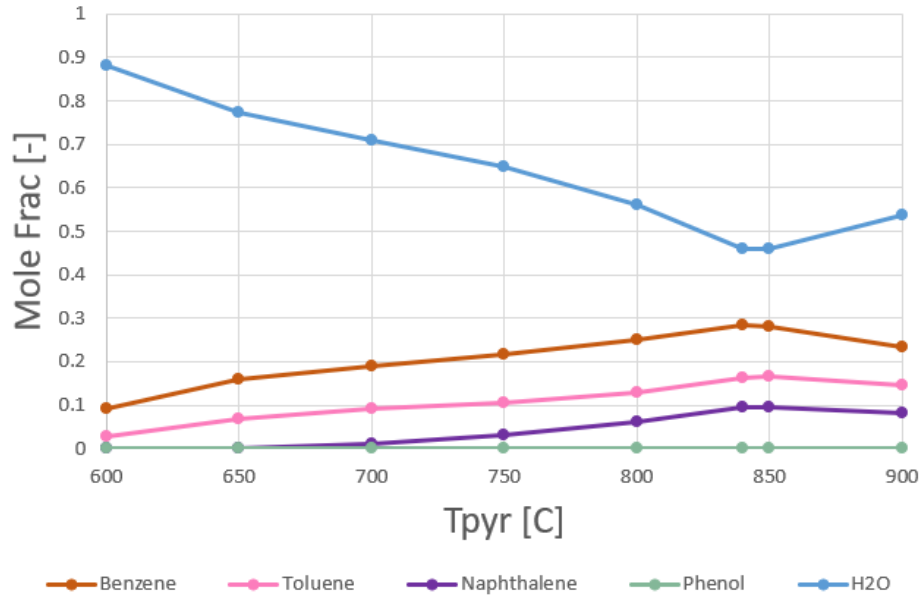
Figure 5.12: The Sensitivity Analysis on the Composition of the Condensable Fraction as Function of the Reactor Temperature $T_r = T_{pyr}$.

5.3.3. Sensitivity of Bedzone Volume

The bed material size has an influence on the volume of the emulsion phase in the bedzone. A smaller size leads to a lower volume of emulsion in the reactor. The experiments have been conducted with three different bed material sizes. In order to illustrate the effect of the bed material size, it is chosen to make a sensitivity analysis of the volume of the emulsion in the bedzone. The bedzone is modelled as a CSTR in ASPEN Plus™. The volume of the CSTR has been varied between $V_{CSTR} = 38 - 56$ [L]. A volume of 56 L represents a bed height that is equal to diameter H4 in figure 4.16. The sensitivity analysis on the product composition as function of the volume of the emulsion is visualized in figure 5.15. The sensitivity analysis on the CC and CGE as function of the volume of the emulsion is visualized in figure 5.14. The corresponding model result data can be found in appendix I. The process conditions for this analysis have been summarized in table 5.7.

Table 5.7: Process Conditions for the Kinetic Model Corresponding to the Sensitivity Analysis of the Volume of the Emulsion

Variable	Symbol	Range	Unit
CSTR Volume	V_{CSTR}	$38 - 56$	[L]
Parameter	**Symbol**	**Value**	**Unit**
Pyrolysis Temperature	T_{pyr}	840	[°C]
CSTR Temperature	T_{cstr}	840	[°C]
PFR Temperature	T_{pfr}	840	[°C]
Biomass Type	-	GB	-
Equivalent Ratio	λ	0.23	-
Biomass Mass Flow	$\dot{m}_{Biomass}$	15	[kg·hr^{-1}]
Air Agent Mass Flow	$\dot{m}_{Air}$	19	[kg·hr^{-1}]
N$_2$ Agent Mass Flow	$\dot{m}_{N_2}$	4	[kg·hr^{-1}]
Steam Agent Mass Flow	$\dot{m}_{Steam}$	0	[kg·hr^{-1}]
Steam to Biomass Ratio	SB	-	-

Figure 5.13: The Sensitivity Analysis on the Product Composition as Function of the Volume of the Emulsion V_{CSTR}.

Figure 5.13 shows that the influence of the bedzone volume on the product composition is relatively low. A slight increase in gas fraction and decrease in solid fraction can be observed for increasing bedzone volume.
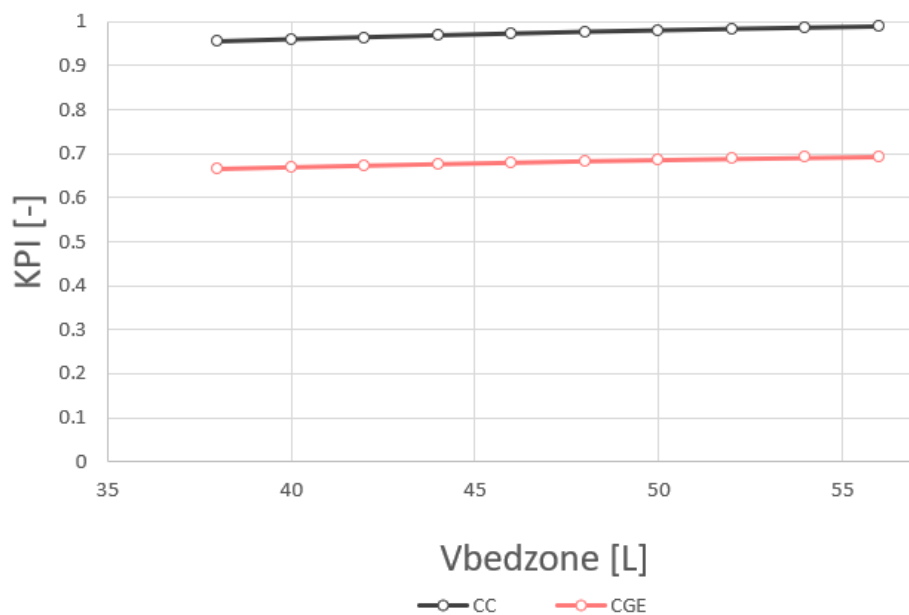
Figure 5.14: The Sensitivity Analysis on the CC and CGE as Function of the Volume of the Emulsion V_{CSTR}.

Figure 5.14 shows that the carbon conversion and CGE increase by 3% for increasing bedzone volume over the selected range of volumes. This seems not much, but an increase of 3% can lead to significant saving when applied at large scale production. The increase is mainly driven by the fact that more solids are being converted into gas and are not necessarily dependent on the change in gas composition.
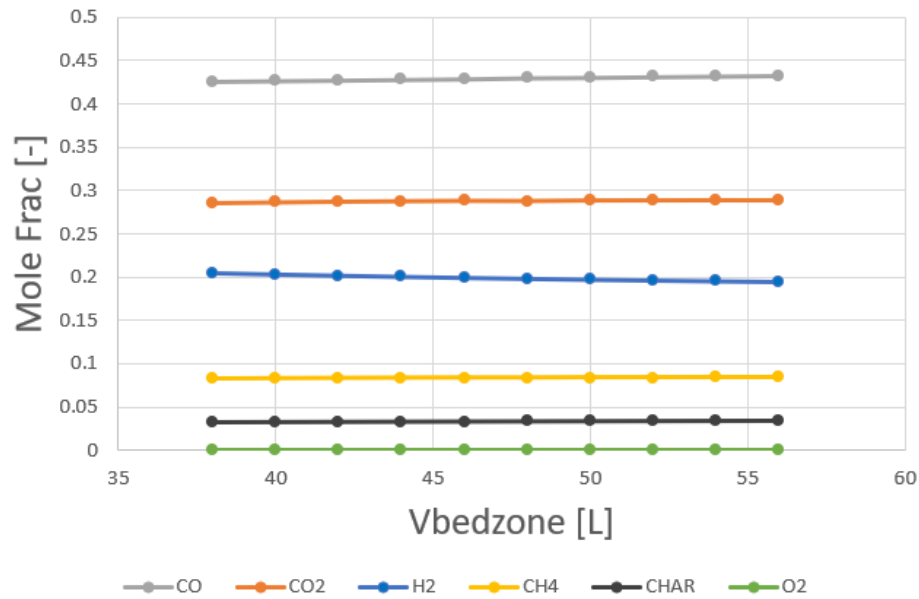
Figure 5.15: The Sensitivity Analysis on the Product Gas Composition as Function of the Volume of the Emulsion V_{CSTR}.

Figure 5.15 shows little increase and decreases in gas composition as function of bezone volume. It is therefore advised not to select the bed material size according to the optimal product gas composition. Instead, it is advised to select the bed material that fluidizes best by minimizing the pressure drop over the bed material. When bed material sizes become too small, there is a risk that the bed does not fluidize at all.
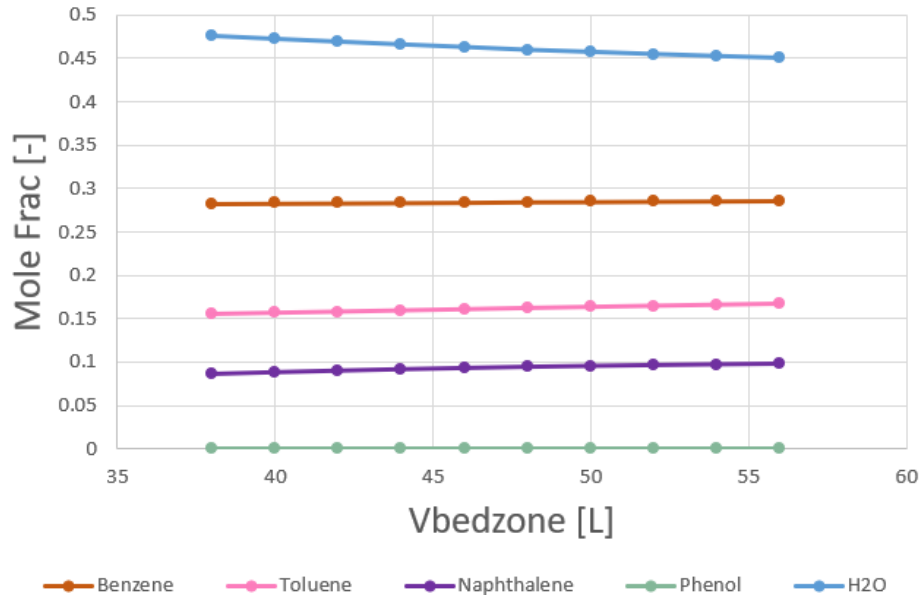
Figure 5.16: The Sensitivity Analysis on the Composition of the Condensable Fraction as Function of the Volume of the Emulsion V_{CSTR}.

From figure 5.16 can be concluded that there is an increase in the fraction of tar species in the condensable product fraction. For the reason that the HHV of these tar species is substantial (between 35 and 45 MJ·kg) they can be a possible additional reason for the slightly increasing CGE.

5.4. Energy Analysis

An energy balance is performed over the five main components of the IHBFBSR set up. The considered components are:

- Burner C-80 (Stoichiometric reactor)

- Burner C-100 (Stoichiometric reactor)

- Pyrolysis zone (Yield reactor)

- Bedzone (CSTR)

- Freeboard (PFR)

A control volume is defined over each component. For each control volume, the energy balance states that:

$$\text{Accumulation} = \text{Energy in} - \text{Energy out} + \text{Generation} \tag{5.1}$$

It is assumed that the reactor operates in steady state conditions. Therefore, the accumulation term becomes zero. The energy entering and leaving each control volume is the energy associated with the chemical species present in the inlet and outlet streams. For each control volume, heat is added or subtracted by chemical reactions. In addition, heat transport between the control volumes is possible. Finally, heat losses to the environment occur. The overall energy balance for each control volume is given by equation 5.2.

$$0 = \Sigma_i^n \dot{m}_i^{\mathrm{ar}} \cdot H_i \mid_{\mathrm{in}} - \Sigma_i^n \dot{m}_i^{\mathrm{ar}} \cdot H_i \mid_{\mathrm{out}} + \dot{Q}_{\mathrm{reaction}} - \dot{Q}_{\mathrm{loss}} - \dot{Q}_{\mathrm{transport}} \tag{5.2}$$

where H_i is the enthalpy of component i in $\mathrm{J \cdot kg^{-1} \cdot K^{-1}}$. $\dot{m}_i^{\mathrm{ar}}$ is the mass flow of component i on an a.r. basis in $\mathrm{kg \cdot m^{-3}}$. $\dot{Q}_{\mathrm{reaction}}$ is the heat production by the chemical reactions in the control volume in Watt. $\dot{Q}_{\mathrm{loss}}$ is the heat loss over the control volume in Watt. $\dot{Q}_{\mathrm{transport}}$ is the heat transport to the control volumes in Watt. A simple heat transfer model for the IHBFBSR is visualized in figure 5.17.
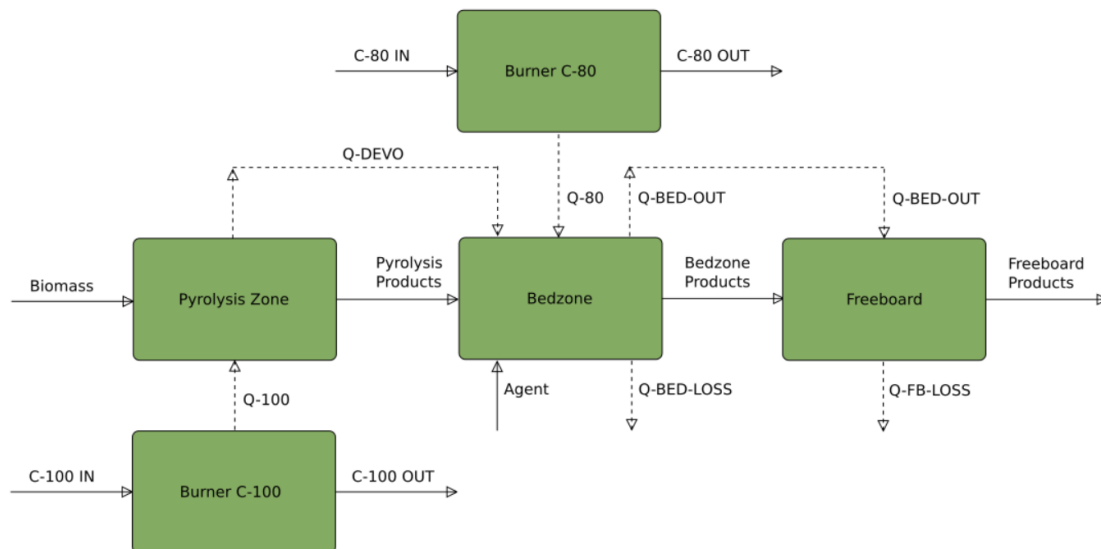
Figure 5.17: Heat Transfer Model for the IHBFBSR with the Five Main Components: Burner C80, Burner C100, the Pyrolysis Zone, the Bedzone and the Freeboard. Heat Transfer Between the Zones is Indicated by the Dotted Arrows. Mass Transfer Between the Zones is Indicated by Normal Arrows.

The burners C80 and C100 both receive methane and air as input. The species enter at room temperature, defined as $T_{\mathrm{room}} = 293.15\mathrm{K}$. Both burners operate at a temperature of $T_{\mathrm{burn}} = 1273.15\mathrm{K}$. The flue gasses contain CO_2, H_2O, N_2 and the remainder of O_2. All methane that enters the burner is fully converted. The surplus of oxygen is about 4% of the atomic ratio. The heat that is produced by burner C-80 is added to the bedzone. that is produced by burner C-100 is added to the pyrolysis zone.

The chemical energy in methane that is combusted in the burners can be calculated by multiplication of the mass flow of methane with its HHV as stated in equation 5.3. The value of $HHV_{\mathrm{CH_4}}$ equals:

$HHV_{\mathrm{CH_4}} = 55.5 MJ \cdot kg^{-1}$

$$\dot{Q}_{\mathrm{reaction}}^{\mathrm{burner}} = \dot{m}_{\mathrm{CH_4}} \cdot HHV_{\mathrm{CH_4}} \tag{5.3}$$

The pyrolysis zone receives the biomass at room temperature. The pyrolysis products leave the pyrolysis zone at the reactor temperature. For this model, the reactor temperature equals $T_r = 1113.15K$. The pyrolysis process requires a substantial amount of energy. Energy is supplied by the bottom burner and is drained from the rest of the bedzone.

The pyrolysis products enter the bedzone. The gasification agent, air in the case of this study, is supplied at a temperature of $T_{\mathrm{agent}} = 923.15K$. Reactions that take place in the bedzone are both oxidation reactions and reduction reactions. The reactions are carried out in isothermal conditions. As the result of these reactions. the bedzone produces heat. This heat is supplied to the pyrolysis zone and the freeboard.

In the freeboard only reduction reactions take place. Heat is supplied to the freeboard zone by the top burner C80 and from the bedzone. Similar to the bedzone, the reactions take place in isothermal conditions. The gasification products exit the reactor at a temperature equal to the reactor temperature.

The enthalpy of each species can be calculated from the enthalpy of formation and a correction for the temperature of the product stream. The relation is given by equation 5.4. It is assumed that all species are at atmospheric pressure for all streams.

$$H_i = H_{\mathrm{f},i}^0 + \int_{T_{\mathrm{room}}}^{T} Cp_i(T') \cdot dT' \tag{5.4}$$

The energy content of the mass steams and the heat flows for the burners as indicated by figure 5.17 have been obtained from the kinetic model in ASPEN Plus™. The heat losses are assumed to be zero. The control volumes have been modelled as adiabatic. The results can be found in table 5.8.

Table 5.8: Energy Analysis for the IHBFBSR System as Described in Figure 5.17. Heat Flows are Given in [kW]. The Reaction Energy of the Pyrolysis Zone, Bedzone and Freeboard Zone are Calculated From the Results From the Kinetic Model.

Burner C80	dQ [kW]	Burner C100	dQ [kW]
C-80-IN	2.2035	C-100-IN	3.6683
C-80-OUT	-15.0500	C-100-OUT	-25.0453
Q-80	-12.8994	Q-100	-21.3771
$\dot{Q}_{\mathrm{reaction}}^{c80}$	25.7458	$\dot{Q}_{\mathrm{reaction}}^{c100}$	42.7541
SUM	0	SUM	0

From table 5.8 can be concluded that the burners operate at an efficiency of 50%. This is the case when the air and methane input is not preheated by the flue gasses. In the experimental set-up, there is heat exchange between the inlet and outlet of the burner. It is advised to maximize this heat transfer in order to increase the efficiency of the burner. A higher efficiency will lead to a lower methane consumption. The cold gas efficiency is calculated by equation 1.2. For the calculation of the CGE it is assumed that the burners have an efficiency of 90% as the result of efficient heat transfer between inlet and outlet gasses.

The energy supply of biomass is assessed as the product of its mass flow and HHV as described by equation 5.5. The value of HHV_{BIO} equals:

$HHV_{\mathrm{BIO}} = 20.5 MJ \cdot kg^{-1}$

$$\dot{Q}_{\mathrm{BIO}} = \dot{m}_{\mathrm{BIO}} \cdot HHV_{\mathrm{BIO}} \tag{5.5}$$

The energy supply of biomass at an equivalent ratio of 0.23 and a mass flow of $\dot{m}_{BIO} = 15\,kg\cdot hr^{-1}$ equals:
$$\dot{Q}_{BIO} = 85.4167\,kW$$

The energy flow of the gasification products at an equivalent ratio of 0.23 is obtained from the kinetic model and equals:
$$\dot{Q}_{GAS} = 93.93\,kW$$

The overall efficiency of the system is maximal when all char is converted. Nevertheless, char build-up has been observed during the experiments. When the process yields a net production of char, it is advised to look into possibilities to use the char for energy production of the IHBFBSR. In addition, it is advised to look into possibilities to separate the tars from the product gas and combust the tars for energy production in the IHBFBSR. This will increase the overall energy efficiency.

5.5. Discussion

The optimal process conditions take place where carbon conversion and cold gas efficiency are maximal. At a temperature of 840 [°C], the optimal equivalent ratio is approximately equal to 0.25. For these conditions, the optimal bedzone volume should be maximized without loosing the fluidization behaviour.

A better more detailed model will theoretically yield a better optimization strategy which could increase productivity of the gasifier and selectivity of the products. Therefore, it is important to reflect on the kinetic model and ensure it is developed to its fullest potential. There is always a trade-off between the level of detail and effort put into the model in contrast with the accuracy of the results. This section lists several potential design improvements to the kinetic model. The considered design improvements are:

- Internal heat transfer limitation in pyrolysis

- Incorporate a more detailed Fluidization Model

- Mass transfer limitation for char oxidation

- Heat transfer model of the bedzone

- Reliability assessment of the kinetics from literature

Most of the suggested improvements can be reviewed in another study, but the improvement of incorporating the internal heat transfer limitation in pyrolysis has been analyzed to some extend.

The pyrolysis model as implemented in section 4.4 assumes that pyrolysis takes place at isothermal conditions and that there is no internal heat transfer limitation. Section 4.2 shows, as the result of calculating the Pyrolysis numbers and thermal Biot number, that internal heat transfer limitation is very likely in the pyrolysis conditions of the IHBFBSR. Taking this heat transfer limitation into account, would provide a more accurate model.

It is proposed to divide the pyrolysis particles into multiple radial sections. For the demonstration of this example, three sections are chosen. More sections can be added if the desired level of detail needs to increase. In the example, a single biomass particle is divided into an outer shell, middle shell and inner core as illustrated by figure 5.18. The particle is divided into three equal volume fractions. A temperature gradient is present over the radius of the particle. It is assumed that the temperature of the outer shell is equal to the pyrolysis temperature. The pyrolysis temperature is equal to the bedzone temperature as steady state conditions prevail in the bedzone. T_0, T_{r_1} and T_{r_0} represent the temperature at the centre, middle and outer shell of the particle respectively.

It is assumed that thermal conduction is the only heat transfer mechanism inside the biomass particle. The average temperature of the inner core and of the middle shell can be calculated by Fourier's Law. The relation between steady state heat flow and the temperature as function of the particle radius is given by equation 5.6[37].
$$\dot{Q} = \frac{4\pi k_{b,eff}(T_{r_2} - T_{r_0})}{1/r_2 - 1/r_0} \tag{5.6}$$
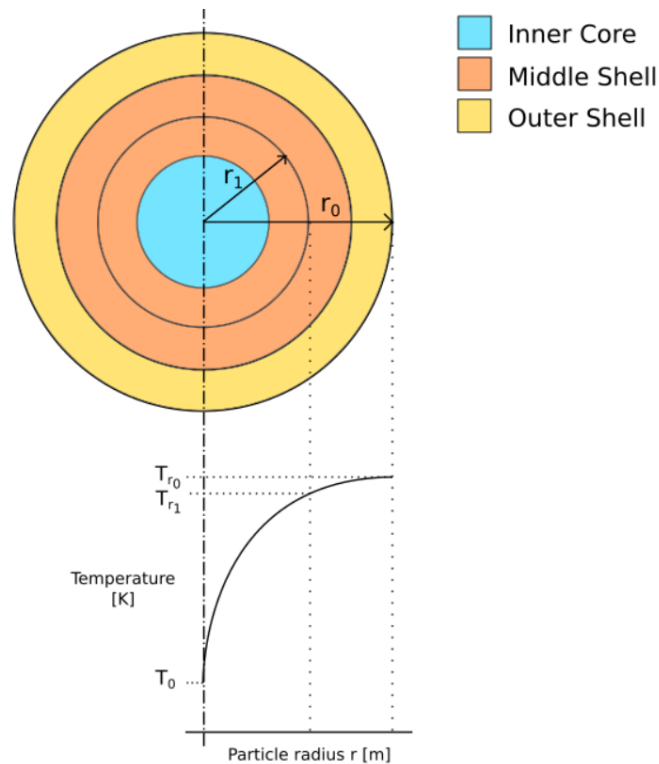
Figure 5.18: Single Biomass Particle Divided into Three Sections for Modelling Internal Heat Transfer Limitation

Both the temperature gradient over the particle and the heat flow are unknown. The biomass particle enters the reactor at $T_{b,0} = 20°$C. The biomass is fastly heated with a heating rate in the range of $600 \ °C \cdot s^{-1}$. The particle shell will reach the pyrolysis temperature within 1.5 seconds. The temperature of the inner core will lag behind due to the internal heat transfer limitation. The description of the temperature profile over the particle radius is complex because in reality steady state is not reached.

Nevertheless, in order to illustrate the effect of this suggested model improvement it is decided to assume the temperature profile over the particle. It is assumed that the temperature of the inner core is 50 degrees below the pyrolysis temperature. The temperature of the middle shell is 20 degrees below the pyrolysis temperature.

The three section have been implemented in ASPEN Plus™by adding two extra yield reactors. The separator splits the biomass feed into three equal shares. The configuration is visualized in figure 5.19.

The results of the model with and without compensation for the internal heat transfer limitation have been compared to the experimental data from section 5.1. The results can be found in figure 5.20.

From the figure can be concluded that the results of the model change significantly and do not resemble the experimental data when internal heat transfer is accounted for. The bars in grey indicate the results from the model that takes Internal Heat Transfer [IHT] into account. The results illustrate that the gas composition of the product stream is highly dependent on pyrolysis conditions. Perhaps the assumed temperatures of the individual particle layers do not represent the reality well.
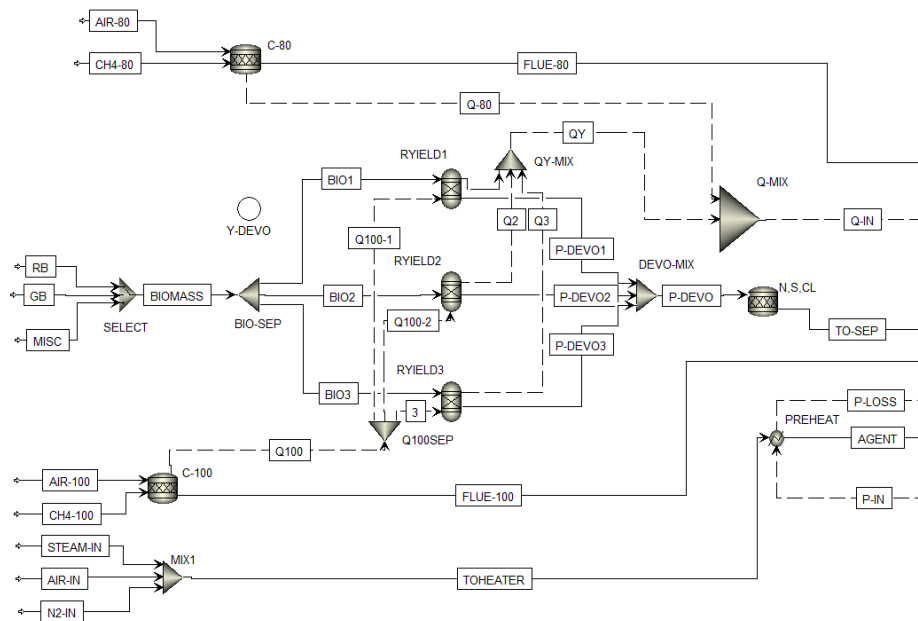
Figure 5.19: ASPEN Plus™Model of Biomass Pyrolysis with Three Different Yield Reactors for Internal Heat Transfer Limitation.
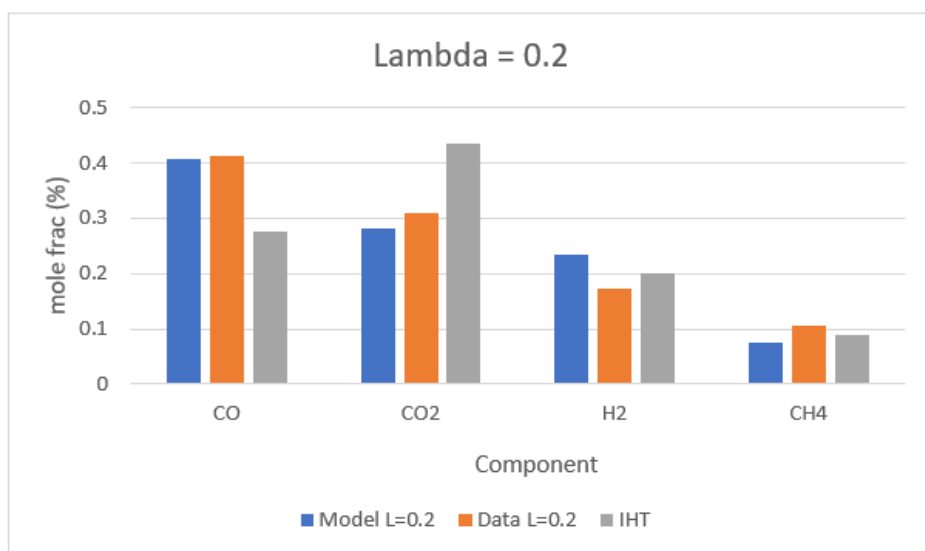
Figure 5.20: Gas Composition from Experimental Data and the Kinetic Model With and Without Internal Heat Transfer [IHT] Included in the Pyrolysis Model

It is advised to study the influence of the pyrolysis process conditions on the composition of the gasification products. It is also advised to look into options for modelling the internal heat transfer limitation in pyrolysis.

6

Conclusions and Further Developments

This chapter concludes the most important findings of this study. The first section will answer the main research question by answering the research sub questions. The second section reflects on the execution of this study and proposes further developments.

6.1. Conclusions

The main research question of this study has been stated as: "How does the Indirectly Heated Fluidized Bed Reactor perform in terms of product yield, product quality and energy efficiency and how does its performance compare to other indirectly heated gasifiers?" In order to answer this question, several sub-questions have been formulated in section 1.3. Each sub questions is repeated in the paragraphs below and the answer is provided as well.

The IHBFBSR set-up at the TU-Delft has had technical difficulties with the steam supply during the duration of this study. The main cause for this problem had been condensation of water in the steam line at the location of the main control valve. This kind of challenges are to be expected when a reactor is still in its commissioning phase. Due to these difficulties, it had not been able to perform experiments with steam as gasifying agent. In addition, technical difficulties have prevented the tars from the experiments to be analyzed. The tar composition is necessary for the determination of the cold gas efficiency of the experiments. This study can therefore only reflect on the CGE as calculated by the model. As the result of these technical difficulties, the amount of experiments with the IHBFBSR had been limited.

The main purpose of the IHBFBSR is to separate combustion and gasification reactions and facilitate efficient heat transfer between the two processes by radiant tubes. For this reason, it is necessary to perform experiments with steam in the future and validate the model for steam gasification as well. For this study, the performance of air gasification with the IHBFBSR is assessed.

During this study, both an equilibrium model and a kinetic model have been design. The molar fractions of the permanent gasses CO, CO_2, H_2 and CH_4, produced by the kinetic model, have been validated by experiments with the IHBFBSR for four different values of the equivalent ratio. In addition, the experimentally determined carbon conversion resembles the carbon conversion as calculated by the model. As mentioned earlier, the cold gas efficiency cannot be validated, but the results from the model are in the range of 65-70% around the sub-optimal process conditions. These values of the CGE resemble the CGE reported in literature of similar allothermal biomass gasification set-ups.

The first sub question is: "What is the effect of Equivalent Ratio ratio on the product selectivity, CC and CGE? For which equivalent ratios can the IHBFBSR be operated optimally?". The sensitivity analysis of the equivalent ratio shows that the gas fraction in the gasification products increases for ER values below the carbon limit. The condensable fraction remains more or less constant and the solid fraction decreases in this domain. At the carbon limit, all solids, besides the ash, have reacted and the solid fraction becomes nearly zero.

The gas fraction decreases for ER values beyond the carbon limit while condensable species slightly increase. This increase is mainly caused by an increase of water (steam) in the product.

The sensitivity analysis of the equivalent ratio also shows that CGE increases for a decreasing equivalent ratio. The carbon limit is reached at an equivalent ratio of 0.25 given that the process takes place at a temperature of 840 °C. This temperature and equivalent ratio are considered sub-optimal operating conditions. At the carbon limit, the carbon conversion equals 100% by definition and the cold gas efficiency equals 65.9%.

The second sub question is: "What is the effect of reactor temperature on the product selectivity, CC and CGE? For which temperature(s) can the IHBFBSR be operated optimally?". For increasing remperatures the gas fraction in the gasification product increases while the solid fraction decreases. This is in line with the expectations. When the carbon limit is reached, the solid fraction equals (nearly) zero and the gas fractions starts to decrease for increasing temperatures beyond the carbon limit. The sensitivity analysis has been performed at an equivalent ratio of 0.23. The corresponding temperature for which the carbon limit is reached equals 850 °C. This temperature and equivalent ratio are considered sub-optimal operating conditions as well. It can now be concluded that both the equivalent ratio and operating temperature influence the carbon limit. It is advized to maximize the temperature to the limits of the reactor set-up. In the case of the IHBF-BSR, the maximum temperature that can be attained for long periods of time equals 850 °C. Optimal process conditions are for an equivalent ratio of 0.23. The corresponding cold gas efficiency equals 69.7%.

The third sub question is: "What is the effect of bed material size on the product selectivity, CC and CGE? For which bed material size can the IHBFBSR be operated optimally?" The carbon conversion and cold gas efficiency increase for an increasing bedzone volume. Over the evaluated range of bezone volume (38-56 L) the CC and CGE both increase by as much as 3%. The volume of the vapour phase in the bedzone, referred to as the modelled bedzone volume, is determined by the bulk density of the bed material given a constant expansion of the bed at fluidization. The bulk density is determined by the particle size of the bed. From the sensitivity analysis of the bedzone volume can be concluded that larger bed material particle size yield a slightly higher CC and CGE. It is important to select a particle size that will not influence the fluidization behaviour of the IHBFBSR. Extremely large or small particles can cause that the bed cannot be fluidized. It is desired to maximize the bed material size given that the particles will still be of Geldart category B. For the bed material corundum that is used at the IHBFBSR, the maximum particle size equals 600 micron. This can be observed in figure 2.14. To be safe and assure fluidization at all times, it is advised to continue working with the currently available bed material with a size of 500 micron.

The fourth sub question is: "What are (sub)optimal operation conditions in terms of ER, temperature and bed material size, given a set of product quality boundaries?" This question has already been answered in the previous paragraphs. Sub-optimal conditions for the IHBFBSR take place at a reactor temperature of 850 [°C], which is the maximal controlable temperature of the reactor. At this temperature, the carbon limit is reached for an equivalent ratio of 0.23. By definition, the carbon conversion equals 100%. In reality, the carbon conversion will not be 100% due to a fraction of unreacted biomass, the condensation and fouling of tars in the reactor or the formation of other contaminants. The only measured carbon conversion of the IHBFBSR from experimental data equals 76%. The cold gas efficiency at the carbon limit equals 69.7%. Optimal process conditions are where the particle size of the bed material is maximized without loosing the fluidization behaviour of the bed. The maximum particle size equals 600 micron.

The fifth sub question is: "How does the performance of the IHBFBSR compare to other allothermal gasifiers?" A comparison has been made between several existing allothermal biomass gasifiers and the IHBFBSR in section 2.5. The results are summarized table 6.1. Several other allothermal technologies reach a 100% carbon conversion by the combustion of residual char. This is not an option for the IHBFBSR. It is important to optimize process conditions that maximize the carbon conversion in order to prevent char build up in the reactor. The reported CGE for the IHBFBSR origins from the model, not from measurements.

Table 6.1: Advantages and Disadvantages of the Discussed Allothermal Biomass Gasification Projects in Section2.5. The CC and CGE of each Gasifier is Reported as well.

Gasifier	Advantages	Disadvantages	CC	CGE
MILENA	- OLGA Tar removal for tar combustion	- Substantial heat loss as a result of the "from outside to inside" heat transfer direction	100%	80%
Heat Pipe Reformer	- Low required heat transfer area	- Hydrogen diffusion from the reformer into the heat pipes - Erosion of the heat pipes	85%	75%
FICFB	- Low char content in fly ash. As a result, fly ash can be processed similarly to ash from the combustor - Proven concept. Continuous operation	- Economic viability is dependent on a local supply of biomass	100%	80%
SilvaGas	- Large production capacity - Economical viability is proven - Process stability	- No disadvantages or challenges mentioned in publications	100%	80%
IHBFBSR	- Effective temperature control by external heat source - Complete separation of combustion and reforming	- Bed removal limitation	76%	69.7%

The sixth sub question is: "How energy efficient is the IHBFBSR?" The burners operate at an efficiency of 50 % when the air and methane input is not preheated by the flue gasses. In the experimental set-up, there is heat exchange between the inlet and outlet of the burner. It is advised to maximize this heat transfer in order to increase the efficiency of the burner. A higher efficiency will lead to a lower methane consumption. The overall efficiency of the system is maximal when all char is converted. Nevertheless, char build-up has been observed during the experiments. When the process yields a net production of char, it is advised to look into possibilities to use the char for energy production of the IHBFBSR. In addition, it is advised to look into possibilities to separate the tars from the product gas and combust the tars for energy production in the IHBFBSR. This will increase the overall energy efficiency. The IHBFBSR is expected to operate at an cold gas efficiency of 69.7%.

The seventh and final sub question is: "What mechanisms, considering chemical rate, heat transfer and mass transfer, are rate limiting in biomass pyrolysis and heterogeneous char reactions?" It is concluded that the pyrolysis step in the IHBFBSR is rate limited by internal heat transfer. The Pyrolysis number is well below one for all considered kinetic rates of pyrolysis. The considered chemical rates and their corresponding Pyrolysis numbers and thermal Biot number have been summarized in table 6.2.

Table 6.2: Values for the Pyrolysis Numbers and Biot Number for Each of the Chemical Rates Stated by Nunn[41], Reina[49] and Pyle and Zaror(1984)[45].

Kinetic Rate	Source	Py	Py'	Thermal Bi
206.24	[41]	$Py = 3.75 \cdot 10^{-5}$	$Py' = 1.38 \cdot 10^{-5}$	$Bi_t = 3.67$
0.035	[49]	$Py = 0.221$	$Py' = 0.810$	$Bi_t = 3.67$
1.81	[45]	$Py = 4.27 \cdot 10^{-3}$	$Py' = 0.016$	$Bi_t = 3.67$

The internal heat transfer limitation is not taken into account in the current kinetic model. This is a point of attention for further development of the model. It is advised to look into this topic for further reseach.

It has been calculated if there is a mass transfer limitation for the heterogeneous char gasification reactions. The Thiele modulus and mass Biot number have been calculated for char oxidation, the water gas and Boudouard reaction. The values for the dimensionless numbers are summarized in table 6.3.

Table 6.3: Values for the Thiele modulus and Mass Biot Number for Char Oxidation, Reforming and the Boudouard Reaction. Included are Corresponding Variables that are Used to Calculate the Dimensionless Numbers.

Reaction	Kinetic Rate	Reactant i	Thiele Modulus Th	Biot number Bi_m	Mass Transfer Limitation?
Char Oxidation	84054.6	O_2	123.62	27.52	Y
Char Reforming	2.9844	H_2O	0.66	25.90	N
Boudouard	0.2717	CO_2	0.24	28.80	N

From the table can be concluded that only char oxidation experiences a mass transfer limitation. This mass transfer limitation has also not been taken into account in the model.

As result of experience with the IHBFBSR it is concluded that several design improvements can be made for scale up of the IHBFBSR. In the current IHBFBSR set-up, the biomass enters at a single entry point in the gasifier. It is expected that the biomass is spread heterogeneously throughout the reactor and therefore the reactor volume is not being utilized to its fullest potential. A second challenge in handling the IHBFBSR has been the removal of bed material an char. As the result of gasification, not all char is converted and char builds up inside the reactor. As a result, the char needs to be removed after some experiments and this counters continuous operation which is desired for commercial scale-up. Also, the bed material needs to be replaced once in a while. For the current set-up, there is no easy way to remove the bed material. This task proves to be even more difficult as the result of the annulus shape of the reaction chamber due to the radiant tube in the center. For commercial scale up, it is advised to make use of a circulating fluidized bed reactor or twin bed reactor.

6.2. Further Developments

This section reflects on the methodology of this study and discusses its limitations. This section will suggest improvements for future work on this topic.

Theoretically, the model can also work for stream gasification, although the model has not been validated for steam gasification. The main purpose of the research on allothermal gasifiers is to remove the combustion process from the gasification process. It is therefore crucial to do experiments with steam in the future. It is proposed to validate the current kinetic model for steam gasification and compare its performance with other allothermal gasifiers.

What makes this allothermal gasifier unique compared to other allothermal gasifiers is the use of radiant tube burners. It is therefore advised to study the heat transfer between these radiant tubes and the gasification reaction chamber thoroughly. In addition, it is advised to look into degradation mechanisms for the radiant tube burners in the process conditions that take place in the gasifier. The hypotheses is that the species present in the reactor might degrade the steel radiant tubes which can be a drawback for continuous operation. Finally, it is advised to look into the fluid dynamics of the annulus shaped gasification chamber. Because of the radiant tubes, the gasification chamber has this unusual geometry which can effect fluid dynamics and therefore its performance.

The current kinetic model, as described in section 4.6, has only been validated for carbon conversion and for the yield of the permanent gasses. Tar samples from the pyroprobe experiments are available in order to redesign the lumped tar model, but due to technical difficulties, this has not been possible yet during this study. The use of four lumped tar groups in the kinetic model is a novel approach compared to other kinetic models for biomass gasifiers. From a scientific perspective, it would be interesting to reflect on the added value of using multiple tars in the model. It is advised to validate the kinetic model with tar samples from experiments with the IHBFBSR.

For now, the tar species have been quantified with data from literature[6]. In the future, it would be better to compose a new lumped tar model based on the tar samples from the pyroprobe experiments. The new model can also be validated with tar samples from experiments with the IHBFBSR. It is advised to review the added value of such a model composed of multiple tar groups.

For this study, it is chosen to use a very limited fluidization model as part of the kinetic model. The bedzone has been modelled as a homogeneous steady state emulsion phase. This has been the result of limited project duration. It is advised to upgrade the kinetic model with a more detailed fluidization model. FM's that can be considered are a two-phase model such as the Davidson-Harrison Model or the three-phase Kunii-Levenspiel Model. An increased level of detail is expected to provide a better resemblance between the model and reality. As a result, the optimal process conditions that can be found by the model, can approach actual optimal process conditions more accurately.

It is advised to model the internal heat transfer limitation in the pyrolysis process and the mass transfer limitation in char oxidation. The resulting model will yield a better description of the biomass conversion in the IHBFBSR.

Biomass is currently disputed as sustainable energy source by the public. The amount of sustainable energy carriers needed in order to lower carbon dioxide emissions to zero exceeds the availability of biomass for energy purposes. Therefore, biomass is not considered as the single solution for lowering greenhouse gas emissions. In the Netherlands, biomass is often directly combusted in CHP-plants. The market for gasification products for energy consumption is very limited. Nevertheless, the chemical industry needs to increase sustainability as well. When fossil fuels will not be the main supply of chemical feed, biomass would be an attractive alternative. Biomass might even be the only attractive sustainable chemical feed source. Gasification is a very attractive approach to quick continuous production of chemical feed species such as hydrogen and carbon monoxide. The production of various carbohydrates through Fischer-Tropsch synthesis in biorefineries has potential as a sustainable, scalable innovation in chemical engineering. Taken into account the limited availability of global biomass for conversion purposes, it is advised to direct biomass resources towards sustainable chemical feed instead of utilizing biomass as sustainable energy source. Nevertheless, it is acknowledged that the energy transition is happening as we speak and that multiple sustainable energy sources, including biomass, must be utilized in order to reach the common goal of preventing global temperature from exceeding an increase of 2.0 $^\circ C$ above pre-industrial levels with a serious effort to stay below 1.5 $^\circ$C [60].

Bibliography

[1] L. Abdelouahed, O. Authier, G. Mauviel, J.-P. Corriou, G. Verdier, and A. Dufour. Detailed modeling of biomass gasification in dual fluidized bed reactors under aspen plus. *Energy & Fuels*, 26(6):3840–3855, 2012.

[2] J. Akhtar and N.A.S. Amin. Liquefaction. *Renewable and Sustainable Energy Reviews*, 15:1615–1624, 2011.

[3] M. Allen, B. Mustafa, P. Shukla, and et al. Global warming of 1.5 °c - an ipcc special report on the impacts of global warming of 1.5 °c above pre-industrial levels and related global greenhouse gas emission pathways, in the context of strengthening the global response to the threat of climate change, sustainable development, and efforts to eradicate poverty. 2018.

[4] J.L. Banyasz, S. Li, J.L. Lyons-Hart, and K.H. Shafer. Cellulose pyrolysis: the kinetics of hydroxyacetaldehyde evolution. *Journal of Analytical and Applied Pyrolysis*, 57(2):223 – 248, 2001. ISSN 0165-2370. doi: https://doi.org/10.1016/S0165-2370(00)00135-2. URL http://www.sciencedirect.com/science/article/pii/S0165237000001352.

[5] Dipal Baruah and D.C. Baruah. Modeling of biomass gasification: A review. *Renewable and Sustainable Energy Reviews*, 39:806–815, 2014.

[6] P. Basu. *Biomass Gasification and Pyrolysis*. John Wiley Sons Inc, 2010.

[7] Bellona. The chemical industry's contributions to climate change. URL https://bellona.org/news/eu/2019-04-the-industrys-chemistry-with-climate-change.

[8] G. Berndes, M. Hoogwijk, and R. van den Broek. The contribution of biomass in the future global energy supply: a review of 17 studies. *Biomass and Bioenergy*, 25(1):1 – 28, 2003. ISSN 0961-9534. doi: https://doi.org/10.1016/S0961-9534(02)00185-X. URL http://www.sciencedirect.com/science/article/pii/S096195340200185X.

[9] M. Boosten and J. Oldenburger. Biomassapotentieel NBLH-sector in 2020 en 2050 . 2014.

[10] M. Boosten, J. Oldenburger, J Kremers, J van den Briel, Spliethof N, and D Borgman. Biomassapotentieel NBLH-sector in 2020 en 2050 . 2018.

[11] F. Chejne and J.P. Hernandez. Modelling and simulation of coal gasification process in fluidised bed. *Fuel*, 81(13):1687 – 1702, 2002. ISSN 0016-2361. doi: https://doi.org/10.1016/S0016-2361(02)00036-4. URL http://www.sciencedirect.com/science/article/pii/S0016236102000364.

[12] W. de Jong. *Biomass as a Sustainable Energy Source for the Future*. template. John Wiley & Sons Inc, 2015.

[13] C. Di Blasi. Modeling chemical and physical processes of wood and biomass pyrolysis. *Progress in energy and combustion science*, 34(1):47–90, 2008.

[14] C. di Blasi. Combustion and gasification rates of lignocellulosic chars. *Progress in Energy and Combustion Science*, 35(2):121–140, 04 2009. doi: 10.1016/j.pecs.2008.08.001.

[15] B. Drift, C. Meijden, and Meijden Boerrigter. Milena gasification technology for high efficient sng production from biomass. 01 2005.

[16] D. Fiaschi and M. Michelini. A two-phase one-dimensional biomass gasification kinetics model. *Biomass and Bioenergy*, 21:121–132, 08 2001. doi: 10.1016/S0961-9534(01)00018-6.

[17] A. Goyal, S. Pushpavanam, and R. Kumar Voolapalli. Modeling and simulation of co-gasification of coal and petcoke in a bubbling fluidized bed coal gasifier. *Fuel Processing Technology*, 91(10):1296 – 1307, 2010. ISSN 0378-3820. doi: https://doi.org/10.1016/j.fuproc.2010.04.012. URL http://www.sciencedirect.com/science/article/pii/S0378382010001256.

[18] A. Gómez-Barea and B. Leckner. Modeling of biomass gasification in fluidized bed. *Progress in Energy and Combustion Science*, 36(4):444 – 509, 2010. ISSN 0360-1285. doi: https://doi.org/10.1016/j.pecs.2009.12.002. URL http://www.sciencedirect.com/science/article/pii/S0360128509000707.

[19] S. Hamel and W. Krumm. Mathematical modeling and simulation of bubbling fluidsed bed gasifiers. *Powder Technology*, 120:105–112, 10 2001. doi: 10.1016/S0032-5910(01)00356-4.

[20] International Energy Agency (IEA). World: Balances for 2016, 2016. URL https://www.iea.org/statistics/?country=WORLD&year=2016&category=Energy%20supply&indicator=TPESbySource&mode=table&dataTable=BALANCES.

[21] International Energy Agency (IEA). World energy balances, 2017. URL https://www.iea.org/statistics/balances/.

[22] International Energy Agency (IEA). Global energy CO_2 status report, 2019. URL https://www.iea.org/geco/.

[23] John A. Dutton Institute. Alternative fuels from biomass sources, 2019. URL https://www.e-education.psu.edu/egee439/node/664.

[24] Paul Scherrer Institute. Green chemicals from lignin, 2019. URL https://www.psi.ch/en/cpe/projects/green-chemicals-from-lignin.

[25] B.M. Jenkins. *Physical properties of biomass*. Gordon Breach Science Publishers, Amsterdam, 1989. ISBN 9780996305310. URL https://books.google.nl/books?id=1GL8sgEACAAJ.

[26] F. Johnsson, S. Andersson, and B. Leckner. Expansion of a freely bubbling fluidized bed. 1991.

[27] J. Karl. Biomass heat pipe reformer—design and performance of an indirectly heated steam gasifier. *Biomass Conversion and Biorefinery*, 4(1):1–14, 2014.

[28] P. Kaushal, J. Abedi, and N. Mahinpey. A comprehensive mathematical model for biomass gasification in a bubbling fluidized bed reactor. *Fuel*, 89(12):3650 – 3661, 2010. ISSN 0016-2361. doi: https://doi.org/10.1016/j.fuel.2010.07.036. URL http://www.sciencedirect.com/science/article/pii/S0016236110003959.

[29] D. Kunii and O. Levenspiel. Chapter 3 - fluidization and mapping of regimes. In D. Kunii and O Levenspiel, editors, *Fluidization Engineering (Second Edition)*, pages 61 – 94. Butterworth-Heinemann, Boston, second edition edition, 1991. ISBN 978-0-08-050664-7. doi: https://doi.org/10.1016/B978-0-08-050664-7.50009-3. URL http://www.sciencedirect.com/science/article/pii/B9780080506647500093.

[30] Hui Liu, A. Elkamel, Ali Lohi, and Mazda Biglari. Computational fluid dynamics modeling of biomass gasification in circulating fluidized-bed reactor using the eulerian–eulerian approach. *Industrial Engineering Chemistry Research*, 52:18162–18174, 12 2013. doi: 10.1021/ie4024148.

[31] C. Loha, H. Chattopadhyay, and P. K. Chatterjee. Thermodynamic analysis of hydrogen rich synthetic gas generation from fluidized bed gasification of rice husk. *Energy*, 36(7):4063 – 4071, 2011. ISSN 0360-5442. doi: https://doi.org/10.1016/j.energy.2011.04.042. URL http://www.sciencedirect.com/science/article/pii/S036054421100291X.

[32] J.D. MacLean. Thermal conductivity of wood. *TPS Termiska Processer AB*, 47(1):323–354, 1941.

[33] I. Matsui, D. Kunii, and Takehiko Furusawa. Study of char gasification by carbon dioxide. 1. kinetic study by thermogravimetric analysis. *Industrial & engineering chemistry research*, 26(1):91–95, 1987.

[34] C. Meijden, H Veringa, B. Drift, and B. Vreugdenhil. The 800 kwth allothermal biomass gasifier milena. 01 2008.

[35] Christiaan Meijden, Berend Vreugdenhil, and Bram Drift. Experimental results from the allothermal biomass gasifier milena. 05 2007.

[36] X. Meng. *Biomass gasification: The understanding of sulfur, tar, and char reaction in fluidized bed gasifiers*. Institutional Repository TU Delft, 2012.

[37] A. Mills and C.F.M. Coimbra. *Basic Heat Transfer*. Temporal Publishing, LLC, 2015. ISBN 9780996305310. URL https://books.google.nl/books?id=1GL8sgEACAAJ.

[38] J. Mitschele. Chemistry: The central science, sixth edition (brown, theodore l.; lemay, h. eugene, jr.; bursten, bruce e.). *Journal of Chemical Education*, 72(5):A107, 1995. doi: 10.1021/ed072pA107.2. URL https://doi.org/10.1021/ed072pA107.2.

[39] JPA Neeft, HAM Knoef, Uwe Zielke, K Sjöström, Philipp Hasler, PA Simell, MA Dorrington, L Thomas, N Abatzoglou, S Deutch, et al. Guideline for sampling and analysis of tar and particles in biomass producer gases. *Energy project ERK6-Ct199-2002 www. tarweb. net*, 1999.

[40] T.D.B. Nguyen, M. W. Seo, Young-Il Lim, Byung-Ho Song, and Sang-Done Kim. Cfd simulation with experiments in a dual circulating fluidized bed gasifier. *Computers & Chemical Engineering*, 36:48–56, 2012.

[41] T. R. Nunn, J. B. Howard, J. P. Longwell, and W. A. Peters. *Studies of the Rapid Pyrolysis of Sweet Gum Hardwood*, pages 293–314. Springer Netherlands, Dordrecht, 1985. ISBN 978-94-009-4932-4. doi: 10.1007/978-94-009-4932-4_16. URL https://doi.org/10.1007/978-94-009-4932-4_16.

[42] M.A. Paisley and R.P. Overend. Verification of the performance of future energy resources' silvagas. 2002.

[43] I. Petersen and J. Werther. Experimental investigation and modeling of gasification of sewage sludge in the circulating fluidized bed. *Chemical Engineering and Processing: Process Intensification*, 44(7): 717 – 736, 2005. ISSN 0255-2701. doi: https://doi.org/10.1016/j.cep.2004.09.001. URL http://www.sciencedirect.com/science/article/pii/S0255270104001916.

[44] J. Piskorz, D. St. A. G. Radlein, D. S. Scott, and S. Czernik. *Liquid Products from the Fast Pyrolysis of Wood and Cellulose*, pages 557–571. Springer Netherlands, Dordrecht, 1988. ISBN 978-94-009-2737-7. doi: 10.1007/978-94-009-2737-7_43. URL https://doi.org/10.1007/978-94-009-2737-7_43.

[45] D.L. Pyle and C.A. Zaror. Heat transfer and kinetics in the low temperature pyrolysis of solids. *Chemical engineering science*, 39(1):147–158, 1984.

[46] L.P.L.M. Rabou and M.H.F. Overwijk. The alkmaar 4 mw bio-sng demo project. In *3rd International Conference on Renewable Energy Gas Technology, REGATEC*, 2016.

[47] Ramin Radmanesh, Jamal Chaouki, and Christophe Guy. Biomass gasification in a bubbling fluidized bed reactor: experiments and modeling. *AIChE Journal*, 52(12):4258–4272, 2006.

[48] Reinhard Rauch, Hermann Hofbauer, Klaus Bosch, Ingmar Siefert, C. Aichernig, K. Voigtlaender, R. Koch, and R. Lehner. *Steam gasification of biomass at CHP plant Guessing-Status of the demonstration plant*. Citeseer, 2004.

[49] J. Reina, E. Velo, and L. Puigjaner. Kinetic study of the pyrolysis of waste wood. *Industrial & engineering chemistry research*, 37(11):4290–4295, 1998.

[50] D. P. Ross, H. Yan, Z. Zhong, and Dong ke Zhang. A non-isothermal model of a bubbling fluidised-bed coal gasifier. *Fuel*, 84(12):1469 – 1481, 2005. ISSN 0016-2361. doi: https://doi.org/10.1016/j.fuel.2005.02.016. URL http://www.sciencedirect.com/science/article/pii/S0016236105000797.

[51] S. Sadaka, A.E. Ghaly, and M. Sabbah. Two phase biomass air-steam gasification model for fluidized bed reactors: Part i - model development. *Biomass and Bioenergy*, 22:439–462, 06 2002. doi: 10.1016/S0961-9534(02)00023-5.

[52] F. Shafizadeh and P.P.S. Chin. Thermal deterioration of wood. *Wood technology: chemical aspects*, 43: 57–81, 1977.

[53] V. Sikarwar. Processing routes. URL `https://www.researchgate.net/figure/Thermochemical-and-biochemical-conversion-routes-for-biomass-to-biofuels-23_fig1_316772405`.

[54] Seethamraju Srinivas, Randall P. Field, and Howard J. Herzog. Modeling tar handling options in biomass gasification. *Energy & Fuels*, 27(6):2859–2873, 2013. doi: 10.1021/ef400388u. URL `https://doi.org/10.1021/ef400388u`.

[55] Study.com. Cellulose in plants: Function structure, 2019. URL `https://commons.wikimedia.org/wiki/File:Cellulose_Sessel.svg`.

[56] Echur Natrajan Sundaram and Elango Natarajan. Pyrolysis of coconut shell: An experimental investigation. 2009.

[57] S. Sundaresan and Neal R. Amundson. Studies in char gasification—ii: The davidson-harrison two phase model of fluidization. *Chemical Engineering Science*, 34(3):355 – 358, 1979. ISSN 0009-2509. doi: https://doi.org/10.1016/0009-2509(79)85067-8. URL `http://www.sciencedirect.com/science/article/pii/0009250979850678`.

[58] H. Thunman and B. Leckner. *Thermo Chemical Conversion of Biomass and Wastes*. 11 2007.

[59] S. R Turns et al. *An introduction to combustion*, volume 499. McGraw-hill New York, 1996.

[60] United Nations (UN). Paris agreement. 2015.

[61] United Nations (UN). World Population 2017. 2017. URL `http://www.unpopulation.org`.

[62] D van de Corput. Labee interview, 2019. URL `http://www.energypellets.nl/`.

[63] Ministerie van Economische Zaken-Directie Groene Groei BioBased Economy-Directoraat-Generaal Bedrijfsleven en Innovatie. Strategische visie voor de inzet van biomassa op weg naar 2030. 2015.

[64] L. Waldheim and T. Nilsson. Heating value of gases from biomass gasification. *TPS Termiska Processer AB*, 2001.

[65] World Data Bank (WDB). Population growth (annual %), 2018. URL `https://data.worldbank.org/indicator/SP.POP.GROW`.

[66] Qingang Xiong, Soroush Aramideh, and Song-Charng Kong. Modeling effects of operating conditions on biomass fast pyrolysis in bubbling fluidized bed reactors. *Energy & Fuels*, 27(10):5948–5956, 2013. doi: 10.1021/ef4012966. URL `https://doi.org/10.1021/ef4012966`.

[67] H. Zheng and R. V. Morey. An unsteady-state two-phase kinetic model for corn stover fluidized bed steam gasification process. *Fuel Processing Technology*, 124:11 – 20, 2014. ISSN 0378-3820. doi: https://doi.org/10.1016/j.fuproc.2014.02.010. URL `http://www.sciencedirect.com/science/article/pii/S037838201400071X`.

Appendices

Appendix A: Basis of Expression for Biomass Composition

Biomass components such as described by the proximate and ultimate analysis are often expressed as a percentage of the total mass. Several bases of expression exist to define this amount of total mass. for this study, it is relevant to mention the difference between the bases listed below;

- Dry ash free [d.a.f.]

- Dry [d.b.]

- As received [a.r.]

The amount of biomass before any processing step is referred to as the biomass 'as received' (a.r.) After devolatilization of the moisture, the mass that remains is the biomass on a 'dry basis' (d.b) All dry biomass except the ash fraction is referred to as biomass on a 'dry, ash- free' (d.a.f.) basis. The basis of expression have been visualized in figure 1. It is common to refer to biomass on an a.r. basis when it comes to comparing its performance and handling capabilities with other fuels. The d.b. and d.a.f. bases are often referred to when in comes to chemical conversion of the dry and ash free components.
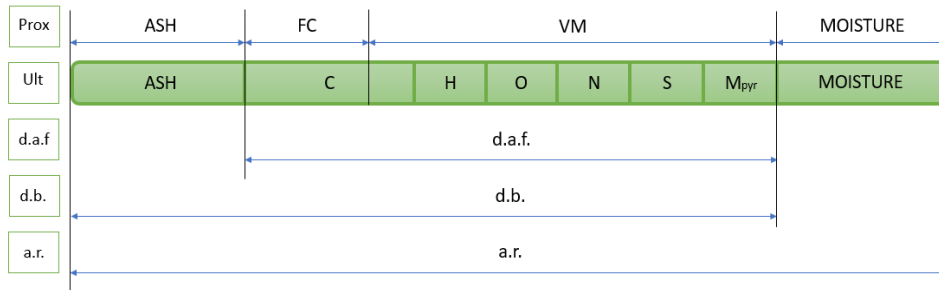
Figure 1: Biomass Composition Visualized for the Proximate and Ultimate Analysis as well for Composition Bases d.a.f., d.b. and a.r.[6].

A distinction can be made between air dry and total dry basis. Air dry refers to all biomass minus the moisture. Total dry refers to all biomass without the moisture and pyrolytic water, also known as inherent moisture content. Dry basis often refers to air-dry basis, for the reason that pyrolysis is needed in order to separate the pyrolytic water from the biomass.

In order to switch between the bases of expression, equations 1 to 2 can be used[12].

$$Y_i^{db} = \frac{100 \cdot Y_i^{ar}}{100 - Y_{moisture}^{ar}} \tag{1}$$

$$Y_i^{daf} = \frac{100 \cdot Y_i^{ar}}{100 - Y_{moisture}^{ar} - Y_{ash}^{ar}} = \frac{100 \cdot Y_i^{db}}{100 - Y_{ash}^{ar}} \tag{2}$$

Appendix B: Particle Size Distribution of the Miscanthus Feed of the IHBFBSR

Particle Size Distribution of the Biomass Feed of the IHBFBSR.

Author: Maarten Kwakkenbos,   MSc. Student Sustainable Energy Technology, TU Delft,   4217462

Introduction

The feeder section of the IHBFBSR makes use of a screw feeder to insert biomass into the reactor. During the feeding process, the brittle biomass can brake and the particle size of the pellets can be reduced. The particle size has a large influence on the reaction kinetics and yield of the reactor. Therefore, it is chosen to make a particle size distribution of the biomass that leaves the feeder section. The results can be used in reactor modelling and to analyse the influence of the particle size on reactor performance. This work gives the size distribution of three biomass types that have passed through the feeder section.

The first biomass type is white pine wood, also referred to as "the red biomass (RB)". The pine wood origins from secondary and tertiary forestry biomass has been imported by Labee group from Scandinavian countries or Russia. The second biomass type is brown leafage wood also referred to as "the green biomass (GB)". The leafage wood origins from secondary and tertiary forestry biomass from the Netherlands[2]. The third and last biomass type is Miscanthus which is cultivated as an energy crop. This particular biomass is grown in Germany and pre-treated in the Netherlands by the company Comgoed.

All three biomass types arrive in a pellet shape with a diameter 6 mm. It has been observed that the biomass preferably breaks perpendicular to the length of the pellet when crossing the feeder section of the IHBFBSR. This process leaves two shorter pellets with a diameter of 6 mm and some small dust particles that are created during the braking process.

Experimental Set Up and Method

The particle size distribution has been determined following a protocol written by the American Society of Agricultural Engineers[1]. For the experiments the following materials have been used:

- Sieve Vibration Plate (Brand and Type)
- Sieves
- Weight Scale
- Three types of biomass (RB, GB, Mis.)

First, Biomass had been taken from a plastic bag with a small bin. The bin was able to carry approximately 600 -700 grams of biomass. It should be mentioned that the particle sizes have not been equally distributed in the plastic bag. Smaller particles (dust) have been observed at the bottom of the bag while larger particles were more abundant at the top of the bag. It is tried to get biomass particles from lower in the bag. Nevertheless, all biomass that is used for the experiments originates from the upper half of the bag.

The biomass is transferred to the top sieve of the stack. All sieves that are present at the stack have been summarized in table 1. All sieves have been weighted individually before the experiment. It has been observed that the weight of the empty sieves do not vary much (a small multiple of 0.01 grams) throughout the experiments. It can therefore be said that the sieves are being cleaned effectively and no biomass is accumulating on the sieves. It has also been chosen to use one weight measurement of the empty sieves for three experiments with the same biomass as reference value.

Sieve Mesh Size	Sieve Brand
4.75 mm	Blue
4.00 mm	Blue
1.40 mm	Blue
850 micron	Blue
600 micron	Blue
500 micron	Blue
300 micron	Green

The stack should have contained a closed bin at the bottom. Unfortunately, no such been had been present and a bucket lid is used instead. The problem with this lid is that some of the dust (<300 micron) did not stay put on the lid but left the sieve stack during vibration. It is therefore impossible to determine the exact amount of particles with a size lower than 300 micron.

The sieve stack is sealed off and the vibration plate is used twice for two minutes. The frequency of the plate is fixed at (search for it) and it was able to adjust the amplitude. For all experiments a vibration of two minutes at an amplitude of 1.0 mm g^{-1} has been performed conform the protocol. It is observed that some of the smaller particles had not been able to pass through the sieves. It is therefore chosen to vibrate another two minutes at an amplitude of 0.5 mm g^{-1}. For larger amplitudes than 1.5 it has been observed that the sieves start moving on the vibration plate. It is therefore chosen not to proceed experiments with higher amplitudes.

After the vibrating process, each of the sieves are weighted starting with the top, largest, sieve and finishing with the 300 micron sieve as well as measuring the weight of the lid. The scale has an accuracy of 0.01 gram. The weight difference between the empty sieve and the sieve with biomass equals the amount of biomass with a particle size larger than that sieve size, but smaller than the sieve size of the sieve on top. When the weight measurement is recorded the biomass is disposed and the sieve is cleaned with paper towel. It has been tried to clean the sieves with water or with different types of brushes, but only paper towels and beating out the dust had proven to be effective.

The experiment has been performed three times for each of the biomass types conform the protocol.

Results and Discussion

For each of the biomass types a table with the measurements can be found in this section. Table 2 gives the measurements for the red biomass RB, Table 3 for green biomass GB and Table 4 for miscanthus. Each table contains the sieve size, weight of the empty sieves and the measurement columns. The measurement columns consist of a measurement of the weight of the full sieves, a weight difference between full and empty sieve indicated by dM and the mass percentage of biomass in that particular sieve.

Table 2: Weight measurements for RB.

Sieve [mm]	Empty [g]	RB1 [g]	dM1 [g]	RB1 [%]	RB2 [g]	dM2 [g]	RB2 [%]	RB3 [g]	dM3 [g]	RB3 [%]
4.75	432.89	887.26	454.37	80.27	939.71	506.82	85.06	1134.68	701.79	87.10
4.00	423.13	432.97	9.84	1.74	428.74	5.61	0.94	431.77	8.64	1.07
1.40	367.15	402.80	35.65	6.30	399.63	32.48	5.45	409.36	42.21	5.24
0.85	339.55	364.42	24.87	4.39	360.79	21.24	3.56	363.63	24.08	2.99

0.6	318.03	332.94	14.91	2.63	329.44	11.41	1.91	329.72	11.69	1.45
0.5	309.94	316.80	6.86	1.21	314.19	4.25	0.71	313.53	3.59	0.45
0.3	319.84	333.58	13.74	2.43	329.35	9.51	1.60	328.74	8.90	1.10
Lid	28.40	34.21	5.81	1.03	32.92	4.52	0.76	33.24	4.84	0.60
Total		3104.98	566.05	100.00	3134.77	595.84	100.00	3344.67	805.74	100.00

Table 3: Weight measurements for GB.

Sieve [mm]	Empty [g]	GB1 [g]	dM1 [g]	GB1 [%]	GB2 [g]	dM2 [g]	GB2 [%]	GB3 [g]	dM3 [g]	GB3 [%]
4.75	432.87	886.93	454.06	83.30	1136.90	704.03	92.06	973.21	540.34	91.67
4.00	423.15	436.66	13.51	2.48	432.99	9.84	1.29	429.24	6.09	1.03
1.40	367.12	415.57	48.45	8.89	397.82	30.70	4.01	391.04	23.92	4.06
0.85	339.55	353.50	13.95	2.56	348.60	9.05	1.18	348.20	8.65	1.47
0.6	318.00	323.74	5.74	1.05	322.12	4.12	0.54	322.37	4.37	0.74
0.5	309.88	312.17	2.29	0.42	311.44	1.56	0.20	311.36	1.48	0.25
0.3	319.73	323.99	4.26	0.78	322.81	3.08	0.40	322.59	2.86	0.49
Lid	28.40	31.20	2.80	0.51	30.78	2.38	0.31	30.11	1.71	0.29
Total		3083.76	545.06	100.00	3303.46	764.76	100.00	3128.12	589.42	100.00

Table 4: Weight measurements for Miscanthus Biomass.

Sieve [mm]	Empty [g]	Mi1 [g]	dM1 [g]	Mi1 [%]	RB2 [g]	dM2 [g]	Mi2 [%]	Mi3 [g]	dM3 [g]	Mi3 [%]
4.75	432.84	708.14	275.30	73.96	707.18	274.34	65.52	958.62	525.78	90.11
4.00	423.08	429.84	6.76	1.82	429.34	6.26	1.50	424.45	1.37	0.23
1.40	367.06	411.98	44.92	12.07	433.23	66.17	15.80	392.01	24.95	4.28
0.85	339.51	357.47	17.96	4.83	364.52	25.01	5.97	352.43	12.92	2.21
0.6	318.02	325.96	7.94	2.13	330.84	12.82	3.06	323.75	5.73	0.98
0.5	309.94	313.29	3.35	0.90	315.40	5.46	1.30	312.09	2.15	0.37
0.3	319.73	329.17	9.44	2.54	336.49	16.76	4.00	325.93	6.20	1.06
Lid	28.85	35.39	6.54	1.76	40.75	11.90	2.84	33.25	4.40	0.75
Total		2911.24	372.21	100.00	2957.75	418.72	100.00	3122.53	583.50	100.00

The results are used to create a graph that shows the particle size distribution of the three biomasses. First, the bulk of the biomass has particle sizes larger than 4.75 mm. This is the normal pellet size for which the biomass enters the feeder section. The remainder consists of dust and small particles of which a particle distribution can be found in figure 1. A visualization of the fraction of small particles in the biomass sample can be found in figure 2. From the first figure can be observed that the individual experiments with the same types of biomass vary substantially with respect to each other. It can also be observed that of the smaller particles a peak can be found around 2000-2500 micron. It is advised to perform the experiment again with several sieve sizes around this optimum for a more accurate size distribution. Another small peak can be observed for particles around 300 micron. For each of the ranges, the geometric mean length of the particles has been calculated conform the protocol as described by the equation below[1].

$$\overline{X_i} = \sqrt{X_i X_{i-1}}$$

In this equation X_i is the diagonal mesh length in sieve i. The geometric mean length is used on the x-axis of figure 1. With this parameter, the overall geometric mean length and corresponding standard deviation, as described by the equations below, have been calculated as well.

$$X_{gem} = log^{-1} \frac{\sum M_i \log \overline{X}_i}{\sum M_i}$$

$$S_{gem} = log^{-1} \left[\frac{\sum M_i (\log \overline{X}_i - \log X_{gem})^2}{\sum M_i} \right]^{0.5}$$
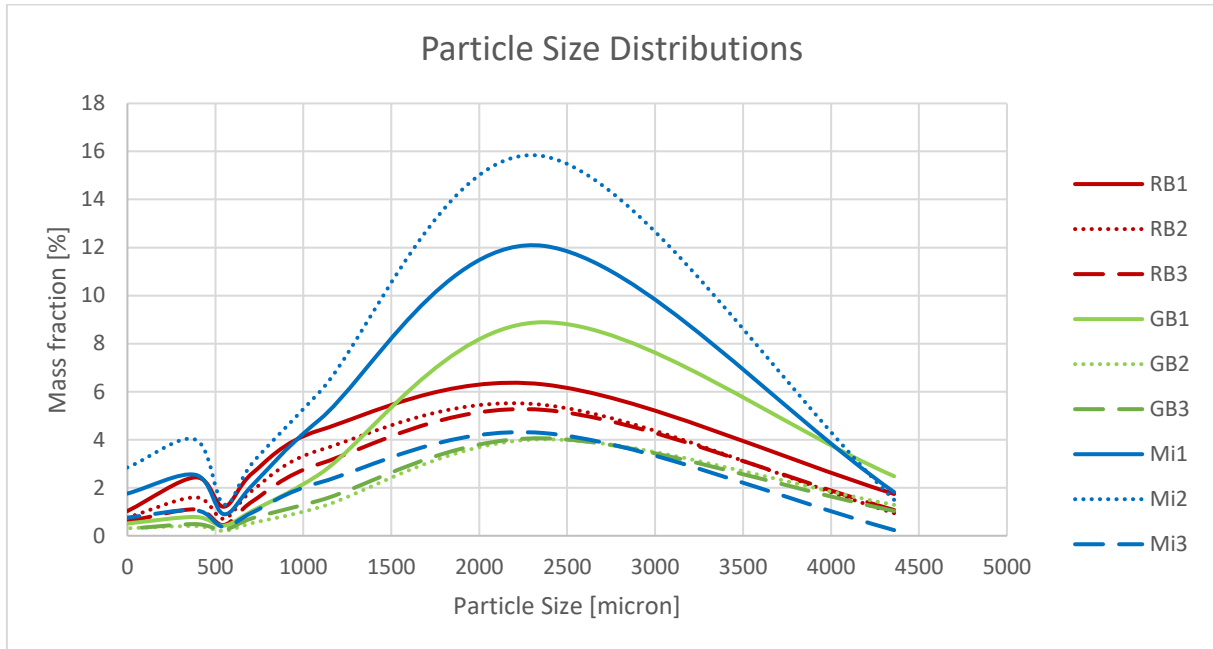
Figure 1: Particle Size Distributions of RB, GB and Miscanthus.
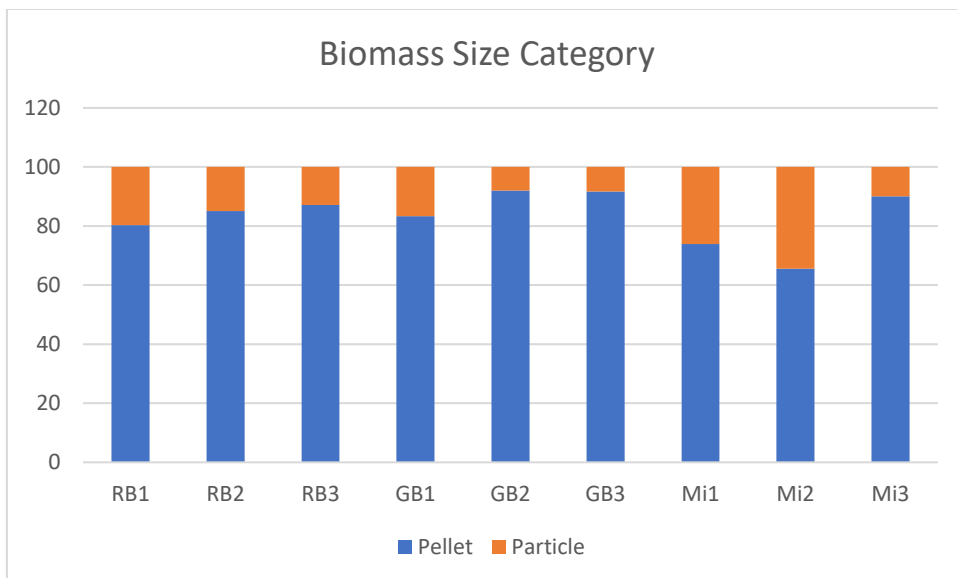
Figure 2: Biomass Size Category

The amount of small particles varies between 12-20% for RB, 7-17% for GB and 9-35% for Miscanthus. The geometric mean length of the small particles (without the bulk pellets) can be found in Table 5 with its corresponding standard deviation.

Table 5: Geometric Mean Length and Standard Deviations of all Biomass Samples [micron].

	RB1	RB2	RB3	GB1	GB2	GB3	Mi1	Mi2	Mi3
X_{gem}	1111.42	1147.60	1277.89	1714.08	1665.79	1543.71	1248.45	1128.76	1098.00
S_{gem}	1.50	1.41	1.37	1.39	1.27	1.27	1.63	1.79	1.35

Conclusion and Recommendations

The three biomass types have been analysed for particle size after passing through the feeder section. The amount of small particles varies between 12-20% for RB, 7-17% for GB and 9-35% for Miscanthus. The mean geometric length of the small particles varies between 1110 and 1278 micron for RB. The mean geometric length of the small particles varies between 1543 and 1715 micron for GB. The mean geometric length of the small particles varies between 1098 and 1249 micron for Miscanthus.

It is expected that the small particle bulk with a size of 2-2.5 mm can be explained by the fact that the fibres, that are used to make the pellets, are also in the size order of 1-3 mm[2]. When a pellets brakes, it is possible for a single or multiple fibres to become separated from the pellet

To compose a more accurate size distribution, it is advised to use more sieves with smaller size ranges. Now, the bulk of the biomass is too large to be analysed by this set up. A geometric mean length would not say anything about these large pellets. Only the smaller particles, smaller than 4.75 mm can be taken into account for calculating such a mean value.

It is advised to repeat the experiment with all the biomass that is present in the storage bag. In this way the effect of the particle size inhomogeneity in the storage bag is accounted for.

References

[1] ASAE-The Society for engineering in agricultural, food, and biological systems 2950 Niles Rd., St. Joseph, MI 49085-9659, USA ph. 269-429-0300, fax 269-429-3852, hq@asae.org

[2] Labee group pelletizing factory visit, Douwe van de Corput.

Appendix C: Technical Supplementary of the IHBFBSR
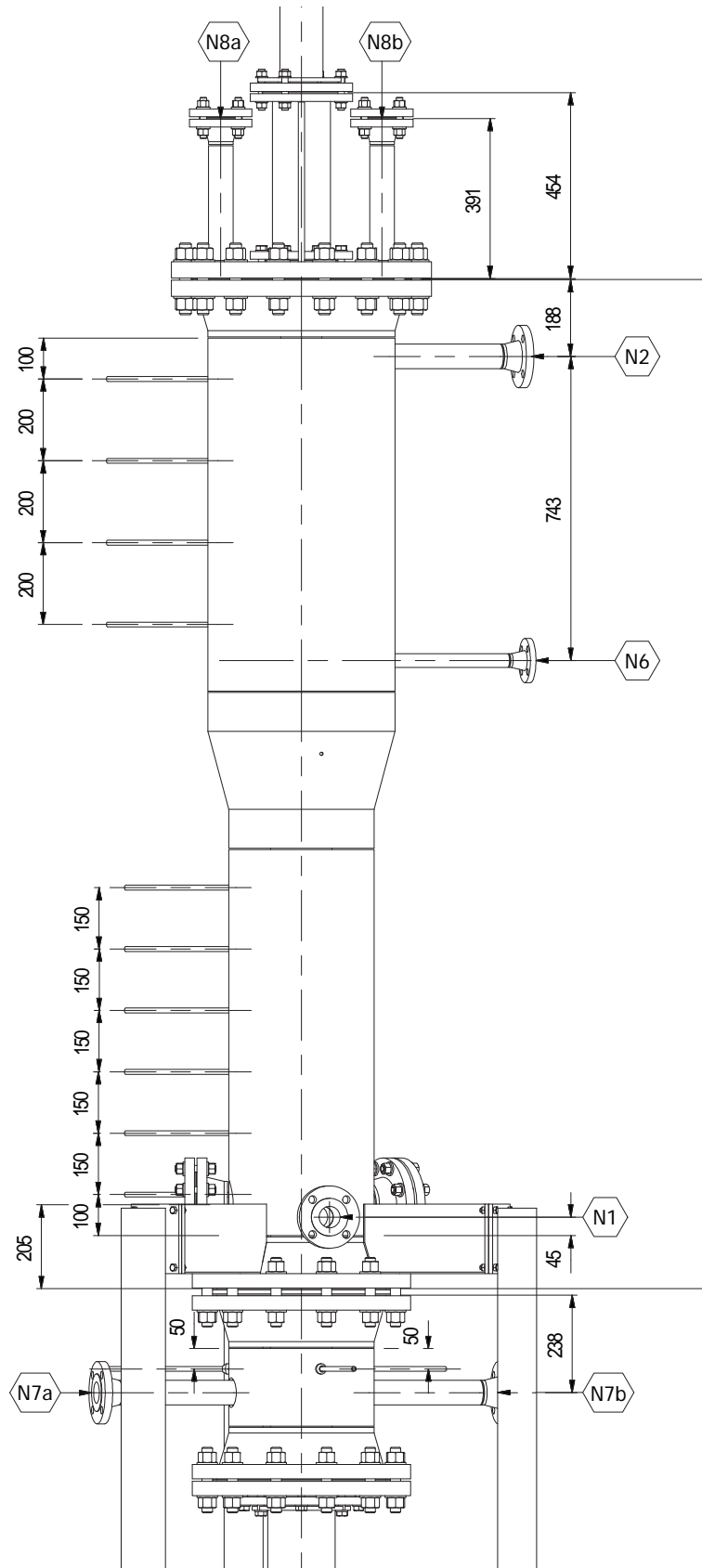
Appendix D: Technical Supplementary of the Burners and Radiant Tubes

velocity of flow < 10 m/s
in each supply line

1300

Ø88 Ø100

474

70

503 443

231

28 ± 5

3

230

700

517 ± 5

Abgas/ exhaust gas
R 1"

Gas/ gas
Rp 3/8"

Verbrennungsluft / air
DN 16 (Ø21,3)

110   89

Test distance for
ceramic falme tube

Verbrennungsluft/ air 127

Abgas/ exhaust gas 148

Gas/ gas 169

ca.312

Ofenflansch
furnace flange

M16

Ø210

Ø250   Ø160

1 x

WS-Order-No.:   BA16/000205
Customer-Order-No.: 16120201
Customer: e-flox, Renningen

WN:

Design by DR. WÜNNING

This drawing contains protected, proprietary
information and may not be copied,
reproduced or made accessible to third parties,
without the express written consent of
WS-Wärmeprozesstechnik GmbH
Copyright protection per DIN 34 / ISO 16016

Burner control box
installed near
the burner

WS Wärme prozess technik			Scale:	(Weight)
			WS-Part-No.: 139-00-xxx	
	Date	Name	REKUMAT® C80S OK m.Spülluft	
Edited	28.10.2016	Pliefke		
Tested			Ion., BohrØ--(550), Ø100x950	
Standard				
			Drawing-No.: WSZ 12647	Sheet 2
			Copyright protection (DIN 34 / ISO 16016)	2 Sh
Pos.	Change	Date	Name	(Orginal)	(Substitute)	(Substituted)

Appendix E: Experimental Results of the Pyro Probe Experiments

Biomass	Mass [mg]	Particle size [µm]	F_{N2} [ml/min]	Heating rate [˚C/s]	Holding time [s]	T_{real} [˚C]	T_{set} [˚C]	Sample name
RB	30 ±0.5	80	10±0.5	600	11.5	600	744	RB_11_4_600
								RB_11_4_600
					11.9	700	876	RB_12_4_700
								RB_17_4_700
					12.5	800	1008	RB_18_4_800
								RB_25_4_800
					12.9	900	1141	RB_26_4_900
								RB_26_4_900
					13.5	1000	1273	RB_2_5_1000
								RB_3_5_1000
GB	30 ±0.5	80	10	600	11.5	600	744	GB_8_5_600
								GB_9_5_600
					11.9	700	876	GB_9_5_700
								GB_10_5_700
					12.5	800	1008	GB_10_5_800
								GB_10_5_800
					12.9	900	1141	GB_15_5_900
								GB_16_5_900
					13.5	1000	1273	GB_16_5_1000
								GB_17_5_1000
Miscanthus	30 ±0.5	80	10	600	11.5	600	744	misc_600_1_6_7
								misc_600_2_6_7
					11.9	700	876	misc_700_2_5_7
								misc_700_3_5_7
					12.5	800	1008	misc_800_1_4_7
								misc_800_2_4_7
					12.9	900	1141	misc_900_1_4_7
								misc_900_2_4_7
					13.5	1000	1273	misc_1000_1_29_6
								misc_1000_5_3_7

Sample name	Treal [°C]	test	Gas	Tar	Char	Mass balance	H2	CO	CH4	CO2
misc_600_1_6_7		_1	11.66%	44.62%	22.74%	79.03%	0.01%	3.86%	0.21%	7.59%
misc_600_2_6_7		_2	11.22%	41.97%	22.61%	75.80%	0.01%	3.77%	0.20%	7.24%
	600	average	11.44%	43.30%	22.68%	77.41%	0.01%	3.81%	0.21%	7.42%
		stdev	0.31%	1.87%	0.09%	2.28%	0.00%	0.07%	0.00%	0.25%
misc_700_2_5_7		_2	15.27%	40.44%	19.12%	74.83%	0.04%	6.56%	0.82%	7.86%
misc_700_3_5_7		_3	16.02%	41.73%	19.17%	76.92%	0.04%	6.95%	0.85%	8.18%
	700	average	15.65%	41.08%	19.15%	75.87%	0.04%	6.76%	0.83%	8.02%
		stdev	0.53%	0.91%	0.03%	1.47%	0.00%	0.28%	0.02%	0.22%
misc_800_1_4_7		_1	23.66%	29.42%	15.36%	68.43%	0.49%	11.10%	1.73%	10.34%
misc_800_2_4_7		_2	19.93%	30.49%	18.08%	68.49%	0.14%	9.91%	1.56%	8.31%
	800	average	21.79%	29.95%	16.72%	68.46%	0.32%	10.51%	1.65%	9.32%
		stdev	2.64%	0.76%	1.92%	0.04%	0.25%	0.84%	0.11%	1.44%
misc_900_1_4_7		_1	26.47%	26.52%	16.19%	69.19%	0.44%	14.16%	2.54%	9.34%
misc_900_2_4_7		_2	25.30%	29.33%	14.68%	69.31%	0.41%	13.35%	2.38%	9.16%
	900	average	25.88%	27.93%	15.44%	69.25%	0.42%	13.76%	2.46%	9.25%
		stdev	0.83%	1.98%	1.07%	0.08%	0.02%	0.58%	0.11%	0.13%
misc_1000_1_29_6		_1	28.80%	25.37%	15.68%	69.84%	0.52%	15.69%	2.86%	9.74%
misc_1000_5_3_7		_5	25.64%	23.29%	15.05%	63.98%	0.42%	14.02%	2.56%	8.64%
	1000	average	27.22%	24.33%	15.36%	66.91%	0.47%	14.85%	2.71%	9.19%
		stdev	2.23%	1.47%	0.44%	4.14%	0.07%	1.18%	0.21%	0.77%

Sample name	Treal [°C]	test	Gas	Tar	Char	Mass balance	H2	CO	CH4	CO2
RB_11_4_600		_3	6.64%	34.90%	39.60%	81.13%	0.004%	1.73%	0.06%	4.84%
RB_11_4_600		_4	6.19%	33.00%	40.67%	79.86%	0.003%	1.70%	0.04%	4.44%
	600	average	6.41%	33.95%	40.13%	80.49%	0.003%	1.72%	0.05%	4.64%
		stdev	0.32%	1.34%	0.76%	0.90%	0.00%	0.02%	0.02%	0.28%
RB_12_4_700		_1	10.06%	37.46%	25.08%	72.60%	0.03%	4.80%	0.53%	4.70%
RB_17_4_700		_3	9.60%	39.07%	27.48%	76.16%	0.02%	3.57%	0.32%	5.70%
	700	average	9.83%	38.27%	26.28%	74.38%	0.03%	4.18%	0.42%	5.20%
		stdev	0.32%	1.14%	1.70%	2.52%	0.01%	0.87%	0.15%	0.70%
RB_18_4_800	800	_2	17.12%	32.78%	18.87%	68.77%	0.097%	9.385%	1.421%	6.215%
RB_25_4_800		_4	0.19379	32.12%	18.87%	70.37%	0.137%	11.523%	1.683%	6.036%
		average	18.25%	32.45%	18.87%	69.57%	0.12%	10.45%	1.55%	6.13%
		stdev	1.60%	0.47%	0.00%	1.13%	0.03%	1.51%	0.19%	0.13%
RB_26_4_900	900	_3	30.70%	20.40%	13.71%	64.81%	0.340%	19.071%	3.210%	8.076%
RB_26_4_900		_4	30.09%	21.59%	15.61%	67.30%	0.334%	18.696%	3.194%	7.866%
		average	30.39%	21.00%	14.66%	66.06%	0.34%	18.88%	3.20%	7.97%
		stdev	0.43%	0.84%	1.35%	1.76%	0.00%	0.27%	0.01%	0.15%
RB_2_5_1000	1000	_3	29.25%	22.52%	17.55%	69.32%	0.437%	20.382%	3.577%	8.277%
RB_3_5_1000		_4	30.13%	21.93%	15.95%	68.00%	0.497%	17.930%	3.419%	7.407%
		average	29.69%	22.22%	16.75%	68.66%	0.47%	19.16%	3.50%	7.84%
		stdev	0.62%	0.42%	1.13%	0.93%	0.04%	1.73%	0.11%	0.62%

Sample name	Treal [°C]	test	Gas	Tar	Char	Mass balance	H2	CO	CH4	CO2
GB_8_5_600	600	_1	5.28%	30.70%	46.36%	82.33%	0.00%	1.23%	0.06%	3.99%
GB_9_5_600		_3	5.24%	32.00%	45.67%	82.91%	0.00%	1.41%	0.06%	3.77%
		average	5.26%	31.35%	46.01%	82.62%	0.00%	1.32%	0.06%	3.88%
		stdev	0.03%	0.92%	0.49%	0.40%	0.00%	0.12%	0.00%	0.16%
GB_9_5_700	700	_1	9.41%	40.20%	26.91%	76.52%	0.01%	3.30%	0.31%	5.79%
GB_10_5_700		_2	10.52%	41.33%	26.00%	77.85%	0.02%	4.18%	0.45%	5.87%
		average	9.96%	40.77%	26.46%	77.18%	0.02%	3.74%	0.38%	5.83%
		stdev	0.78%	0.80%	0.64%	0.93%	0.00%	0.62%	0.09%	0.06%
GB_10_5_800	800	_1	17.86%	31.89%	21.26%	71.01%	0.12%	9.90%	1.53%	6.32%
GB_10_5_800		_2	18.68%	32.78%	20.53%	71.99%	0.11%	10.25%	1.55%	6.78%
		average	18.27%	32.34%	20.90%	71.50%	0.11%	10.07%	1.54%	6.55%
		stdev	0.58%	0.63%	0.52%	0.69%	0.01%	0.25%	0.02%	0.33%
GB_15_5_900	900	_1	26.81%	20.33%	18.00%	65.14%	0.28%	16.50%	2.85%	7.17%
GB_16_5_900		_2	26.84%	21.40%	18.39%	66.64%	0.28%	16.66%	2.87%	7.03%
		average	26.82%	20.87%	18.20%	65.89%	0.28%	16.58%	2.86%	7.10%
		stdev	0.02%	0.76%	0.28%	1.06%	0.00%	0.11%	0.01%	0.10%
GB_16_5_1000	1000	_1	27.04%	20.67%	17.67%	65.37%	0.28%	16.77%	2.88%	7.10%
GB_17_5_1000		_2	26.47%	20.60%	17.28%	64.35%	0.27%	16.42%	2.82%	6.96%
		average	26.76%	20.64%	17.47%	64.86%	0.28%	16.60%	2.85%	7.03%
		stdev	0.40%	0.05%	0.28%	0.72%	0.00%	0.25%	0.04%	0.10%

Appendix F: Submodels for Kinetic Models of Fluidized Bed Reactors

Fluid Dynamics Sub Models for Kinetic FBR modelling

Fluid dynamics describe the motion of components in the reactor. In a BFB gasifier, both solids and gasses are present. Their motion can be modelled into various levels of detail. Section 4.1 has categorized fluid dynamics model variations into three groups: CFD, FM and BBM. The following subsections will elaborate on the model variations within these groups.

CFD Models

CFD Models give the mass, momentum, species and energy balance for a pre-defined volume increment[18]. The model can provide a detailed description of the reactor dynamics, but the models can be quite time consuming to solve. Often a compromise is made for the amount of detail that is requested from the CFD calculations in order to reduce the simulation time. Main categories of CFD Models are:

- Eulerian-Eulerian Model [EEM]

- Eulerian-Lagrangian Model [ELM]

The Eulerian-Lagrangian Model [ELM] models a gas phase as described by the Navier-Strokes equation and a discrete solid phase. Numerically solving the Navier-Strokes equation for turbulent flow can be done by using Direct Numerical Simulation [DNS], but this method is extremely time consuming. An option for solving the Navier-Strokes equation in turbulent flow is by Large Eddy Simulation [LES]. This method solves the equation up to a predefined step-size. In the ELM, the trajectory of each individual particle is calculate according to Newton's Law of motion. This method is also referred to as a Discrete Particle Model [DPM]. The collisions between the particles are either described by soft- or hard-sphere model. Phase parameters such as gas concentration, temperature are calculated by solving energy and mass balances for each particle[30]. Because each solid particle is modelled individually, ELM has a high computational time and is only suitable for low amounts of particles[40].

The Eulerian-Eulerian Model [EEM] models both the gas phase and fluid phase are modelled according to the Eulerian framework. This method is also referred to as a Two-Fluid Model [TFM]. It means that large volumes of multiple particles can be modelled at once by solving momentum and energy balances for that volume. EEM's are more often used for CFD modelling fluidized bed reactors as the result of their compromise between detail and computational time.

CFD is often not selected to describe the fluid dynamics in a kinetic model of a BFB gasifier. This is due to the considerable computational time required for CFD calculations. Fluidization Models are a good compromise between complex CFD calculations and overall non-realistic equilibrium models by assuming a multi-phase pattern in the reactor.

Fluidization Models

Fluidization models assume multiple phases to be present in the reactor. These phases do not correspond to the thermodynamic phases, but indicate a region with similar gas/solid composition. The model describes the dynamics of the phases as the result of semi-empirical relations. Mass and heat transfer is modelled between the phases. Several fluidization models exist. Considered mechanisms are:

- Two-phase of BFB with a bubble phase and emulsion phase

- Three phase of BFB with a bubble phase, emulsion phase and cloud phase

- FB divided into horizontal slices

The two-phase model defines a gas phase in the form of a bubble. The second emulsion phase is modelled as a perfectly mix of all solids and a fraction of gas. Semi-empirical relations exist in order to define the fraction of gas in the bubble and emulsion phases as well as the bubble velocity and size. Mass transport between the emulsion and bubble phase is modelled as well. A visual representation of the two-phase model can be found in figure 2. An example of the two-phase fluidization model is the Davidson-Harrison Model [DHM][57]

The three phase model consists of the same bubble and emulsion phase, but has a third defined phase:
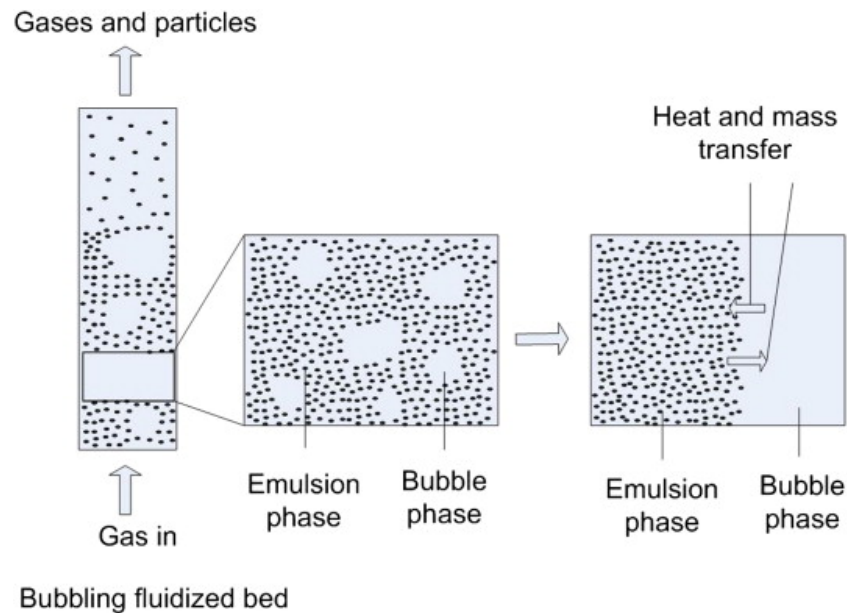
Figure 2: Visualization of the two-phase fluidization model with a bubble and emulsion phase[67]

the wake. A cloud of solids dispersed in gas is present around the bubble. The movement of these solids differs from the rest of the emulsion. Solid particles are dragged upward in the wakes of rising bubbles. Solid particles drift downward in the emulsion phase, but the cloud travels upwards with the same velocity as the bubble. A visual representation of the three phase model is given in figure 3. An example of a commonly used three-phase model is the Kunii-Levenspiel model [KLM][29].

The Counter Current Back Mixing model [CCBM] makes use of two phases: an ascending and a descending
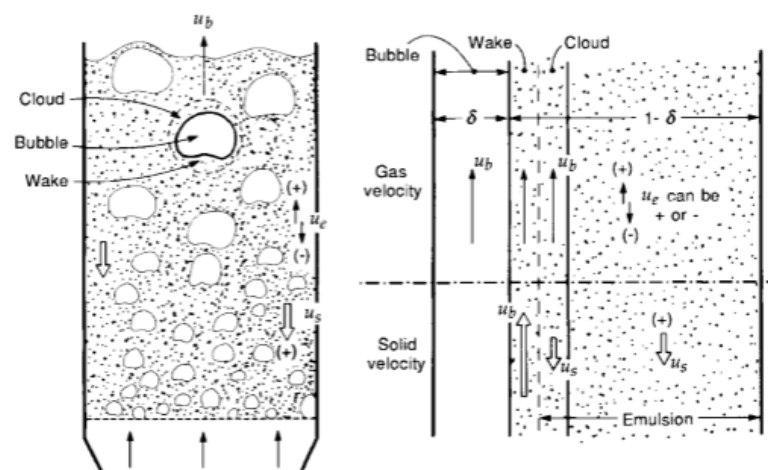

Figure 3: Visualization of the Three-Phase Fluidization Model with a Bubble, Wake and Emulsion phase[29]

phase. Mass and heat transfer between the phases is calculated over a volume element of the reactor. This model makes use of the horizontal slice principle. A visualization of this fluidization model is given in figure

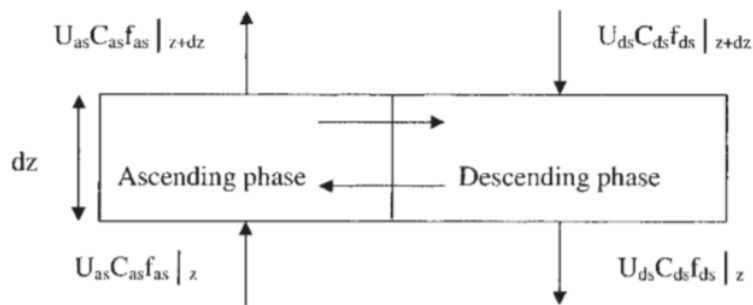4. An example of the CCBM is Fryer and Potter[18].

Figure 4: Visualization of the Two-Phase Counter Current Back-Mixing Fluidization Model with an Ascending and Descending Phase[47].

Besides minor differences in the semi-empirical correlations for phase dynamics, there are no significant differences between the aforementioned models according to Gómez-Barea et al.[18].
All fluidization models divide the gasifier into multiple sections. A bedzone and freeboard for bubbling fluidized bed and a core-annulus for circulating fluidized bed. Gas flow through the bed can be modelled by different modelling component. The considered options are[6]:

- Plug flow in the bubble phase (PFR) and an ideally mixed gas in the emulsion phase (CSTR)

- Ideally mixed gas in both phases (CSTR)

- Plug flow in both phases with mass transfer between the phases (PFR)

- Plug flow in both phases without mass transfer between the phases (PFR)

- Plug flow of the gas upwards (PFR) and a solid back flow in the annulus (PFR)

The freeboard is often modelled as one-dimensional plug flow since mainly a gas phase is present and radial mixing is limited.

Chemical Conversion Sub Models for Kinetic FB modelling

Chemical reactions convert substances that have well-defined properties into other substances with different properties[38]. The reaction rate indicates the change in concentration of reactants and products throughout the conversion process as function of time and process conditions. This sections describe the models that are considered for the quantification of the chemical reaction rate. In gasification, different models are used for pyrolysis, homogeneous gas phase reactions and heterogeneous solid-gas char conversion. The considered options will be introduced in the following three subsections.

Pyrolysis Models

Pyrolysis is the thermochemical conversion of biomass into various products such as permanent gasses, vapours and solids. This process occurs in the absence of an oxidizer. modelling pyrolysis is quite a challenge due to the fact that the composition is highly dependent on process conditions and reactor configurations. Pyrolysis models often make use of yields or kinetic rates that origin from experimental data. It could be that the process conditions of that particular experiment are different from the process conditions in which pyrolysis will be modelled. In that case, the model will either be less accurate or own experiments in the right process conditions are required to obtain the parameters that are needed for the pyrolysis model.

For pyrolysis modelling, three options are considered[13]:

- One Component Model

- Multi-Component Model

- Distributed Activation Energy Model [DAE]

In all cases, biomass is pyrolyzed and the amount of products can be identified either by an experimental determination of the mass yields [wt% of x] or experimental determination of the reaction rate expressed by Rate Law with an Arrhenius constant and activation energy. In the case of a mass yield model, the amount of pyrolysis products is obtained after the biomass particle has been fully pyrolyzed. In the case of a reaction rate model, the quantification of pyrolysis products is time dependent and also depends on the concentration of the biomass reactant.

In case of a one component model, biomass is assumed to be a single non-conventional substance. The mass yields of each pyrolysis product is expressed in mass yield [wt%] with respect to the a.r. mass of the biomass in the case of a mass yield model. In the case of a reaction rate model, the reaction rate is expressed for the conversion of biomass into a char, gas and tar fraction. A visualization of the one compound model by Shafizadeh and Chin [52] can be found in figure 5 .
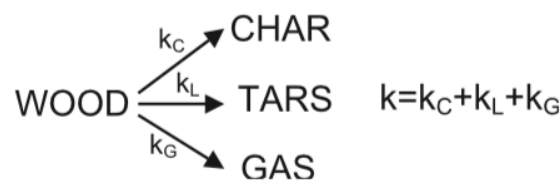
Figure 5: Visualization of the pyrolysis of wood in a one-compound pyrolysis model[52]

In case of the multi component model biomass is considered to consist of multiple conventional components. Examples are the models reviewed by Di Blasi[13]. In these model, biomass is modelled to consist only out of cellulose, hemi-cellulose and lignin. The mass fractions of these components present in the biomass still need to be determined experimentally and are different for each type of biomass. The multi-component model describes the conversion of the three components into the pyrolysis products by rate law equation. The reaction pathways of multi component models are often rather complex for the reason that reactions between pyrolysis products can also occur. A visualization of the pyrolysis kinetics of cellulose as described by Piskorz et al.[44] is given in figure 6. The same process with a different kinetic model, described by Banyesz et al.[4], is visualized in figure 7. The rate of pyrolysis depends on time, process conditions and the concentrations of cellulose, hemi-cellulose and lignin.
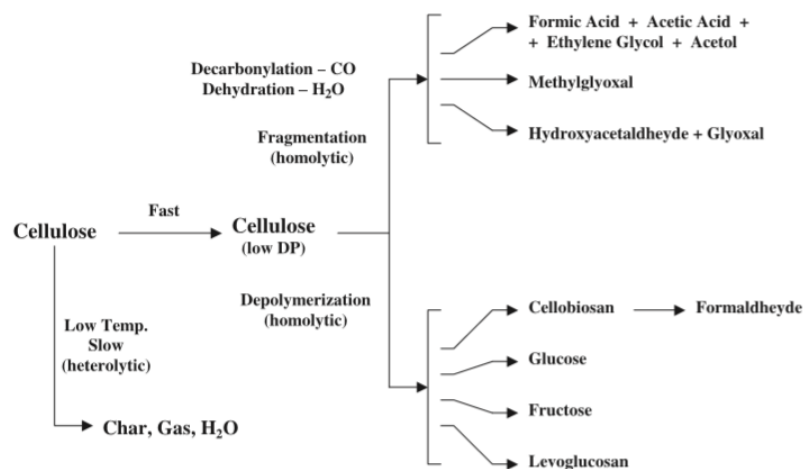
Figure 6: Visualization of the pyrolysis of cellulose in a multi-compound pyrolysis model[44]
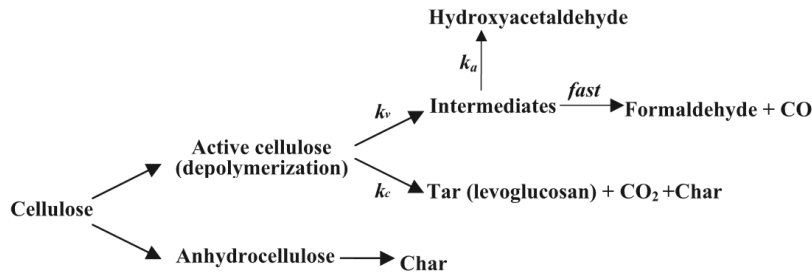
Figure 7: Visualization of the pyrolysis of cellulose in a multi-compound pyrolysis model[4]

Both models can be validated by closing the elemental balance. The C,H,O,N content from the ultimate analysis of the biomass should match the elemental sum of the pyrolysis products.

Homogeneous Reaction Model

Homogeneous reactions in the gasifier are the reactions between species present in the bubble phase, the gas phase of the emulsion and in the gas phase present in the freeboard. These reactions include the oxidation of carbon monoxide, hydrogen and methane as well as the oxidation of all tars. In addition, the reforming reactions of methane and tars and the water gas shift reaction are also homogeneous. The reaction rate is described by the rate law equation as stated in equation 3.

$$r_i = k_i [\text{A}]^a [\text{B}]^b \tag{3}$$

In the case of a simple reaction equation, such as:

$$a\text{A} + b\text{B} \longrightarrow c\text{C} + d\text{D} \tag{4}$$

With a rate constant described by Arrhenius' Law:

$$k_i = A_i \exp(\frac{-E_{a,i}}{R_g T}) \tag{5}$$

In the equation of the Arrhenius constant, A_i is the pre-exponential factor of reaction i and $E_{a,i}$ is the activation energy of reaction i in [kJ·kmol^{-1}]. According to the rate law equation, the reaction rate depends on time, concentration of the reactants and temperature. The values of A_i and $E_{a,i}$ can be found in literature from experiments. It is important to pay attention to the process conditions of the experiment, to see if the kinetics are compatible for the modelled chemical conversion.

Heterogeneous Reaction Models

Heterogeneous reactions in the gasifier are the reactions between char and gaseous reactants. In ordinary solid-gas reactions, the reaction can be divided into seven process steps[38]:

1. Mass transfer of the reactants from the gas phase to the film around the reacting particle

2. Pore diffusion inside the particle

3. reactant adsorption onto the particle surface

4. Elemental reaction

5. product desorption

6. diffusion of products towards the film

7. Mass transfer of the products from the film to the gas phase

The process steps 1,2,6 and 7 depend on the hydrodynamics of the BFB reactor. The Thiele modulus and Biot number indicate if and which of these processes can be rate limiting. For each of the heterogeneous reactions, the Thiele modulus and Biot number can be calculated. For the case that mass and heat transfer are not controlling the reaction rate, the chemical rate is limiting. For these solid-gas reactions, only processes step 3,4 and 5 need to be taken into account for the reaction rate expression.

Kinetics that take into account the rate of chemical reaction and species adsorption are Langmuir-Hinshelwood [LMHW] kinetics. for LMHW kinetics, reactions take place in isothermal conditions. The LMHW mechanism takes into account the adsorption of a gaseous reactant on the surface of a solid reactant as well as the chemical reaction rate. The reaction rate for LMHW kinetics is described by equation 6 and 7.

$$r_i = \frac{[\text{KineticTerm}] \cdot [\text{DrivingForceTerm}]}{[\text{AdsorptionTerm}]} \tag{6}$$

$$r_i = \frac{k_i [\text{A}]^a}{1 + k_a [\text{A}]^a + k_c [\text{C}]^c + k_d [\text{D}]^d} \tag{7}$$

In the case of a simple reaction equation, such as:

$$a\text{A(g)} + b\text{B(s)} \longrightarrow c\text{C(g)} + d\text{D(g)} \tag{8}$$

With a reaction constant, and adsorption constants described by Arrhenius' Law:

$$k_j = A_j \exp(\frac{-E_{a,j}}{R_g T}) \tag{9}$$

($j = i, a, c, d$)

As a result of the chemical conversion, the physical composition of char is changed. Several models exist that describe the conversion of solids in solid-gas reactions. The considered options are:

- Uniform Conversion Model [UCM]

- Shrinking Unreacted Particle Model [SUPM]

- Shrinking Unreacted Core Model [SUCM]

For the uniform conversion model there is no distinction between local conversion and conversion over the geometry of the particle. The rate of conversion is determined by the intrinsic reactivity evaluated for emulsion conditions. Both SUPM and SUCM are particle surface conversion models. For SUPM, reaction rate is higher compared to mass transfer into the particle. The ash and products that are formed on the char's surface are assumed to peel of immediately and as a result, the particle size reduces. For the SUCM model, the reactions also take place at the surface but the formed ash keeps its geometry. Therefore the density of the char particle reduces from outside to inside along the chemical conversion.

Kinetic Model Comparison
Previous studies of fluidized bed gasifiers have made use of kinetic models in order to optimize their processes. This section will provide examples of gasifier set-ups and their corresponding models. From the previous sections of this chapter can be concluded that there are various configurations of kinetic models of fluidized bed gasifiers. The comparison of multiple gasifier models has been described thoroughly by [31]. The configurations with a two-phase fluidization model will be discussed. An overview of all considered gasifier models is given in table 1.

Table 1: A List of Kinetic FB Gasifier Models with a Two-Phase Fluidization Model[31].

Authors	Year	Source	Conversion Model	Reactor Type	Feed	Agent
Hamel and Krumm	2001	[19]	1-D, steady state, non-isothermal	BFB	Brown coal, Peat, Lignite	Air/steam and O2/steam
Fiaschi and Michelini	2001	[16]	1-D, non-isothermal	BFB	Biomass	Air
Sadaka et al.	2002	[51]	1-D, unsteady state, non-isothermal	FB	Biomass	Air/Steam
Chejne and Hernandez	2002	[11]	1-D, steady state, non-isothermal	BFB	Coal	Air/Steam
Ross et al.	2005	[50]	1-D, steady state, non-isothermal	BFB	Coal	Air/Steam
Petersen and Werther	2005	[43]	1.5-D, unsteady state	CFD	Sewage Sludge	Air
Radmanesh et al.	2006	[47]	1-D, steady state, Isothermal	BFB	Biomass	Air/Steam
Kaushal et al.	2010	[28]	1-D, steady state, non-isothermal	BFB	Biomass	Air/Steam
Goyal et al.	2010	[17]	1-D, non-isothermal	BFB	Coal	Air/Steam

Appendix G: Devolatilization Curves derived from Pyro Probe Experiments

Table 2 shows the coefficients of each of the polynomials. They relate to the fourth degree polynomial described in equation 10 where i is the chemical component for which the yield is calculated. For completeness, the coefficients of the pyrolytic water model have been included in the table as well[1].

$$Y_i = aT^4 + bT^3 + cT^3 + dT + e \tag{10}$$

Table 2: Coefficients for the Devolatilization Curves

RB					
Component	a	b	c	d	e
Solid	+2.6416667E-09	-1.1349700E-05	+1.8419703E-02	-1.3438756E+01	+3.7509808E+03
Liquid	+5.7458333E-09	-2.2760283E-05	+3.3234326E-02	-2.1205559E+01	+5.0234410E+03
H2	-1.2083330E-10	+5.0611670E-07	-7.8676770E-04	+5.3905650E-01	-1.3753190E+02
CO	-3.6083333E-09	+1.4490300E-05	-2.1573920E-02	+1.4162384E+01	-3.4650211E+03
CH4	-6.7916670E-10	+2.7391500E-06	-4.0928670E-03	+2.6940660E+00	-6.6055220E+02
CO2	-1.4250000E-09	+5.9211000E-06	-9.1564079E-03	+6.2556923E+00	-1.5900540E+03
GB					
Component	a	b	c	d	e
Solid	+4.2666667E-09	-1.9314200E-05	+3.2798721E-02	-2.4790093E+01	+7.0631348E+03
Liquid	-2.2083333E-10	+3.3719833E-06	-9.4786951E-03	+9.6620002E+00	-3.2948295E+03
H2	-1.0833330E-10	+4.4496670E-07	-6.7890050E-04	+4.5684100E-01	-1.1454160E+02
CO	-1.2250000E-09	+4.3910330E-06	-5.6512180E-03	+3.0871510E+00	-5.9680010E+02
CH4	-3.3750000E-10	+1.2677170E-06	-1.7379640E-03	+1.0329590E+00	-2.2458800E+02
CO2	-6.2916670E-10	+2.7512170E-06	-4.5121080E-03	+3.2951880E+00	-8.9905610E+02
MISC					
Component	a	b	c	d	e
Solid	-3.1691900E-23	+8.3333300E-09	+3.0675000E-05	-1.1324500E-01	+9.2620200E+01
Liquid	-1.1962500E-08	+5.1953883E-05	-8.4027787E-02	+5.9916476E+01	-1.5842390E+04
H2	+2.3333330E-10	-1.0264670E-06	+1.6810020E-03	-1.2128960E+00	+3.2514600E+02
CO	-1.5000000E-10	+3.9713300E-07	-2.6567600E-04	-2.2860200E-02	+4.9144300E+01
CH4	-1.4166670E-10	+5.4470000E-07	-7.7384300E-04	+4.8811010E-01	-1.1626610E+02
CO2	+1.4375000E-09	-6.2272500E-06	+1.0032430E-02	-7.1174416E+00	+1.8832121E+03

Appendix H: Reaction Kinetics for the Considered Gasification Reactions

The considered reactions have been summarized in table 3.

Table 3: Typical Reactions Occurring during Gasification

Reaction Nr	Reaction Name	Reaction Equation	Source
R1	Boudouard	$C + CO_2 \longrightarrow 2CO$	[33]
R2	Water Gas Shift	$CO + H_2O \longrightarrow CO_2 + H_2$	[18],[43]
Oxidation			
R3	Char Oxidation	$\alpha C + O_2 \longrightarrow 2(\alpha - 1)CO + (2 - \alpha)CO_2$	[18],[43]
R4	H_2 Oxidation	$H_2 + 0.5O_2 \longrightarrow H_2O$	[18],[36]
R5	CO Oxidation	$CO + 0.5O_2 \longrightarrow CO_2$	[18]
R6	CH_4 Oxidation	$CH_4 + 0.5O_2 \longrightarrow CO + 2H_2$	[18]
R7	C_6H_6 Oxidation	$C_6H_6 + 3O_2 \longrightarrow 6CO + 3H_2$	[36]
R8	C_7H_8 Oxidation	$C_7H_8 + 3.5O_2 \longrightarrow 7CO + 4H_2$	[54]
R9	$C_{10}H_8$ Oxidation	$C_{10}H_8 + 7O_2 \longrightarrow 10CO + 4H_2O$	[18]
Reforming			
R10	Water Gas	$C + 1.2H_2O \longrightarrow 0.8CO + 0.2CO_2 + 1.2H_2$	[18],[43]
R11	CH_4 Reforming	$CH_4 + H_2O \longleftrightarrow CO + 3H_2$	[43]
R12	C_6H_6 Reforming	$C_6H_6 + 2H_2O \longrightarrow 1.5C + 2.5CH_4 + 2CO$	[54]
R13	C_7H_8 Reforming	$C_7H_8 + 21H_2O \longrightarrow 7CO_2 + 29H_2 + 7CO$	[54]
R14	C_6H_5OH Reforming	$C_6H_5OH + 3H_2O \longrightarrow 2CO + CO_2 + 2.95CH_4 +$ $0.05C + 0.1H_2$	[54]

The kinetics for these reactions have been summarized in table 4. The unit of reaction rate r_i is $kmol \cdot m^{-3} \cdot s^{-1}$. The unit of activation energy $E_{a,i}$ is $kJ \cdot kmol^{-1}$. The unit of reaction constant k_i depends on the order of reaction i. A general description is given by equation 11 for an n-th order reaction[12].

$$\text{unit of } r_i = [(m^3 \cdot kmol^{-1})^{n-1} \cdot (m \cdot s^{-1})] \tag{11}$$

Table 4: Reaction Kinetics for the Reactions as Described in Table 3.

Reaction Nr	Reaction Name	Reaction Kinetics	Source
R1	Boudouard	$r_1 = \frac{k_1 F_1 [CO_2]}{1+K^1_{CO_2}[CO_2]+K^1_{CO}[CO]}$ $k_1 = 4.89 \cdot 10^{10} \exp\left(\frac{-268000}{RT}\right)$ $F_1 = \frac{\rho_{char} \cdot (1-X)}{MW_{char}}$ $K^1_{CO_2} = 66$ $K^1_{CO} = 120 \exp\left(\frac{-255000}{RT}\right)$ $\rho_{char} = 250\,kg \cdot m^3$ In the bedzone (CSTR)[45] $\rho_{char} = 125\,kg \cdot m^3$ In the freeboard (PFR) due to the SDM.	[33]
R2	Water Gas Shift	$r_2 = k_2\left([CO][H_2O] - \frac{[CO_2][H_2]}{K^2_{eq}}\right)$ $k_2 = 2778 \exp\left(\frac{-12560}{RT}\right)$ $K^2_{eq} = 0.022 \cdot 10^{14} \exp\left(\frac{37730}{RT}\right)$	[18],[43]
Oxidation			
R3	Char Oxidation	$r_3 = k_3 F_3 [O_2]$ $k_3 = 595.7 \cdot T^2 \cdot \exp\left(\frac{-149440}{RT}\right)$ $F_3 = \frac{6}{d_p}$ $d_p = 0.006\,[m]$ $\alpha = \frac{1+2\cdot f_r}{1+f_r}; f_r = 4.72 \cdot 10^{-3} \cdot \exp\left(\frac{3773.7}{R_g T_r}\right)$	[18],[43],[36]
R4	H$_2$ Oxidation	$r_4 = k_4 [O_2][H_2]$ $k_4 = 1.08 \cdot 10^{13} \cdot \exp\left(\frac{-125525}{RT}\right)$	[18],[36]
R5	CO Oxidation	$r_5 = k_5 [O_2]^{0.25}[CO][H_2O]^{0.5}$ $k_5 = 2.32 \cdot 10^{12} \cdot \exp\left(\frac{-167000}{RT}\right)$	[18]
R6	CH$_4$ Oxidation	$r_6 = k_6 [O_2]^{0.25}[CH_4]^{0.5}$ $k_6 = 4.4 \cdot 10^{11} \cdot \exp\left(\frac{-126000}{RT}\right)$	[18]
R7	C$_6$H$_6$ Oxidation	$r_7 = k_7 [O_2][C_6H_6]$ $k_7 = 1.58 \cdot 10^{15} \cdot \exp\left(\frac{-202641}{RT}\right)$	[36]

R8	C_7H_8 Oxidation	$r_8 = k_8[O_2]^{0.5}[C_7H_8][H_2O]^{0.5}$ $k_8 = 1.3 \cdot 10^{11} \cdot \exp\left(\frac{-125600}{RT}\right)$	[54]
Reforming			
R9	$C_{10}H_8$ Oxidation	$r_9 = k_9[O_2]^{0.5}[C_10H_8]^{0.5}$ $k_9 = 9.2 \cdot 10^6 \cdot T \cdot \exp\left(\frac{-80000}{RT}\right)$	[18]
R10	Water Gas	$r_{10} = \frac{k_{10}[H_2O]}{1 + K_{H_2O}^{10}[H_2O] + K_{H_2}^{10}[H_2] + K_{CO}^{10}[CO]}$ $k_{10} = 2.39 \cdot 10^5 \exp\left(\frac{-129000}{RT}\right)$ $F_{10} = \frac{\rho_{char} \cdot (1-X)}{MW_{char}}$ $K_{H_2O}^{10} = 31.6 \exp\left(\frac{30100}{RT}\right)$ $K_{H_2}^{10} = 5.36 \exp\left(\frac{59800}{RT}\right)$ $K_{CO}^{10} = 0.0825 \exp\left(\frac{96100}{RT}\right)$ $\rho_{char} = 250\,\text{kg} \cdot \text{m}^3$ In the bedzone (CSTR)[45] $\rho_{char} = 125\,\text{kg} \cdot \text{m}^3$ In the freeboard (PFR) due to the SDM.	[18],[43]
R11	CH_4 Reforming	$r_{11} = k_{11}\left([CH_4][H_2O] - \frac{[H_2]^3[CO]}{K_{eq}^{11}}\right)[C(s)]$ $k_{11} = 4.916 \cdot 10^{-10} \cdot T^2 \cdot \frac{1}{M_c \cdot \rho_c \cdot d_p} \exp\left(\frac{-36150}{RT}\right)$ $K_{eq}^{11} = 3.106 \cdot 10^{14} \exp\left(\frac{-208800}{RT}\right)$	[43]
R12	C_6H_6 Reforming	$r_{12} = k_{12}[H_2O]^{0.2}[C_6H_6]^{1.3}[H_2]^{-0.4}$ $k_{12} = 3.39 \cdot 10^{16} \cdot \exp\left(\frac{-443000}{RT}\right)$	[54]
R13	C_7H_8 Reforming	$r_{13} = k_{13}[C_7H_8]$ $k_{13} = 2.323 \cdot 10^5 \cdot \exp\left(\frac{-356000}{RT}\right)$	[54]
R14	C_6H_5OH Reforming	$r_{14} = k_{14}[C_6H_6O]$ $k_{14} = 1 \cdot 10^8 \cdot \exp\left(\frac{-100000}{RT}\right)$	[54]

Appendix I: FORTRAN Code in ASPEN Plus Block YDEVO for Implementing Temperature Dependent Pyrolysis Curves

```
IF (SELECT .EQ. 1) THEN
H2 = -1.2083330E-10*T**4 + 5.0611670E-07*T**3 +- 7.8676770E-04*T**2 + 5.3905650E-01*T -1.3753190E+02
CO2 = -1.4250000E-09*T**4 + 5.9211000E-06*T**3 +- 9.1564079E-03*T**2 + 6.2556923E+00*T - 1.5900540E+03
CO = -3.6083333E-09*T**4 + 1.4490300E-05*T**3 -2.1573920E-02*T**2 ++ 1.4162384E+01*T -3.4650211E+03
CH4 = -6.7916670E-10*T**4 +2.7391500E-06*T**3 -4.0928670E-03*T**2 ++ 2.6940660E+00*T -6.6055220E+02
SOLID = 2.6416667E-09*T**4 -1.1349700E-05*T**3 +1.8419703E-02*T**2 +- 1.3438756E+01*T + 3.7509808E+03
LIQUID = 5.7458333E-09*T**4 -2.2760283E-05*T**3 ++3.3234326E-02*T**2 -2.1205559E+01*T +5.0234410E+03
N2 = 0.06
S = 0.01
ASH = 0.49
O2 = 0
LGASSES = 0
CHAR = SOLID - ASH
PW = 5.157E-05*T**2 - 11.86E-02*T + 84.91
MOIST = 5.57
DMASS = 100 - CO - H2 - CO2 - CH4 - LIQUID - SOLID - N2 - S
LIQUIDS = LIQUID + DMASS
H2O = PW + MOIST
BENZENE= 0.379 * (LIQUIDS - H2O)
TOLUENE= 0.282 * (LIQUIDS - H2O)
NAPHTHA = 0.218 * (LIQUIDS - H2O)
PHENOL = 0.121 * (LIQUIDS - H2O)
CL2 = 0
TCSTR = T
TPLUG = T
TSTOIC = T
FR = 4.72E-3*exp(37737 / (8.31445985 * T))
BETAC = -((1+2*FR) / (1+FR))
BETACO = 2*((-BETAC) - 1)
BETACO2 = 2 + BETAC
LCSTR = (VCSTR+(24.7E-3)) / 0.076353
LFB = 2.454 - LCSTR
DFB2 = (1.068 - LCSTR) / LFB
DFB3 = (1.207 - LCSTR) / LFB
DFB4 = (1.453 - LCSTR) / LFB
DFB5 = (1.454 - LCSTR) / LFB
DFB6 = (1.704 - LCSTR) / LFB
DFB7 = (1.705 - LCSTR) / LFB

ELSE IF (SELECT .EQ. 2) THEN

H2 = -1.083333E-10*T**4 + 4.449667E-7*T**3 - 0.000678901*T**2 ++ 0.456841*T -114.5416
CO2 = -6.291667E-10*T**4 + 2.751217E-06*T**3 - 0.004512108*T**2 ++ 3.295188*T - 899.0561
CO = -1.225E-09*T**4 + 4.391033E-06*T**3 - 0.00565122*T**2 ++ 3.087151*T - 596.8001
CH4 = -3.375E-10*T**4 + 1.267717E-06*T**3 - 0.001737964*T**2 ++ 1.032959*T - 224.588
```

```
SOLID = 4.2666667E-09*T**4 - 1.93142E-05*T**3 + 0.032798721*T**2 +- 24.790093*T + 7063.1348
LIQUID = -2.2083333E-10*T**4 + 3.3719833E-06*T**3 +- 0.0094786951*T**2 + 9.662*T - 3294.83
N2 = 0.3
S = 0.01
ASH = 0.73
O2 = 0
LGASSES = 0
CHAR = SOLID - ASH
DMASS = 100 - CO - H2 - CO2 - CH4 - LIQUID - SOLID - N2 - S
LIQUIDS = LIQUID + DMASS
PW= 5.157E-05*T**2 - 11.86E-02*T + 84.91
MOIST = 5.08
H2O = PW + MOIST
BENZENE= 0.379 * (LIQUIDS - H2O)
TOLUENE= 0.282 * (LIQUIDS - H2O)
NAPHTHA = 0.218 * (LIQUIDS - H2O)
PHENOL = 0.121 * (LIQUIDS - H2O)
CL2 = 0
TCSTR = T
TPLUG = T
TSTOIC = T
FR = 4.72E-3*exp(37737 / (8.31445985 * T))
BETAC = -((1+2*FR) / (1+FR))
BETACO = 2*((-BETAC) - 1)
BETACO2 = 2 + BETAC
LCSTR = (VCSTR+(24.7E-3)) / 0.076353
LFB = 2.454 - LCSTR
DFB2 = (1.068 - LCSTR) / LFB
DFB3 = (1.207 - LCSTR) / LFB
DFB4 = (1.453 - LCSTR) / LFB
DFB5 = (1.454 - LCSTR) / LFB
DFB6 = (1.704 - LCSTR) / LFB
DFB7 = (1.705 - LCSTR) / LFB


ELSE


H2 = 2.3333330E-10*T**4 -1.0264670E-06*T**3 +1.6810020E-03*T**2 +-1.2128960E+00*T +3.2514600E+02
CO2 = 1.4375000E-09*T**4 -6.2272500E-06*T**3 +1.0032430E-02*T**2 +-7.1174416E+00*T + 1.8832121E+03
CO = -1.5E-10*T**4 + 3.97133E-07*T**3 -2.65676E-04*T**2 +-2.2860200E-02*T +4.9144300E+01
CH4 = -1.416667E-10*T**4 +5.447E-07*T**3 -7.73843E-04*T**2 ++ 4.8811010E-01*T -1.1626610E+02
SOLID = -3.16919E-23*T**4 +8.33333E-09*T**3 +3.0675E-05*T**2 +-1.1324500E-01*T + 9.26202E+01
LIQUID = -1.19625E-08*T**4 +5.1953883E-05*T**3 +-8.4027787E-02*T**2 +5.9916476E+01*T -1.5842390E+04
N2 = 0.49
S = 0.07
ASH = 4.1
O2 = 0
LGASSES = 0
CHAR = SOLID - ASH
DMASS = 100 - CO - H2 - CO2 - CH4 - LIQUID - SOLID - N2 - S
LIQUIDS = LIQUID + DMASS
PW = 5.157E-05*T**2 - 11.86E-02*T + 84.91
MOIST = 6.7
H2O = PW + MOIST
BENZENE= 0.379 * (LIQUIDS - H2O)
TOLUENE= 0.282 * (LIQUIDS - H2O)
NAPHTHA = 0.218 * (LIQUIDS - H2O)
```

```
PHENOL = 0.121 * (LIQUIDS - H2O)
CL2 = 0
TCSTR = T
TPLUG = T
TSTOIC = T
FR = 4.72E-3*exp(37737 / (8.31445985 * T))
BETAC = -((1+2*FR) / (1+FR))
BETACO = 2*((-BETAC) - 1)
BETACO2 = 2 + BETAC
LCSTR = (VCSTR+(24.7E-3)) / 0.076353
LFB = 2.454 - LCSTR
DFB2 = (1.068 - LCSTR) / LFB
DFB3 = (1.207 - LCSTR) / LFB
DFB4 = (1.453 - LCSTR) / LFB
DFB5 = (1.454 - LCSTR) / LFB
DFB6 = (1.704 - LCSTR) / LFB
DFB7 = (1.705 - LCSTR) / LFB

END IF
```

Appendix J: Model Data for the Sensitivity Analysis of the Equivalent Ratio

Fbio	YCO	YCO2	YH2	YCH4	ER	O2/BIO	YCHAR	Ybenz	Ytolu	Ynaph	Yphen
kg/hr	kmol/hr	kmol/hr	kmol/hr	kmol/hr	-	2.50685	kmol/hr	kmol/hr	kmol/hr	kmol/hr	kmol/hr
10	0.10552	0.15084	0.05794	0.02434	0.34817	0.25069	0	0.01835	0.0098	0.00548559	0
11	0.12798	0.14995	0.06948	0.02678	0.31652	0.2279	0	0.02019	0.01097	0.00630486	0
12	0.15093	0.14881	0.08114	0.02922	0.29015	0.2089	0	0.02203	0.01215	0.00708972	0
13	0.1744	0.14744	0.09293	0.03165	0.26783	0.19283	0	0.02386	0.01334	0.007846	0
14	0.19856	0.14583	0.10502	0.03407	0.2487	0.17906	0	0.0257	0.01454	0.00857917	0
15	0.22076	0.14591	0.11861	0.03649	0.23212	0.16712	0	0.02754	0.01574	0.00929398	0
16	0.22555	0.15119	0.12526	0.0389	0.21761	0.15668	0.01243	0.02937	0.01693	0.00999438	0
17	0.23007	0.15654	0.13183	0.04132	0.20481	0.14746	0.02528	0.03121	0.01813	0.01068352	0
18	0.23476	0.16181	0.13843	0.04373	0.19343	0.13927	0.03816	0.03304	0.01933	0.01136388	0
19	0.23882	0.16727	0.14484	0.04614	0.18325	0.13194	0.05153	0.03488	0.02052	0.01203736	0
20	0.2431	0.17264	0.1513	0.04855	0.17409	0.12534	0.06485	0.03672	0.02172	0.01270545	0
21	0.24736	0.17799	0.15773	0.05096	0.1658	0.11937	0.07826	0.03855	0.02291	0.01336927	0
22	0.25151	0.18335	0.16412	0.05336	0.15826	0.11395	0.09181	0.04039	0.0241	0.01402971	0
23	0.25552	0.18875	0.17043	0.05577	0.15138	0.10899	0.10551	0.04222	0.02528	0.01468744	0
24	0.25929	0.19421	0.17664	0.05819	0.14507	0.10445	0.11943	0.04406	0.02647	0.01534299	0

Appendix K: Model Data for the Sensitivity Analysis of the Isothermal Reactor Temperature

Tr C	YCO kmol/hr	YCO2 kmol/hr	YH2 kmol/hr	YCH4 kmol/hr	YCHAR kmol/hr	Ybenz kmol/hr	Ytolu kmol/hr	Ynaph kmol/hr	Yphen kmol/hr
600	0.00729	0.14956	0.03328	0.01349	0.55437	0.01601	0.00305	0.00000	0.00000
650	0.02977	0.16591	0.07455	0.02072	0.39328	0.02517	0.00956	0.00004	0.00000
700	0.05359	0.17237	0.08576	0.02625	0.27789	0.02898	0.01322	0.00181	0.00000
750	0.10270	0.17240	0.10043	0.03124	0.16244	0.02941	0.01402	0.00543	0.00000
800	0.19556	0.15347	0.11439	0.03627	0.02642	0.02795	0.01529	0.00897	0.00000
810	0.21961	0.14642	0.11695	0.03729	0.00000	0.02754	0.01573	0.00929	0.00000
850	0.23489	0.17782	0.04718	0.12223	0.00000	0.03276	0.01025	0.01375	0.00000
900	0.35619	0.13827	0.00569	0.18579	0.00000	0.02552	0.01503	0.00838	0.00000
950	0.36707	0.13836	0.00430	0.20125	0.00000	0.02228	0.01462	0.00819	0.00000
1000	0.50527	0.05944	0.00089	0.22460	0.00000	0.00250	0.01442	0.00630	0.00000

Appendix L: Model Data for the Sensitivity Analysis of the Bedzone Volume

Vbed L	YCO kmol/hr	YCO2 kmol/hr	YH2 kmol/hr	YCH4 kmol/hr	YCHAR kmol/hr	Ybenz kmol/hr	Ytolu kmol/hr	Ynaph kmol/hr	Yphen kmol/hr
40	0.21829	0.14434	0.12967	0.03657	0.04077	0.02752	0.01401	0.00682	0
45	0.21859	0.14462	0.12789	0.03656	0.03405	0.02752	0.01418	0.00731	0
50	0.21865	0.14497	0.12614	0.03655	0.0279	0.02753	0.01438	0.00775	0
55	0.21878	0.14528	0.12452	0.03654	0.02217	0.02753	0.01459	0.00813	0
60	0.21905	0.1455	0.12306	0.03653	0.01686	0.02753	0.01481	0.00846	0
65	0.21949	0.14564	0.12179	0.03652	0.01196	0.02753	0.01503	0.00873	0
70	0.21976	0.1458	0.12062	0.03651	0.00773	0.02753	0.01526	0.00895	0
75	0.22035	0.14582	0.11968	0.0365	0.00384	0.02753	0.01548	0.00913	0
80	0.2207	0.14589	0.11883	0.03649	0.00063	0.02754	0.01568	0.00926	0
81.3	0.22076	0.14591	0.11861	0.03649	0	0.02754	0.01574	0.00929	0
85	0.21865	0.14632	0.11649	0.03648	0	0.02754	0.01587	0.00937	0
90	0.21594	0.14713	0.11444	0.03647	0	0.02754	0.01605	0.00944	0
95	0.21331	0.14805	0.11284	0.03646	0	0.02754	0.0162	0.0095	0
100	0.21121	0.14883	0.11162	0.03645	0	0.02754	0.01633	0.00954	0